UNIVERSITY OF KWAZULU-NATAL

SOFT-OUTPUT DETECTION FOR TRANSMIT ANTENNA INDEX MODULATION-BASED SCHEMES

Abdulmajeed Adekilekun Tijani

2016

(EXAMINER'S COPY)

SOFT-OUTPUT DETECTION FOR TRANSMIT ANTENNA INDEX MODULATION-BASED SCHEMES

Abdulmajeed Adekilekun Tijani

214584641

Submitted in fulfilment of the academic requirements of

Master of Science in Engineering

Discipline of Electrical, Electronic and Computer Engineering

School of Engineering, College of Agriculture, Engineering and Science

University of KwaZulu-Natal, Durban, South Africa

Supervisor: Dr. Narushan Pillay

Co-Supervisor: Prof. HongJun Xu

July 2016

Preface

The research contained in this dissertation was completed by the candidate while based in the School of Engineering, Discipline of Electrical, Electronic and Computer Engineering, in the College of Agriculture, Engineering and Science, University of KwaZulu-Natal, Howard College, South Africa.

The contents of this work have not been submitted in any form to another university and, except where the work of others is acknowledged in the text, the results reported are due to investigations carried out by the candidate.

As the candidate's supervisor, I agree to the submission of this dissertation.

Signed: _____

Name: Dr. Narushan Pillay

Designation: Supervisor

Date:

Declaration 1

Plagiarism

I, Abdulmajeed Adekilekun TIJANI, declare that:

i. the research reported in this dissertation, except where otherwise indicated, is my original research;

ii. this dissertation has not been submitted for any degree or examination at any other university;

iii. this dissertation does not contain other person's data, pictures, graphs or other information unless specifically acknowledged as being sourced from other persons;

iv. this dissertation does not contain other person's writing unless specifically acknowledged as being sourced from other researchers. Where other written sources have been quoted, then

   a. their words have been re-written but the general information attributed to them has been referenced,

   b. where their exact words have been used, then their writing has been placed in italics and inside quotation marks, and referenced;

v. this dissertation does not contain texts, graphics or tables copied from the internet, unless specifically acknowledged, and the source being detailed in the dissertation and in the reference section.

Signed:

_____

Name: Abdulmajeed A. TIJANI

Designation: Student

Date:

Declaration 2

Publications

Publication 1:

A. A. Tijani, N. Pillay, H. Xu, "Soft-Output Decision Based Detectors for SSK, Bi-SSK, and QSM Modulations" *International Journal of Communication Systems (IJCS-16-0569)* [under review].

Publication 2:

A. A. Tijani, N. Pillay, H. Xu, "Soft-Output Detection for Bi-Space Shift Keying Modulation" in *Proceedings of the Southern Africa Telecommunications Network and Applications Conference (SATNAC)*, Sep. 2016 [under review].

Signed:

_____

Name: Abdulmajeed A. TIJANI

Designation: Student

Date:

Dedication

to

Muslihudeen Adekilekun TIJANI

B. Pharm. Hons (Ibadan), PGDip Pharm (Aston)

my brother, mentor, and sponsor,
who has invested so many resources in me and my education,
right from the cradle.

O Allah! Continue to increase his blessings, wealth, health, and wisdom.

Abstract

The use of multiple-input multiple-output (MIMO) techniques in wireless communication systems has led to substantial improvements in spectral efficiency and reliability. However, challenges such as inter-antenna synchronization, inter-channel interference, and computational/hardware complexity remains.

In recent times, innovative MIMO systems based on transmit antenna index modulation, such as spatial modulation (SM), quadrature SM (QSM), space shift keying (SSK) and Bi-SSK, have been proposed. These schemes address the abovementioned challenges of MIMO; hence, rendering them as promising schemes for integration into the next generation of wireless communication systems.

In this dissertation, the error performances of these transmit antenna index modulation-based schemes are firstly investigated. It is evident that the schemes are able to achieve a good combination of high spectral efficiencies/improved reliability and relatively low hardware complexities.

In practice, channel coding would be employed with the above mentioned transmit antenna index modulation-based schemes. However, the available detectors for SSK/Bi-SSK and QSM are hard-decision and will not exploit the coding gains achievable with soft-decision detection combined with soft-input channel decoding.

On this note, in this dissertation, soft-output maximum-likelihood detectors (SOMLD) for the above schemes are formulated. Monte Carlo simulation results demonstrate the substantial improvements in error performance that can be achieved in comparison to the conventional hard-decision ML detector (HDMLD).

For example, at a BER of 10^{-6}, coded SOMLD for 6 bits/s/Hz SSK system achieves an SNR gain of 4.3 dB over the coded HDMLD. At the same BER and spectral efficiency, the coded Bi-SSK-SOMLD system performs better than its coded HDMLD counterpart by 4.2 dB SNR gain. For coded QSM system, the receiver with SOMLD achieve 5.1 dB gains over HDMLD, at 6 b/s/Hz spectral efficiency and a BER of 10^{-6}. It was clear that further improvements in error performance are observed in coded SOMLD systems over uncoded conventional HDMLD systems. Finally, the SOMLD is shown to impose no additional computational complexity at the receiver; and without channel coding, the proposed detector yields identical error performance as the HDMLD.

Acknowledgements

ألحمد لله رب ألعلمبن . The biggest thanks goes to الله (Allah) for seeing me through the years of pursuing the degree of Master of Science in Engineering (MSc.Eng).

Many thanks to my amiable supervisor, Dr. Narushan Pillay, from whom I have learnt a lot in the field of Electronic Engineering. He also taught me how best to prepare technical reports. I appreciate his patience in dealing with me and the time spent in going through this dissertation over and over again to make sure it is error-free. Thanks to Professor HongJun Xu, for impacting so much knowledge of wireless communication engineering in me. Both of them are the pillars on which I stand to be able to see the research world.

The financial contributions of the duo of Rx. Muslihudeen and Dr. Ahmad are very well appreciated. Indeed, you guys saved me from the shame that accompanied my youth exorbitance. Kudos to my beloved parents, Alhaji and Alhajas Tijani Adekilekun Abdulhameed, who always support me with prayers. My sincere appreciation goes to my siblings: Muhammad, Mustapha and Murtadha, who stood by me, unconditionally. I acknowledge the patience and endurance of my wife, Faizat Anike, and my beautiful daughter, Rayhaanat Moyanjuola.

I wish to extend my heart of gratitude to all staff and postgraduate fellows of the Discipline of Electrical, Electronic and Computer Engineering at the Howard College of UKZN. You all made the department a great place to be for me. To my friends, '*Muchas gracias*'; and to members of the ADEKILEKUN dynasty, "*Jazakumullahu-khayran"*.

Abdulmajeed Adekilekun TIJANI

B.Tech (LAUTECH)

Durban, July 2016.

Table of Contents

2. Spatial Modulation

3. SSK and Bi-SSK Modulations

4. Quadrature Spatial Modulation

List of Figures

List of Tables

List of Acronyms

AS	Antenna Selection
APM	Amplitude/Phase Modulation
AWGN	Additive White Gaussian Noise
APP	a-Posteriori Probability
BER	Bit Error Rate
Bi-SSK	Bi-Space Shift Keying
BLAST	Bell Laboratories Layered Space-Time Architecture
BPSK	Binary Phase Shift Keying
CC	Computational Complexity
CM	Coded Modulation
CSI	Channel State Information
DIV	Diversity
FEC	Forward Error Correction
FRF	Flat Rayleigh Fading
GSM	Generalised Spatial Modulation
GSSK	Generalized Space Shift Keying
HDMLD	Hard Decision Maximum Likelihood Detection/Detector
IAS	Inter-Antenna Synchronization
ICI	Inter-Channel Interference
IEEE	Institute of Electrical and Electronic Engineers
i.i.d.	Independent and Identically Distributed
IP	Internet Protocol
LLR	Log-Likelihood Ratio
LTE	Long Term Evolution
LUT	Look-Up Table
MAP	Maximum a-posteriori
MIMO	Multiple-Input Multiple-Output

ML	Maximum Likelihood
MMSE	Minimum Mean-Squared Error
MRC	Maximum Ratio Combining
NMRC	Normalized Maximum Ratio Combining
OSIC	Ordered Successive Interference Cancellation
PEP	Pairwise Error Probability
PDF	Probability Density Function
PSK	Phase Shift Keying
QAM	Quadrature Amplitude Modulation
QPSK	Quadrature Phase Shift Keying
QSM	Quadrature Spatial Modulation
SD	Sphere Decoding
RF	Radio Frequency
SER	Symbol Error Rate
SM	Spatial Modulation
SM-OD	Spatial Modulation with Optimal Detection
SNR	Signal-to-Noise Ratio
SOMLD	Soft-output Maximum-Likelihood Detection/Detector
SSK	Space Shift Keying
STBC	Space-Time Block Code
SVD	Signal Vector-based Detection
TV	Television
V-BLAST	Vertical Bell Laboratories Layered Space-Time Architecture
WiMAX	Worldwide Interoperability for Microwave Access
WLAN	Wireless Local Area Network
WRAN	Wireless Regional Area Network

Chapter 1

Introduction

1.1. Digital Communication Systems

Digital communication has to do with transmitting a sequence of binary digits from a source to one or more destinations. Achieving this involves a number of processes as depicted in Figure 1.1, which clearly illustrates the basic constituent elements of a typical digital communication system. The source output (i.e. message) can further be compressed into a digital information sequence (i.e. binary digits) by source encoder and, in turn, passed into the channel encoder so that redundancy is introduced in a controlled manner to overcome the effects of interferences and noise that will be encountered in the process of transmitting the information through a physical channel. At the output of the channel encoder is a digital modulator that is capable of mapping the channel coded sequence into signal waveforms which are interfaced with the communication channel. Through the channel, the signal travels from the transmitter (i.e. source) to the receiver (i.e. destination) along the line, gets corrupted in a random manner due to its nature. The received signal is fed into a digital demodulator which reduces it to an estimate of the channel coded data. At this point, a channel decoder is used to reconstruct the transmitted information sequence from the foreknowledge of the introduced redundancy and characteristics of the channel encoder. A source decoder is employed to obtain the desired output [1].

A general problem of sending information through channels is the additive noise. Components, such as resistors, as well as other solid-state devices used in the construction of communication systems, are majorly responsible for this. Interferences and noise can also come from other external sources. Attenuation, phase and amplitude distortion and other

multipath distortions are responsible for degradations encountered in digital communication systems. Noise effects may, therefore, be minimized by increasing the signal transmit power. However, the power level in transmission is usually limited by equipment and other practical constraints. The limited channel bandwidth available and the electronic components used in the construction of transceivers are other rampant constraints in communication systems. Signal transmission is made through wireline and wireless channels; such as free space, fibre-optic, storage, and underwater acoustic [2].

This dissertation is interested in wireless communication systems, where electromagnetic energy is united to the propagation medium by the radiating antenna(s). To the content and context of this dissertation, the "channel encoding/decoding" and "digital modulation/demodulation" elements of the communication system remain very important. In this section, therefore, we will take a broader look into channel encoding and decoding techniques that are used in this research and leave the digital modulation and demodulation aspects for later discussion at the appropriate sections of the dissertation.

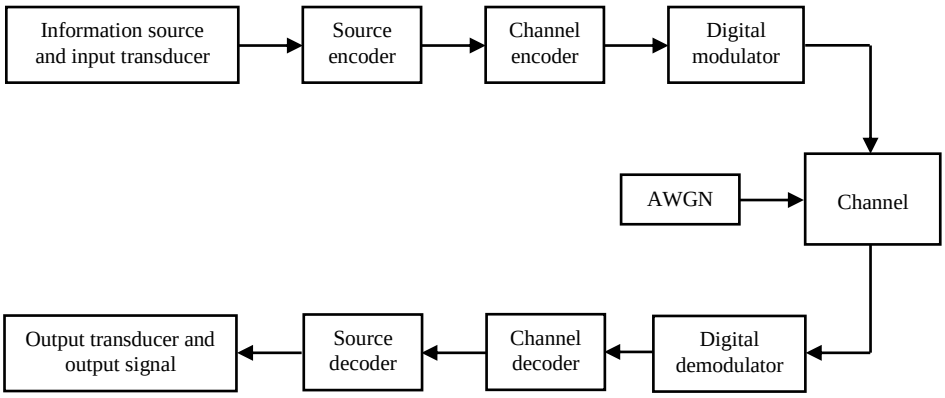

Figure 1.1: Basic elements of a digital communication system [1]

1.1.1. Channel Encoding and Decoding

Generally, coding techniques are a major feature of digital data transmission with an aim to protect the original information being transmitted over the channel [1]. Additional protection is thus given to digital information sequences by the introduction of extra bits in a meticulous manner which translates to more reliable transmission, even in the presence of noise and interferences on the physical channel. Channel encoding gives receivers the ability

to detect and/or correct errors in transmission. In turn, this improves the quality of transmission in terms of the bit errors. Simply put, coding can be employed to improve the effective SNR and, thus, enhance the performance of the digital communication system. In [1], coding is said to have improved the performance of a practical digital communication systems by up to 9 dB depending on the application and the type of the code employed.

Codes can be simple - such as block codes and convolutional codes, or derived - such as concatenated codes, turbo codes and product codes. In this section, we discuss, briefly, the two simple encoding standards available for applications based on the transmission mode involved in the communication system. These, again, are block codes and convolutional codes. In block codes, each block of k input bits is mapped into a block of length n of output bits by a rule defined by the code and regardless of the previous inputs to the encoder. Convolutional codes are different from block codes by the existence of memory in the encoding scheme. In convolutional codes, each block of k bits is again mapped into a block of n bits to be transmitted over the channel, but these n bits are not only determined by the present k-information bits but also by the previous information bits. This dependence on the previous information bits causes the encoder to be a finite state machine [1].

In telecommunication, a convolutional code is a type of error-correcting code that generates parity symbols via the sliding application of a Boolean polynomial function to a data stream. The sliding application represents the 'convolution' of the encoder over the data, which gives rise to the term 'convolutional coding'. The sliding nature of the convolutional codes facilitates trellis decoding using a time-invariant trellis which allows it to be maximum-likelihood soft-decision decoded with reasonable complexity. Thus, the convolutional codes are of major interest in this dissertation, due to its ability to perform economical maximum-likelihood soft-decision decoding. Their block length and code rate flexibility have also made them very popular for digital communications [1]. It is therefore considered necessary, in the next sub-section, to briefly look into the structures of encoders and decoders of convolutional codes.

1.1.1.1. Convolutional Encoder

The major aim of the channel coding is to reduce the probability of erroneous transmission over noisy communication channels [3]. A convolutional encoder generates codewords from

a linear sequential circuit that requires a block of k bits as input and outputs a block of n bits, with or without feedback. Consequently, convolutional encoders are described with a ratio of k/n, known as 'rate'. For example, a $1/2$ rate encoder, shown in Figure 1.2, generates two output bits for every input bit. Meanwhile, each output (v_n) of the convolutional encoder simply depends not only on the present input bit (u_k), but also on the previous input bits.

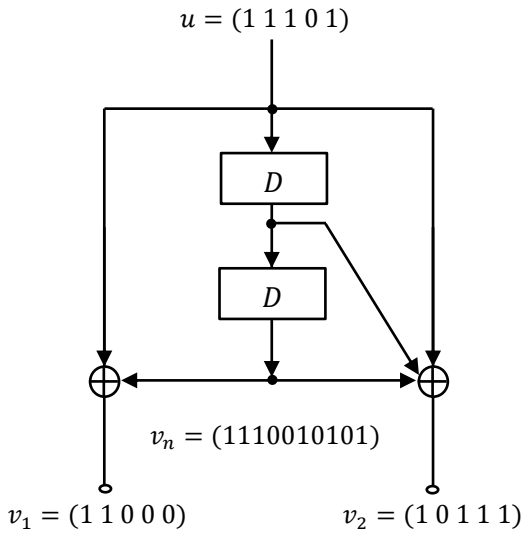

Figure 1.2: A three-tuple (*2,1,2*) convolutional encoder [4]

Usually, the encoder memory m is limited to K bits, which is the number of input bits required for the processing of encoded output bits. $K = k(m-1)$ is otherwise known as the 'constraint length' of the encoder. It determines how complex and powerful the code would be. In simple terms, convolutional codes are denoted by a three-tuple (n, k, K), which corresponds to an encoder for which k input bits generates n output bits and for which the current *n* output bits are linear combinations of the present k input bits and the previous $k \times K$ input bits. [1, 4].

In Figure 1.2., the k/n convolutional encoder has a sequence of u of k-tuples and the coded output is a sequence of v of n-tuples, as represented in (1.1) and (1.2), respectively:

$$\boldsymbol{u}_t = (u_t^1, u_t^2, \dots, u_t^k) \tag{1.1}$$

$$\boldsymbol{v}_t = (v_t^1, v_t^2, \dots, v_t^n) \tag{1.2}$$

In composite forms, these input and output sequences of the convolutional encoder can be written as;

$$\boldsymbol{u} = \left(u_0^1, u_0^2, \dots u_0^k;\ u_1^1, u_1^2, \dots u_1^k;\ u_2^1, u_2^2, \dots u_2^k; \dots\right) \tag{1.3}$$

$$\boldsymbol{v} = (v_0^1, v_0^2, \dots v_0^n;\ v_1^1, v_1^2, \dots v_1^n;\ v_2^1, v_2^2, \dots v_2^n; \dots) \tag{1.4}$$

Again, these can also be represented by (1.5) and (1.6) using the delay elements *D*, as operators;

$$\boldsymbol{u}(D) = (u_0 + Du_1 + D^2u_2 + \cdots) \tag{1.5}$$

$$\boldsymbol{v}(D) = (v_0 + Dv_1 + D^2v_2 + \cdots) \tag{1.6}$$

In representing convolutional codes, the following terms are also involved and accordingly, they are briefly discussed [5]:

Generator Matrix: the generator matrix is used to define a convolutional code. It is regarded as being semi-indefinite because its outputs are semi-indefinite in length, and so it is not an easy way of representing a convolutional code.

Generator Polynomial: for each of the n modulo-2 adders used in convolutional coding, a set of n vectors is specified; such that the connection of the encoder to that modulo-2 adder is indicated by each of the $2k$ dimension vectors. For example, a '0' in the i^{th} position of the vector indicates that the corresponding shift register is not connected while a '1' indicates connection.

Logic Table: this is a table built to show the outputs of the convolutional encoder as well as the states of the encoder for all input sequences present in the shift register.

State Diagram: this is being used to represent the encoding process; as the output of the encoder is determined by the input and the current state of the encoder. The state diagram is simply a graph of the possible states of the encoder and the possible transitions from one state to another.

Tree Diagram: with the tree diagram, the structure of the encoder is shown in the form of a tree with branches to represent the various states and outputs of the coder.

Trellis Diagram: once the number of stages is greater than the constraint length, the tree is observed to repeat itself. A closer observation reveals that all branches emanating from two nodes and also having the same state are identical as they generate identical output sequences. This suggests that, two nodes with the same labels can be merged; doing this

throughout the tree diagram gives rise to a new and more compact diagram which is called the trellis diagram.

1.1.1.2. Decoding of Convolutional Codes

Decoding of forward error correcting (FEC) codes like convolutional codes can be carried out with either of two decision methods: hard decision and soft decision. The input to a hard-decision decoder consists of a single level of the binary bits 0 and 1. The low complexity but high maturity of hard decision decoding makes it widely used in a variety of scenarios. On the other hand, the input to a soft-decision decoder is a multilevel quantization signal. While offering the same coding rate as hard decision, soft-decision provides a higher coding gain, albeit with a greatly increased processing complexity. A hard-decision decoder receives data streams consisting only of the binary digits 0 and 1. Hard-decision decoding will normally be performed based on the algebraic code format. With this decoding mode, statistical characteristics of channel interference in a signal are lost [5].

Soft decision decoding scheme is often realized using Viterbi decoders. Such decoders utilize soft output Viterbi Algorithm (VA) which takes into account the priori probabilities of the input symbols producing a soft output indicating the reliability of the decision. [6]. The VA provides maximum-likelihood decoding for convolutional codes. However, the complexity of the algorithm is proportional to the number of states in the trellis diagram. This means that the complexity of the algorithm increases exponentially with the constraint length of the convolutional code. For higher constraint-length codes, other sub-optimal decoding schemes have been proposed. These include the Fano's sequential algorithm [7], the Stack algorithm [8] and the feedback decoding algorithm [9].

Although VA suffers from a high decoding complexity with long constraint lengths of convolutional codes, this is addressable in practice by applying it to codes with constraint lengths that are less than or equal to nine [1, 5]. In [13], VA is identified to be an optimal maximum-likelihood (ML) procedure for decoding convolutional codes. It can be said, in other words, that the use of VA decoders on the received message enables error correction in the sense of ML [3, 4, 6, 10, 14]. VA, perhaps, remains the most popular decoding algorithm deployed in practice, due to the fact that its computational complexity is reduced by using recursion and because it is an optimal ML decoder [1, 5]. The above form the justification on

which the choice of the VA technique is made for decoding; thus a brief discussion of it is hereby made in the following paragraphs.

The VA can be used to perform convolutional decoding, where every user data in the bit sequence is logically explored [6]. After receiving coded transmitted signals, a typical VA will use the trellis tree to perform branch metric calculation, path metric calculation, the traceback calculation and then, output a decoded bit stream. Meanwhile, calculation of the branch metrics for hard decision decoding is quite different from that of soft-decision decoding, but the major task is to find the path through the trellis which has a minimum distance from a given sequence. In soft-decision decoding, the minimum distance is called Euclidean distance, while it is called Hamming distance in hard-decision decoding [6, 10].

Add-Compare-Select (ACS) is a 3-in-1 procedure for calculating the path metrics. For every encoder state, the three processes are repeated. For the "Add" process; there are always two known states on the previous step which can move to this state and the output bit pairs that correspond to these transitions. To calculate new path metrics, the previous path metrics is added to the corresponding branch metrics, thereby making two paths available and both will end in a given state. To carry out the "compare" and "select" processes; the available path with greater metric is dropped. Because there are two encoder states, we usually have 2 survivor paths at any given time. The difference between two survivor path metrics must be made to be less than or equal to $\delta \log (K-1)$, where δ is the difference between minimum and maximum possible branch metrics [1, 11].

At this point, some survivor paths are left behind; and merging them together after decoding a sufficiently large block of data will make them differ only in their endings and have the common beginning as shown in Figure 1.3. If a continuous stream of data is decoded, and when some part of the path at the beginning of the graph belongs to every survivor path, the decoded bits corresponding to this part can be sent out as output. For quality and reasonable decoding, an important parameter called decoding depth, D is required, which should be made considerably large (usually not less than $5 \times K$). An increase in D increases latency but decreases the probability of a decoding error. Another important parameter is the number of bits sent to the output after each traceback; this can be denoted as N. If N is assumed to have a value of 1, then latency in the decoder is minimal,

but the decoder traces the whole tree every step, which is computationally considered ineffective. Anyway, N is usually equal to D in hardware implementations [10, 12].

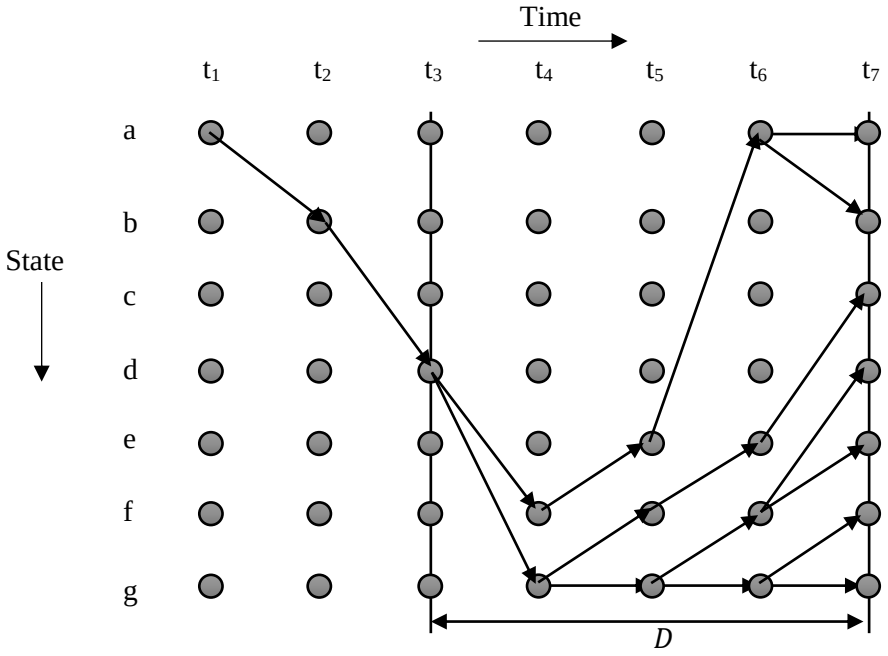

Figure 1.3: Trellis diagram showing survivor paths

Summarily, decoding of convolutional codes can be performed according to the following Steps:

1. Locate the survivor paths for $N + D$ input pairs of bits.
2. Trace back from the end of any survivor paths to the beginning.
3. Send N bits to the output.
4. Find the survivor paths for another N pairs of input bits.
5. Repeat Step 2 to 4 in D times.
6. Stop.

However, under certain channel conditions, the number of errors may be small or nearly equal to zero when the VA is employed in decoding convolutional codes. In such a case, simpler techniques should be sufficient to produce similar results [6, 14]. Accordingly, a new low complexity algorithm for decoding convolutional codes has been proposed by Dany *et*

al. [15]. The approach presented a soft decoding technique, where the VA is applied to identify the error vector rather than the information message. In the scheme, the exhaustive computation of a vast majority of state to state iterations is not necessary. This new system is shown to have achieved a performance close to the optimum, in addition to reduction in complexity.

1.2. MIMO Systems

Over the years, the desire to reliably communicate at higher data rates across wireless communication links has been on the increase. It has since resulted in the need for improved spectral efficiency as an important quality required in the next generation cellular communication systems. A conventional approach to enhance data rates is the use of high order modulation schemes. Doing this, however, has a disadvantage of poor reliability with an increase in the modulation order. That is, at a particular transmit power, high order modulation schemes yield performances that are inferior to that of the lower order modulation schemes. An effective way to achieve reliability is 'diversity', where the transmitter/receiver provides/is provided with independently faded copies of the transmitted signal, with the expectation that at least one of these replicas is received correctly [16]. Multiple-input multiple-output (MIMO) is, thus, a new 'spatial diversity' technique that consists of point-to-point communication links with multiple antennas at both the transmitter and receiver. Goldsmith [2] pointed out that the use of MIMO techniques provides improved performance over diversity systems, where either the transmitter or receiver, but not both, have multiple antennas.

A typical model for a MIMO system is shown in Figure 1.4. It consists of m transmit and n receive antennas and a channel such that each and every antenna receives direct components intended for it and also the indirect components intended for the other antennas. On the assumption of a time-independent, narrowband channel, the direct connection from transmit antenna 1 to receive antenna 1 is specified with h_{11}, and that from transmit antenna 2 to receive antenna 2 is specified with h_{22}, etc. On the other hand, the indirect connection from transmit antenna 1 to receive antenna 2 is identified as cross-component h_{21}, etc [17]. Assuming that m ranges from 1 to N_t and n from 1 to N_r, then a channel matrix $\boldsymbol{H}$ with the dimensions $N_r \times N_t$ is obtained as:

$$\boldsymbol{H} = \begin{bmatrix} h_{11} & h_{12} & h_{13} & \cdots & h_{1m} \\ h_{21} & h_{22} & h_{23} & \cdots & h_{2m} \\ \vdots & \vdots & \vdots & \ddots & \vdots \\ h_{n1} & h_{n2} & h_{n3} & \ldots & h_{nm} \end{bmatrix} \tag{1.7}$$

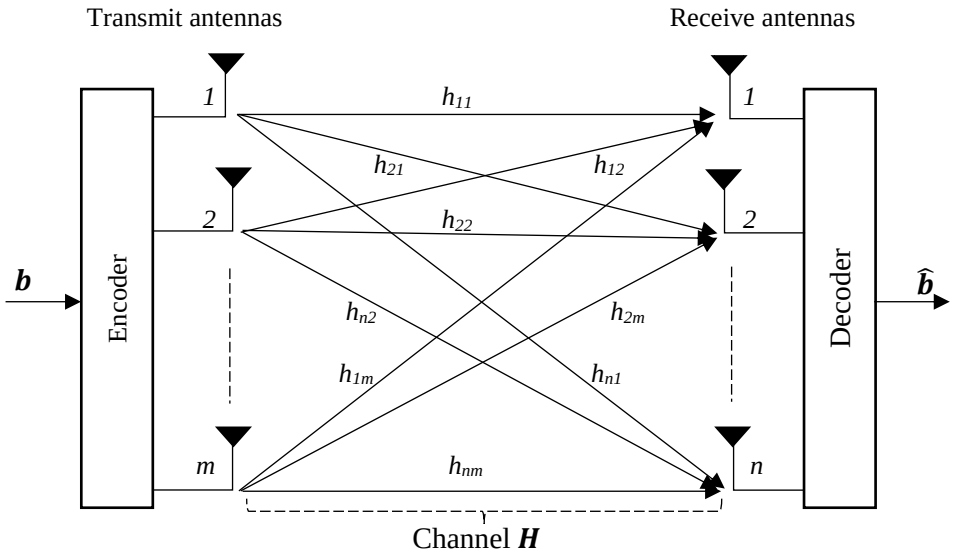

Figure 1.4: General MIMO system model

A transmit vector $\boldsymbol{x}$, which is to be transmitted over the $N_r \times N_t$ wireless channel usually contains an encoded sequence of random and independent information bits $\boldsymbol{b}$, and will experience a N_r-dim additive white Gaussian noise (AWGN), $\boldsymbol{w}$. The transmission through the channel $\boldsymbol{H}$ results in a receive signal vector $\boldsymbol{y}$, which is modelled as:

$$\boldsymbol{y} = \sqrt{\rho}\boldsymbol{H}\boldsymbol{x} + \boldsymbol{w} \tag{1.8}$$

where $\boldsymbol{H}$ and $\boldsymbol{w}$ are complex, distributed as $CN(0, 1)$ and are assumed to be independent and identically distributed (i.i.d.). ρ is the average signal-to-noise ratio (SNR) at each receive antenna and a power constraint of unity is assumed (i.e. $E_{\boldsymbol{x}}[\boldsymbol{x}^H\boldsymbol{x}] = 1$). The received signal is accordingly decoded in order to estimate the transmitted bits as $\widehat{\boldsymbol{b}}$.

In the last decade, MIMO techniques have consistently continued to receive interest from research industries and academia because of its promising high data transmission rate, more channel capacity, and superior error performance. It has therefore become one of the most important models for deployment in the existing and emerging wireless communication

systems [18]. Recent standards such as the Wireless Local Area Network (WLAN), Long Term Evolution (LTE), IEEE 802.11n and the Worldwide Interoperability for Microwave Access (WiMAX) have witnessed the presence and importance of MIMO in their various designs. At present, standards such as LTE-Advanced, WiMAX 802.16m, and 1×EV-DO Rev.C are being worked on with MIMO. It is expected that future standards will continue to use MIMO technologies [16]. It is currently being considered for the IEEE 802.20 and 802.22 standards. IEEE 802.20 standard aims to put in place mobile broadband wireless access specifications internet protocol (IP)-based services, while the IEEE 802.22 standards aim at utilizing the white spaces within the already allocated television (TV) frequency spectrum to construct wireless regional area networks (WRAN).

It is to be noted that synchronisation is a critical aspect for wireless communication. In time-division multiple access (TDMA) systems, data frame and symbol need to be accurately synchronised; in code-division multiple access (CDMA) systems, code-timing need to be performed in asynchronous multi-user detectors; while carrier frequency synchronisation is most important in multi-carrier communication systems. The deployment of MIMO, which has been considered a promising scheme to increase system capacity and link reliability over fading channels, has effectively addressed the synchronisation by implementing space-time coding to utilize diversity sufficiently [1].

In digital communication systems, the objective of signal detection is to retrieve the transmitted signal from the noise corrupted received waveforms. The detection process begins from receiving a transmitted signal, processing it based on the statistical properties of the waveforms received, and ends at making decisions in order to recover the transmitted signal with minimum error probability. It must be added that all these take place at the receiver, and decision making can be hard or soft in nature [19].

The hard detection has to do with making a firm decision at the receiver based on the incoming signal, and provides a single bit of information (1 or 0) to the decoder. When a signal is received, it compares it to a threshold and anything above the threshold is made “1” otherwise it is a “0.” On the other hand, a soft-detection uses additional data bits to provide a finer, more granular indication of the incoming signal. In other words, the decoder not only determines whether the incoming signal is a “1” or a “0” based on the threshold, but also provides a “confidence” factor in the decision [1]. This provides an indication of how far the signal is from the threshold crossing. In practice, these additional “confidence” or

“probability” bits are exploited by the soft-decision decoder, along with an FEC coding algorithms, to provide a net coding gain [16].

As earlier mentioned in sub-section 1.1.1.2., the input to a hard-decision decoder consists of a single level of the binary bits 0 and 1. The low complexity but high maturity of hard decision decoding makes it widely used in a variety of scenarios. On the other hand, the input to a soft-decision decoder is a multilevel quantization signal. While offering the same coding rate as hard decision, soft-decision provides a higher coding gain, albeit with a greatly increased processing complexity. A hard-decision decoder receives data streams consisting only of the binary digits 0 and 1. Hard-decision decoding will normally be performed based on the algebraic code format. With this decoding mode, statistical characteristics of channel interference in a signal are lost [5].

To fully utilize the information in a received waveform and improve the decision accuracy of the decoder, sampling and quantization can be performed for the received signal. When the information is sampled, the decoder provides higher decoding accuracy and therefore greatly improves system performance. When working at the same rate, soft-decision provides a higher net coding gain than hard-decision. However, the soft-decision algorithm is very complex because it must consider the changes in noise probability distribution caused by channel performance deterioration. Fortunately, the rapid development of integrated circuits has made commercial use of soft-decision a reality.

Summarily, the difference between hard and soft decision decoder is that: in hard decision decoding, the received codeword is compared with the all possible codewords and the codeword which gives the minimum Hamming distance is selected, while in Soft decision decoding, the received codeword is compared with the all possible codewords and the codeword which gives the minimum Euclidean distance is selected. Thus the soft decision decoding improves the decision making process by supplying additional reliability information (calculated Euclidean distance or calculated log-likelihood ratio). Because of the techniques involved in soft decision decoding, its combination with FEC schemes like convolution codes helps in recovering data more effectively. We can understand that the soft decision decoders uses all of the information in the process of decision making whereas the hard decision decoders does not fully utilize the information available in the received signal [6].

In MIMO systems, there are a wide variety of algorithms to obtain an estimate of the transmitted message from the received signal, which includes but are not limited to: maximum-likelihood (ML) detection, maximal ratio combining (MRC) detection, minimum mean square error (MMSE), and the log-likelihood (LLR) or soft-output detection [1], [16], [19].

1.3. Transmit Antenna Index Modulations

Without a corresponding increase in transmit power, modulation order or bandwidth, research has shown that MIMO techniques can considerably increase the data rates of wireless communication systems but majorly at the expense of the cost of deploying multiple antennas, space and spacing required for the multiple antennas, synchronization needed for transmit antennas, complexity in multi-dimensional signal processing and inter-channel interference (ICI) at the receiver [20-23]. A number of schemes have since been proposed to address these seeming problems to make sure that the advantages presented by MIMO are fully taken and deployed into the existing and emerging wireless communication systems.

To solve the problem of ICI at the receiver, multiplexing MIMO systems called the Bell Laboratory layered space-time architecture (BLAST) [24] and vertical-BLAST (V-BLAST) [25] were proposed. The V-BLAST scheme separates multiple transmitted spatial data streams and detects them successively using a combination of array processing and interference cancellations. Research results illustrated that better spectral efficiency can be achieved by the V-BLAST algorithm assuming a practical SNR range [25]. The ICI at the receiver can be avoided totally when a block of N_t (number of transmitting antennas) symbols is compressed into a single symbol before transmission so that an algorithm that maps the single symbol to just one of the N_t antennas can be used to retain the information. The receiver detects the antenna number from which the symbol is transmitted after it must have first estimated the symbol itself. Although the task of the receiver is doubled, it is able to retrieve the entire block of N_t symbols by combining both information, and carrying out the inverse of information encoding, while achieving multiplexing gain and avoiding ICI in the MIMO system [26, 27].

It is obvious from literature that the schemes discussed above are able to address some of the numerous challenges of MIMO at inception. In particular, the scheme in [27] employed

the use of parity symbols and when compared with V-BLAST suffered from degradation in spectral efficiency, even though it avoided ICI at the receiver.

Recently, schemes, which we have termed as "transmit antenna index modulation-based schemes" for the purpose of this dissertation, were beginning to spring up in research, and within the shortest possible period, different versions have been proposed. The general idea in them is to use the transmit antenna number as an additional means of transmitting information. This points out that all members of "transmit antenna index modulation-based schemes" are based on the golden idea of the spatial modulation (SM). First among these SM-based or transmit antenna index modulation-based schemes is the conventional SM itself. Others are generalised SM (GSM), space shift keying (SSK) modulation, bi-space shift keying (Bi-SSK) modulation and the quadrature SM (QSM). The following sub-sections are designated to look into the major works that have been done on each and every technique identified to be a member of the 'transmit antenna index modulation-based schemes'.

1.3.1. Conventional Spatial Modulation

Mesleh *et. al.* [28] proposed the pioneer SM, which achieved an increased spectral efficiency compared to V-BLAST, while, at the same time, improved on the achievable error performance as compared to the previous MIMO systems. The SM scheme makes use of the amplitude/phase modulation (APM) present in the conventional MIMO systems in a novel manner, by extending the available two-dimensional plane to a third one. Each symbol was made to represent a constellation point in the two-dimensional signal plane, while a third dimension, known as the spatial dimension is included. At any given time, only one transmit antenna is made to be active and its index is used as an additional source of information, which is added to the transmitted bit stream.

It should be noted that the inactive antennas transmit zero power during each and every transmission. This clearly gives the SM scheme the ability to completely avoid ICI at the receiver. In turn, it results in a relatively low receiver complexity. In addition to this, the ability of SM to operate on one active antenna results in no need for inter-antenna synchronization (IAS) between transmit antennas. It also ensures that only one radio frequency (RF) chain is required at the transmitter. Apart from a relatively high spectral efficiency achieved by SM, it also improves on the error performance achieved by V-

BLAST. With these merits, the SM scheme has therefore been proven to be a good candidate for deployment in wireless communication systems [28-31].

On the other hand, the SM scheme has drawbacks such as: inability to exploit transmit diversity because of its single active transmit antenna [28, 29]; limited spectral efficiency by base-two logarithm of the number of transmit antennas and which can only be increased in proportion of same [29]; and relatively high receiver/hardware complexity. The point is that an optimal performance in error is achieved in SM only with the maximum-likelihood (ML) algorithm at the receiver and this increases its detection complexity linearly with respect to N_t. This is unlike alternative MIMO systems whose complexity increases exponentially with N_t. It, therefore, means that the ML-based SM detector is relatively low in complexity compared to the ML detection of other MIMO systems; but despite this, the complexity of optimal SM detection remains considerably high [28-32]. These drawbacks have actually disallowed the scheme from achieving its full potential. They form the platform on which the SM scheme is being criticized.

An immediate work that attempted to enhance the overall efficiency of SM was reported in [33] as GSM, where a group of transmit antennas are considered as a spatial constellation point and activated simultaneously. However, slight performance degradation of this system as compared with its SM counterpart is reported. Meanwhile, several other works have been done to improve on the above-discussed drawbacks of SM.

1.3.2. Other Transmit Antenna Index Modulation-based Schemes

All other SM-based schemes possess similar advantages to the conventional SM, in addition to making improvements on one or two of its drawbacks. It must be noted that the use of transmit antenna number as an additional means of transmitting information form the basis on which we have grouped them all into the same family of 'transmit antenna index modulation-based schemes'. The previous section has discussed the SM as the pioneer member of the family, with its advantages, as well as drawbacks, clearly stated. In this sub-section, other SM-based schemes (i.e. SSK, Bi-SSK, and QSM) are briefly surveyed.

SSK modulation is a special case of SM that was proposed in [34], where only the spatial domain is exploited to relay information. The elimination of the APM gives SSK some

strengths and advantages over its SM counterpart; such as lowered detection complexity, less stringent transceiver requirements, and simplicity. The Bi-SSK modulation [35], like SSK, employs only spatial domains to relay information. But, unlike SSK, it uses two set of antenna indices that are respectively associated with real and imaginary numbers to carry information at once. It possesses the same benefits as SSK in addition to doubling the transmission rate of SSK.

The QSM scheme, proposed in [36], also has its roots based on conventional SM. It sets out to enhance the overall throughput of conventional SM system, while still retaining almost all its advantages by extending the SM idea to in-phase and quadrature-phase dimensions. This was done by using an extra spatial dimension on the conventional SM. The QSM system activates one or two transmit antennas at a time as spatial constellation points, and utilizes them to carry information, in addition to the APM present in SM, so as to boost the overall spectral efficiency of SM. It, therefore, means that, in QSM, an additional base-two logarithm of the number of transmit antennas bit can be transmitted.

Table 1.1: Advantages and disadvantages of Transmit Antenna Index Modulation-based Schemes

Advantages	- Simple and flexible design of the transceiver - High throughput - Robustness to phase noise - No need for synchronization at the transmitter - Simple receiver design - High and reasonable spectral efficiency - High energy efficiency - Avoidance of ICI at the receiver - No need for IAS between transmit antennas - Only one RF chain in required - Lowered detection complexity
Disadvantages	- High cost of antenna array design - Inability to exploit transmit diversity - Spectral efficiency is limited by logarithm base of transmit antennas - Relatively high receiver/ hardware complexity

In Table 1.1, we give a summary of the advantages and disadvantages of the SM-based schemes which are studied and called Transmit Antenna Index Modulation-based Schemes, in this dissertation. On a general note, research results have shown that each and every member of the transmit antenna index modulation-based family outperforms the previously proposed techniques of MIMO transmissions. This set of schemes formed a major breakthrough in the quest of researchers to overcome the key challenges – such as cost of deploying multiple antennas, spacing for the multiple antennas, synchronization for transmit antennas, complexity in multi-dimensional signal processing, limited spectral efficiency, and ICI at the receiver – encountered in MIMO systems.

1.4. Research Objectives and Motivations

With the aim of further improving the error performances of member of the transmit antenna index modulation-based schemes, the objectives of this research, therefore, are:

i. to detect the received signals from different transmit antenna index modulation-based schemes by using developed soft-output decision-based ML demodulators (i.e. SOMLDs),
ii. to numerically evaluate the error performances of the uniquely formulated SOMLDs on each member of the transmit antenna index modulation-based schemes,
iii. to investigate the computational complexities of the developed/formulated SOMLDs.

The application of the developed demodulators in the next generation wireless communication systems promises to provide users with the same data rates achievable from each and every members of the transmit antenna index modulation-based schemes, in addition to ensuring higher reliability and effective power efficiency. In actualising these, the target is to effectively reduce errors, induced by noise and unreliable channels. This is achieved by employing the FEC techniques for channel coding at the transmission end, and then process the received signals by developed soft-output ML detectors (SOMLDs) coupled with soft-input decoders.

The motivational bases of this research includes the fact that transmit antenna index modulation-based MIMO schemes are able to avoid ICI at the receiver in a novel fashion. This has been well established in the conclusion of the previous section. As such, the schemes do not require any synchronization between the transmit antennas. Furthermore, transmit antenna index modulation-based schemes retain MIMO advantages of high spectral efficiency and reliability without a corresponding increase in transmit power, modulation order or bandwidth. It is also notable that the complexity of multi-dimensional signal processing of MIMO systems is lowered in these schemes and space requirement for the multiple antennas is reduced to a minor challenge. More importantly, only one RF chain is required at the transmitter, thereby resulting in reduced cost of deploying transmit antennas. We are also motivated by the fact that MIMO transmission technique becomes more realizable when transmit antenna index modulation-based schemes are deployed in it. These qualities that have definitely put the schemes at the forefront as reliable candidates of choice in the next generation cellular communication systems.

1.5. Research Contributions

Summarized below are the major contributions of this dissertation:

1. Development of a soft-output ML detector (SOMLD) for SSK modulation scheme (i.e. SSK-SOMLD)
2. Numerical evaluation of the error performance of the formulated SSK-SOMLD detector for coded and uncoded channels.
3. Investigation of the computational complexity of the proposed SSK-SOMLD.
4. Development of a SOMLD for Bi-SSK modulation scheme
5. Numerical evaluation of the error performance of the formulated Bi-SSK-SOMLD detector for coded and uncoded channels.
6. Investigation of the computational complexity of the proposed Bi-SSK-SOMLD.
7. Development of a SOMLD for the QSM modulation scheme
8. Numerical evaluation of the error performance of the formulated QSM-SOMLD detector for coded and uncoded channels.
9. Investigation of the computational complexity of the proposed QSM-SOMLD.

1.6. Contributions to the Literature

1. A. A. Tijani, N. Pillay, H. Xu, "Soft-Output Decision Based Detectors for SSK, Bi-SSK, and QSM Modulations" *International Journal of Communication Systems (IJCS-16-0569)* [under review].

2. A. A. Tijani, N. Pillay, H. Xu, "Soft-Output Detection for Bi-Space Shift Keying Modulation" in *Proceedings of the Southern Africa Telecommunications Network and Applications Conference (SATNAC)*, Sep. 2016 [under review].

1.7. Overview of Dissertation Structure

In the previous sections of Chapter 1, we had a brief look into the digital communication systems, MIMO system structure and its various detection schemes. Discussion was made of convolutional encoder and decoders that are useful in this dissertation. It has also been noted that this entire work is focused on a particular set of MIMO system called "transmit antenna index modulation-based schemes", where only the selected transmit antennas are employed for transmission instead of all available transmit antennas. Our research motivations, as well as target objectives, have been clearly stated while the contributions of our work are itemized in Section 1.5. Section 1.6 stated the contributions we have made to the body of knowledge.

Having discussed the above, the rest of the dissertation is outlined such that in Chapter 2, we present some preliminary background knowledge of SM, which includes; SM transmission process, various SM detection schemes, and performance analyses. We also refreshed our memory of the soft-output detection algorithm for SM that is available in existing literatures. Simulation results are provided to support our discussion at the end of the chapter.

Chapter 3 discusses space shift keying (SSK) and Bi-SSK modulation schemes, while Chapter 4 is dedicated to the QSM scheme. In both chapters, we discuss the models and transmission processes for the respective schemes. Their conventional detection techniques, computational complexities, as well as performance analyses are presented for discussion. Monte Carlo simulation results showing the error performances of the schemes with optimal

ML-detectors also are presented to support the outcome of our investigations in each chapter. These are later compared to the performances obtained for SM in Chapter 2.

In Chapter 5, we propose soft-output ML-based detectors (SOMLD) for SSK and Bi-SSK. Mathematical models for the proposed detectors are derived. Simulation results are thereafter presented to show what the SM-SOMLD is able to achieve, under coded and uncoded channel conditions. Similarly, in Chapter 6, we propose a soft-output ML-based detector for QSM and a clear mathematical model of it is shown. Results from Mote Carlo simulations are used to show the error performances of the QSM-SOMLD in coded and uncoded channels. Finally, Chapter 7 summarizes the achievements of our research and outlines the possible future direction.

Chapter 2

Spatial Modulation

2.1. Introduction

SM is a novel transmission technique that is capable of avoiding ICI as well as inter-antenna synchronization (IAS) in MIMO systems. At an instance of time, it uses an amplitude and or phase modulation (APM) signal constellation together with an index-based active antenna to convey information. Only one antenna is made active in the process thereby reducing the amount of power needed for transmission. This is because zero power is needed by other non-active antennas. SM creates a transmission scenario that is contrary to the case of V-BLAST, where all antennas are active for simultaneous transmission, while it maintains a high data rate by carrying information through both the active antenna and the symbol constellation. In addition to these, the scheme requires only one RF chain at the transmitter [28, 29, 38]. Basically, this chapter serves to provide as an overview of the SM scheme. Further explanations of the SM system model, transmission technique, detection schemes and analytical performance can be found in the succeeding subsections.

2.2. System Model and Transmission of SM

The key idea in SM is to use the index of the transmit antenna as an additional means to convey information. It involves dividing the original information bits, which is meant for transmission, into two blocks. The first part is mapped to a chosen symbol from the APM signal constellation, while the remaining part determines the transmit antenna index that is to be used for transmission. This approach was demonstrated as a simple and flexible transmission mechanism that achieves a high spectral efficiency as well as a relatively low

receiver complexity. It is noteworthy that the type of modulation used in SM determines the number of bits per symbol in one transmission instance. Antenna indexing/selection in SM, therefore, depends on the incoming data stream and should not be confused with the concept of antenna selection in conventional MIMO systems, which has to do with the received signal strength and channel states [39-41]. Figure 2.1 illustrates the system model for SM transmission.

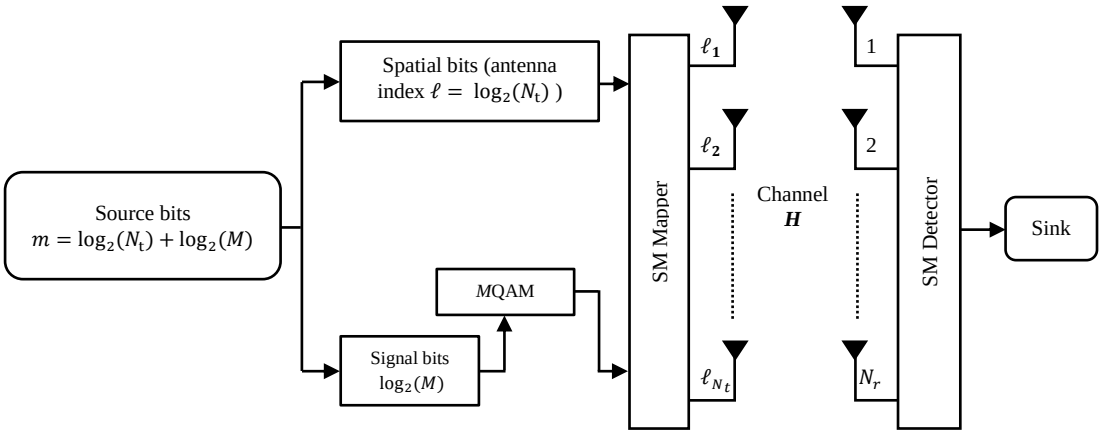

Figure 2.1: System model for SM

In SM, a group of $m = \log_2(N_t) + \log_2(M)$ data bits is transmitted at once. For a MIMO configuration with N_r receive antennas and N_t transmit antennas, using the well-known MQAM modulation, one of the transmit antennas is made active and one of the complex symbol constellation points ($\boldsymbol{\chi}$) is selected by $\log_2(N_t)$ and $\log_2(M)$ bits, respectively. That is, the vector of the m data bits is grouped and mapped to form a constellation vector $\boldsymbol{x}_{q\ell}$ of size $N_t \times 1$, where q and ℓ represent the selected signal constellation and active transmit antenna, respectively, and written as:

$$\boldsymbol{x}_{q\ell} \triangleq [\,0 \ldots \underbrace{\boldsymbol{x}_q}_{\ell^{th}\ position} \ldots 0\,]^T \tag{2.1}$$

where $q \in [1:M]$ and $\ell \in [1:N_t]$, such that only the ℓ^{th} number of the resulting vector is non-zero.

The ℓ^{th} antenna, therefore, transmits the selected complex symbol constellation. The received signal from the transmission of an M-ary symbol, $\boldsymbol{x}_q$, on the ℓ^{th} antenna over a wireless MIMO channel $\boldsymbol{H}$, in the presence of AWGN $\boldsymbol{w}$, is given in [28] as:

$$\boldsymbol{y} = \sqrt{\rho}\boldsymbol{H}\boldsymbol{x}_{q\ell} + \boldsymbol{w} \tag{2.2}$$

where $\boldsymbol{H}$ and $\boldsymbol{w}$ are complex and assumed to be i.i.d as $CN(\mu = 0, \sigma^2 = 1)$. ρ is the average SNR at each receive antenna and $\boldsymbol{x}_{q\ell}$ represents the chosen complex M-ary symbol $\boldsymbol{x}_q$, transmitted via the ℓ^{th} antenna.

It is to be noted that the transmit antenna number ℓ, used at a time, may change at the next time of transmission, but at a given time, only one transmit antenna is active [28].

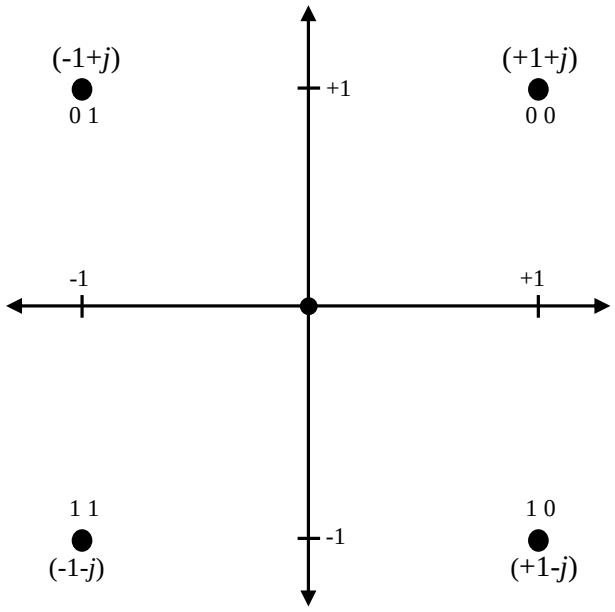

Figure 2.2: Constellation diagram for 4QAM with Gray coding

Table 2.1: Example of the grouping and mapping processes in SM

Input Bits ($b_3b_2b_1b_0$)	**Symbol bits** (b_3b_2)	**Symbol Number** (q)	**Symbol** x_q	**Antenna bits** (b_1b_0)	**Antenna Number** (ℓ)	**SM signal vector** $\boldsymbol{x}_{\ell q}$
[1 1 0 0]	1 1	4	-1-j	0 0	1	[-1-j 0 0 0]^T
[1 0 0 1]	1 0	3	+1-j	0 1	2	[0 +1-j 0 0]^T
[0 1 1 0]	0 1	2	-1+j	1 0	3	[0 0 -1+j 0]^T
[1 0 1 1]	1 0	3	+1-j	1 1	4	[0 0 0 +1-j]^T
[0 0 1 0]	0 0	1	+1+j	1 0	3	[0 0 +1+j 0]^T

An example of the grouping and mapping processes in SM is tabulated in Table 2.1, where we assume that 4QAM complex symbols (i.e. M = 4) and 4 transmit antennas (i.e. N_t = 4) are used for transmission. As earlier discussed, a total of $\log_2(N_t)$ + $\log_2(M)$ information bits are transmitted in SM. In this example, 4 bits (i.e. $b_3b_2b_1b_0$) will be transmitted because $\log_2(N_t)$ = 2 and $\log_2(M)$ = 2. The mapping rule therefore stipulates that $\log_2(M)$ group (i.e. b_3b_2) is mapped to select one of the 4 symbols of 4QAM and $\log_2(N_t)$ group (i.e. b_1b_0) selects only one of the 4 transmit antennas. In Figure 2.2., the constellation diagram showing the symbols $\boldsymbol{x}_q$ for 4QAM in the example is given.

2.3. SM Detection Schemes

In literature, a good number of algorithms have been proposed for the detection of SM signals. In this section, we survey the notable ones. Later, three of these detectors, which are important to the context of this dissertation, are presented for more elaborate discussion in Sub-sections 2.3.1, 2.3.2, and 2.3.3, respectively.

Mesleh *et al.* [28] proposed the SM scheme and based its detection on the iterative-maximum ratio combining (*i*-MRC) algorithm. The detector estimates the active transmit antenna index by iteratively computing the product of the channel gain and received signal vectors. The estimated active transmit antenna index is then used to estimate the modulated symbol. However, the *i*-MRC-based detection for SM was seen in [30] to be sub-optimal and applicable only to constrained channels. On this note, SM optimal detection (SM-OD) scheme was proposed. The new detector which is based on the ML detection principle, performs a joint detection of the active transmit antenna index and transmit symbol. SM-OD is shown to achieve a better error performance compared to the *i*-MRC, as well as the MIMO V-BLAST architecture [30].

In addition, SM-OD possesses a reduced computational complexity, which increases linearly with respect to N_t, N_r and the modulation order M, compared to ML-based detectors for other spatial multiplexing MIMO schemes. Despite this, its computational complexity would still be considered relatively high, when high spectral efficiencies (i.e. MN_t is large) and diversity gains are required (i.e. N_r is large) [30]. A modified sub-optimal SM detector was proposed in [42], and was termed ‘normalized maximum ratio combining (NMRC)’. As the name suggests, the detector first normalizes each column of the channel by its Frobenius

and then estimates the active transmit antenna index before the MRC-based algorithm is finally applied to obtain the symbol estimate. NMRC advantage lies in its application to unconstrained/conventional channels, as compared to the *i*-MRC.

In [30], the sub-optimal detectors (i.e. *i*-MRC and NMRC) are confirmed to be inadequate in providing a good performance-complexity trade-off. Note also that the computational complexity of SM-OD is still being considered relatively high. Therefore, developing novel low-complexity detection schemes for SM formed the primary focus of recent literature works.

Younis *et al.* [43], [44], presented three sphere decoding (SD) algorithms for low-complexity SM detection. The detectors are based on three search structures referred to as receiver-centric (Rx-SD) [43], transmitter-centric (Tx-SD) [44] and combined-SD (C-SD) [44], respectively. They all show significant reduction in receiver complexity, while achieving system error performances which closely match that of SM-OD. We note that these detectors reduce transmit/receiver search spaces before applying the ML principle. Thus, Rx-SD reduces the receiver search-space, Tx-SD reduces the transmit search-space and C-SD reduces both the receiver and transmitter search-spaces [44]. It was demonstrated that no specific SD detector is superior to others: rather, the MIMO configuration employed in the SM system determines the optimal SD algorithm for a detection process. Rx-SD therefore was shown to be suitable for SM systems with large N_r; Tx-SD can appropriately be deployed for use when either or both N_t and M are large, while C-SD is applicable when either N_r is low or M is high.

A novel low-complexity detection that combines the operations of the sub-optimal and optimal SM detectors was presented in [31] by Naidoo *et al.* This was called a multi-stage (MS) detection scheme for SM. The detector inherits the desirable characteristics of sub-optimal detectors to obtain N_s most probable estimates of the active transmit antenna index, where $N_s < N_t$, thus reducing the search-space from MN_t to MN_s. It further employs the optimal SM detector to search over the reduced space to obtain the final estimates of the active transmit antenna index and transmit symbol. This detector achieves a substantial reduction in receiver complexity for signal constellations with large modulation orders (i.e. $M > 16$), while closely matching the performance of SM-OD.

In [45], Xu proposed a simplified ML-based detection scheme for *M*QAM SM. In contrast to the conventional SM-OD, which searches over all possible MN_t pairs for the active transmit antenna index and transmit symbol estimate, the proposed scheme searches through a partitioned signal sets for the ML estimates, starting at the most probable signal set. This scheme is shown to achieve near ML-performance at significantly reduced, complexity relative to the conventional SM-OD. In addition, this idea is extended to MS detection [31] and a further reduction in receiver complexity was demonstrated. In the same vein, a signal vector based detection (SVD) scheme [46], searches for the smallest angle between the channel gain vectors and the received signal vector in order to obtain the estimate of the active transmit antenna index. The estimate of the transmitted symbol is then obtained by applying the ML detection principle.

In addition, Wang *et al.* [46] noted that the SVD scheme is able to achieve near-ML performance, while significantly reducing receiver complexity, such that the receiver complexity is independent of the modulation order. However, Pillay *et al.*, in [47], demonstrated that the performance of the SVD scheme is unable to match that of the optimal SM-OD, especially for moderate to high SNR values. A list of variant SVD scheme was, therefore, proposed in [48]. The List SVD selects a list of candidate transmit antennae by searching for L smallest angles between the channel gain vectors and received signal vector. ML detection principle is thereafter applied to this list of candidate antennae to obtain the final estimates of the active transmit antenna index and transmit symbol. List SVD has been shown to outperform the SVD scheme, while approaching near-ML performance. However, the improved performance is achieved at the expense of an increased complexity relative to SVD scheme.

The complexity of the ML-based detector can become independent of the modulation order as long as a square-QAM or a rectangular-QAM signal constellation is employed. This was proposed and demonstrated by Rajashekar *et al*. in [49]. In addition to this, two novel SD detectors were presented, and are shown to achieve the optimal performance of SM-OD, while imposing a lower computational complexity compared to existing SD detectors and SM-OD. The authors concluded that SD detectors only become essential for low-complexity SM detection when N_t is large and not necessarily when M is large.

A low-complexity SM detection scheme that separately detects the active transmit antenna index and transmit symbol was proposed in [50]. However, as experienced in the

sub-optimal detector, decoupling the estimation processes for active transmit antenna index and transmitted symbol can result in a substantial performance loss since both fade together. The proposed scheme is, therefore, able to achieve near-ML performance by taking into account the correlation between the transmit antenna index and transmit symbol. Although the receiver complexity is reduced relative to the optimal SM-OD, it remains a function of the modulation order and therefore imposes high complexity when large signal constellations are used.

To further reduce receiver complexity, Tang *et al.* [51] proposed a distance-based ordered detection (DBD) scheme for SM system. The key idea is to first equalize the symbol from each transmit antenna element in the antenna array and then use the output of the equalizer to determine the corresponding transmit symbol estimate. The estimates are compared with the received signal vector and the closest is used to jointly determine the final estimates for active transmit antenna index and transmit symbol. Contrary to the SM-OD, which performs the ML search over M constellation points for each transmit antenna element, in DBD there is only a single constellation point for each antenna element. This reduces the ML search-space from MN_t to N_t and consequently, the receiver complexity is significantly reduced.

Finally, a soft output ML detection (SOMLD) scheme was formulated for SM systems in [37]. In coded channels, the SOMLD was shown to outperform the hard decision ML detector (HDMLD) for SM or SM-OD. However, the proposed soft-output ML detector results in high computational complexity due to the application of ML principle. Motivated by the need to reduce the computational complexity of the soft-output detection for SM, the authors of [51] presented a soft-output low-complexity detector, which employs a distance-based ordered detection algorithm. The low-complexity soft-output detector is shown to achieve near-ML performance while achieving a substantial reduction in computational complexity.

On this note, three of the above discussed SM detection algorithms are selected for further background discussion, due to their importance to the context of this dissertation. These are sub-optimal (*i*-MRC) detection for SM [28], optimal ML detection for SM (SM-OD) [30] and the soft-output ML detection for SM (SOMLD-SM) [37].

2.3.1. Sub-Optimal Detection

The MRC-based sub-optimal detection, is used to demodulate SM received signals in [28]. We note that MRC scheme is traditionally being used for SIMO channels with a diversity of L^{th} order. Taking a brief look into this, $m = \log_2(M)$ bits are mapped to select a symbol $\boldsymbol{x}_q$, from the APM constellation points. The channel output is given by [28]:

$$\boldsymbol{y} = \sqrt{\rho}\boldsymbol{h}_\ell \boldsymbol{x}_{q\ell} + \boldsymbol{w} \tag{2.3}$$

where $\boldsymbol{h}_\ell$ is the ℓ^{th} column of the $\boldsymbol{H}$ matrix that represents the wireless channel, and the symbol is estimated by the rule [29]:

$$\boldsymbol{x}_{\hat{q}} = \arg\max_{\boldsymbol{x}_q} p_Y(\boldsymbol{y} \,|\, \boldsymbol{x}_{q\ell}, \boldsymbol{H}) \tag{2.4}$$

where

$$p_Y(\boldsymbol{y} \,|\boldsymbol{x}_q, \boldsymbol{H}) = \pi^{-N_r} \exp\left(-\left\|\boldsymbol{y} - \sqrt{\rho}\boldsymbol{h}_\ell \boldsymbol{x}_{q\ell}\right\|_F^2\right) \tag{2.5}$$

The MRC rule is therefore given by [28]:

$$\boldsymbol{x}_{\hat{q}} = \arg\max_{\boldsymbol{x}_q} \sqrt{\rho}\left[\Re\left\{\left(\boldsymbol{h}_\ell \boldsymbol{x}_{q\ell}\right)^H \boldsymbol{y}\right\} - \frac{1}{2}\left\|\boldsymbol{h}_\ell \boldsymbol{x}_{q\ell}\right\|_F^2\right] \tag{2.6}$$

The received signal of SM transmission is then equalized to yield [28]:

$$\boldsymbol{z}_\ell = \frac{\boldsymbol{h}_\ell^H \boldsymbol{y}}{\|\boldsymbol{h}_\ell\|_F^2} \tag{2.7}$$

such that the transmit antenna and transmitted symbol index, respectively, are estimated with MRC as $\hat{\ell}$ and $\hat{q}$;

$$\hat{\ell} = \arg\max_{\ell} (\boldsymbol{z}_\ell) \tag{2.8}$$

$$\hat{q} = S(\boldsymbol{z}_{\ell}) \tag{2.9}$$

where S is the constellation demodulator or the slicing function [28].

De-mapping is done in a similar one-to-one manner of the mapper by taking $\hat{\ell}$ and $\hat{q}$ as inputs of the de-mapper in order to obtain an estimate of the transmitted bits. However, the MRC based detector suffers from some restrictions, which does not allow the SM scheme to attain the expected full potential proposed for it. It was pointed out in [34, 52] that substituting (2.3) for $\boldsymbol{y}$ in (2.8) reduces $\boldsymbol{z}_{\ell}$ to $\frac{\sqrt{\rho}|\boldsymbol{h}_{\ell}^{H}\boldsymbol{h}_{\ell}\boldsymbol{x}_{q}|}{\|\boldsymbol{h}_{\ell}\|_{F}^{2}}$. Meanwhile, $\frac{|\boldsymbol{h}_{\ell}^{H}\boldsymbol{h}_{\ell}|}{\|\boldsymbol{h}_{\ell}\|_{F}^{2}}$ should be less than unity if the correct antenna index must be detected, but the MRC based detector provided no means to ensure this; and as such, if a conventional MIMO channel is assumed, the simulation results of the MRC detection method in [28] could not be constructed.

2.3.2. Spatial Modulation with Optimal Detection (SM-OD)

To solve the problem encountered in the sub-optimal MRC-based detection of SM, we have to ensure that $\frac{|\boldsymbol{h}_{\ell}^{\mathrm{H}}\boldsymbol{h}_{\ell}|}{\|\boldsymbol{h}_{\ell}\|_{F}^{2}}$ is less than unity. A simple way to do this is to normalize the channels before transmission [52]; that is, $\|\boldsymbol{h}_{\ell}\|_{F}^{2}$ is made constant for all ℓ. Consequently, a new optimal detector based on ML was proposed to jointly detect the transmitting antenna and the symbol using the ML principles [30], [52].

The probability density function (PDF) of $\boldsymbol{y}$, given by (2.10) is conditioned on $\boldsymbol{x}_{q\ell}$ and $\boldsymbol{H}$ as [52]:

$$p_{Y}(\boldsymbol{y}\,|\boldsymbol{x}_{q\ell}, \boldsymbol{H}) = \pi^{-N_r}\exp\left(-\left\|\boldsymbol{y} - \sqrt{\rho}\;\boldsymbol{h}\boldsymbol{x}_{q\ell}\right\|_{F}^{2}\right) \tag{2.10}$$

Therefore, $\hat{l}$ and $\hat{q}$ are estimated as [30]:

$$[\,\hat{\ell}\,,\hat{q}\,] = \arg\max_{\ell,q} p_{Y}(\boldsymbol{y}\;|\,\boldsymbol{x}_{q\ell}, \boldsymbol{H}) \tag{2.11}$$

$$[\,\hat{\ell}\,,\hat{q}\,] = \arg\min_{\ell,q}\left\|\boldsymbol{y} - \sqrt{\rho}\,(\,\boldsymbol{h}_{\ell}\,\boldsymbol{x}_{q})\right\|_{F}^{2} \tag{2.12}$$

Suppose that $\boldsymbol{g}_{\ell q} = \boldsymbol{h}_{\ell}\, \boldsymbol{x}_{q}$ such that $1 \leq \ell \leq N_t$ and$1 \leq q \leq M$, the optimal detector for SM scheme can be modelled as [30]:

$$[\,\hat{\ell}\,,\hat{q}\,] = \arg\min_{\ell,q} \sqrt{\rho}\,\left\|\boldsymbol{g}_{\ell q}\right\|_F^2 - 2\Re\{\boldsymbol{y}^{\mathrm{H}}\boldsymbol{g}_{\ell q}\} \tag{2.13}$$

SM requires that the number of transmit antennas be a power of 2. Consequently, the logarithmic increase in spectral efficiency unnecessarily requires a large number of antennas. This constraint was noted in [33], and overcome by the introduction of generalized SM (GSM). GSM, like the SM, maps the block of source information bits to a constellation symbol and a spatial symbol. The difference is that; instead of activating only one antenna (as in the case of SM), a combination (or pair) of transmit antenna is activated to transmit the same constellation symbol simultaneously. Therefore, the overall spectral efficiency of SM is increased by base-two logarithm of the number of antenna pairs. GSM scheme would obtain the same spectral efficiency as SM while reducing the number of transmit antennas needed in SM by more than half. Complete avoidance of ICI at the receiver is maintained in GSM by transmitting the same data symbol from more than one antenna at once; hence, the major advantage of SM is retained. However, ISI must be avoided by synchronizing the activated transmit antennas [33]

2.3.3. Soft-Output Detection for SM

Soft-decision technology for SM is developed in [51], [37], where the authors saw a room to improve the performances of SM receivers and thus derived a soft-output maximum-likelihood (ML) detector to recover the signal (data bit and antenna index) by soft decision approach, when coding is employed. The developed soft-output detector, which practically marries SM to coded systems, computes the a-posteriori log-likelihood ratio (LLR) for the a^{th} antenna bit and b^{th} modulated bit on the assumption of N_t transmit antennas and *M*-ary data input.

From (2.2), the estimate of the a^{th}antenna bit is expressed as [37]:

$$LLR(\ell^a) = \log\left[\frac{\sum_{\hat{\ell} \in \ell_1^a, \hat{\boldsymbol{x}} \in \boldsymbol{x}} \exp\left(\frac{-\left\|\boldsymbol{y} - \boldsymbol{h}_\ell \boldsymbol{x}_{q\ell}\right\|_F^2}{2\sigma^2}\right)}{\sum_{\hat{\ell} \in \ell_0^a, \hat{\boldsymbol{x}} \in \boldsymbol{x}} \exp\left(\frac{-\left\|\boldsymbol{y} - \boldsymbol{h}_\ell \boldsymbol{x}_{q\ell}\right\|_F^2}{2\sigma^2}\right)}\right] \tag{2.14}$$

In the same vein, the b^{th} symbol bit is estimated as:

$$LLR(\boldsymbol{x}^b) = \log\left[\frac{\sum_{\hat{\boldsymbol{x}} \in \boldsymbol{x}_1^b, \hat{\ell} \in \ell} \exp\left(\frac{-\left\|\boldsymbol{y} - \boldsymbol{h}_\ell \boldsymbol{x}_{q\ell}\right\|_F^2}{2\sigma^2}\right)}{\sum_{\hat{\boldsymbol{x}} \in \boldsymbol{x}_0^b, \hat{\ell} \in \ell} \exp\left(\frac{-\left\|\boldsymbol{y} - \boldsymbol{h}_\ell \boldsymbol{x}_{q\ell}\right\|_F^2}{2\sigma^2}\right)}\right] \tag{2.15}$$

where σ^2 is the variance of the AWGN while ℓ_1^a and ℓ_0^a are the vectors of the antenna indices with '1' and '0' at the a^{th} antenna bit, respectively, while $x_1^b$and x_0^b are the vectors of the data symbols with '1' and '0' at the b^{th} symbol bit, respectively.

2.4. Analytical Performance Bounds for SM

An analytical union bounding technique was employed to derive the performance analysis for *M*QAM SM with sub-optimal detection [28] in Rayleigh fading channels, as presented by Mesleh *et al.* [29], [53]. The same approach was adopted to derive the performance analysis for BPSK SM-OD by Jeganathan *et al.* in [52]. However, as against the assumption of joint detection in [29], [52] and [53], the estimation of the transmit antenna index and transmit symbol are assumed by Naidoo *et al.* [31] to be independent processes. It was believed that this assumption yields the best achievable performance (i.e. lower bound performance).

The approach presented in [29], [53] was followed in [31] to derive a performance bound for *M*QAM SM-OD, where the overall average bit error probability (BEP) is bounded as:

$$P_e = 1 - (1 - P_a)(1 - P_d) \tag{2.16}$$

In (2.16), P_a and P_d denote the bit error probability due to the incorrect estimation of the transmit antenna index and transmit symbol, respectively.

Then, the analytical BER of transmitted symbol estimation was done based on the assumption that the active transmit antenna index is perfectly detected. Consequently, the authors approximate P_d as:

$$P_d \cong \frac{SER(\rho)}{m} \tag{2.17}$$

where $m = \log_2 M$ and $SER(\rho)$ is the symbol error rate (SER) of MQAM with MRC detection over i.i.d Rayleigh flat fading channel and is given in [54] as:

$$SER(\rho) = \frac{a}{c}\left\{\frac{1}{2}\left(\frac{2}{b\rho+2}\right)^{N_r} - \frac{a}{2}\left(\frac{1}{b\rho+1}\right)^{N_r} + (1-a)\sum_{i=1}^{c-1}\frac{1}{2}\left(\frac{S_i}{b\rho+S_i}\right)^{N_r} + \sum_{i=1}^{2c-1}\frac{1}{2}\left(\frac{S_i}{b\rho+S_i}\right)^{N_r}\right\} \tag{2.18}$$

where c is the number of simulation (c>10, and the choice of c is explained in [31]), such that $\theta_i = \frac{i\pi}{4c}$, $S_i = 2\sin^2\theta_i$, $a = \left(1 - \frac{1}{\sqrt{M}}\right)$ and $b = \frac{3}{M-1}$.

To derive the analytical BER for the estimated transmit antenna index, P_a was formulated using the union bound technique of [1] in a similar way to [30], [34]. Therefore, P_a is bounded in [31], as:

$$P_a \leq \sum_{q=1}^{M}\sum_{r=1}^{N_t}\sum_{\hat{r}=1}^{N_t}\frac{N_{SM}(r,\hat{r})\gamma_{SM}^{N_r}\sum_{k=0}^{N_r-1}\binom{N_r-1+k}{k}[1-\gamma_{SM}]^2}{MN_t} \tag{2.19}$$

where $\gamma_{SM} = \frac{1}{2}\left(1 - \sqrt{\frac{\sigma_{SM}^2}{1+\sigma_{SM}^2}}\right)$, $\sigma_{SM}^2 = \frac{\rho(|\boldsymbol{x}_q|^2+|\boldsymbol{x}_{\hat{q}}|^2)}{4}$, while the number of bits in error between the transmit antenna index r and the estimated transmit antenna index $\hat{r}$ is represented as $N_{SM}(r,\hat{r})$.

2.5. Computational Complexity of SM-OD Receiver

The number of complex multiplications required in the detection process was used as a metric for determining the computational complexities (CC) of SM-OD receiver. This was written in [52] as:

$$CC_{\mathrm{SM-OD}} = 2N_r N_t + N_t M + M \tag{2.20}$$

where N_r, N_t, M are number of receive antennas, number of transmit antennas, and modulation order, respectively.

2.6. Simulation Results and Discussion

In this section, simulation results for SM scheme are presented. We validate the results with the performance analysis presented in Section 2.4. Furthermore, an attempt was made to compare SM scheme to V-BLAST architecture. In all our simulations, we assume flat-fading MIMO channels with i.i.d. entries distributed according to *CN*(0,1), in the presence of AWGN. We perform Monte Carlo simulations that are terminated at a bit error rate (BER) of 10^{-6}. The results presented herein are therefore in terms of the BER as a function of the SNR. Simulations have been carried out using MATLAB and the parameters used are shown in Table 2.2.

Table 2.2: Simulation parameters for SM and V-BLAST systems

	SM				**V-BLAST**
Antenna configuration ($N_t \times N_r$)	4×4	16×4	2×4	4×4	4×4
Modulations order	4QAM	4QAM	BPSK	16QAM	4QAM
Simulation Tool used	MATLAB				
Iterations	1,000,000				
Spectral efficiency	4 b/s/Hz	6 b/s/Hz	2 b/s/Hz	6 b/s/Hz	8 b/s/Hz
Channel model	Uncoded Rayleigh, coded Rayleigh with $1/2$ rate convolutional encoder (constraint length 9 $[g_1, g_2] = [(561)_o, (753)_o]$)				
Decoding algorithms	HDMLD, SOMLD (using the Viterbi)				
Target BER	10^{-6}	10^{-6}	10^{-6}	10^{-6}	10^{-6}

Before the discussion of results obtained, it is equally important to give an elaborate picture of the steps/processes that have been followed in arriving at the results for SM schemes; hence a generic flowchart of the MATLAB processes involved in our simulations is hereby presented.

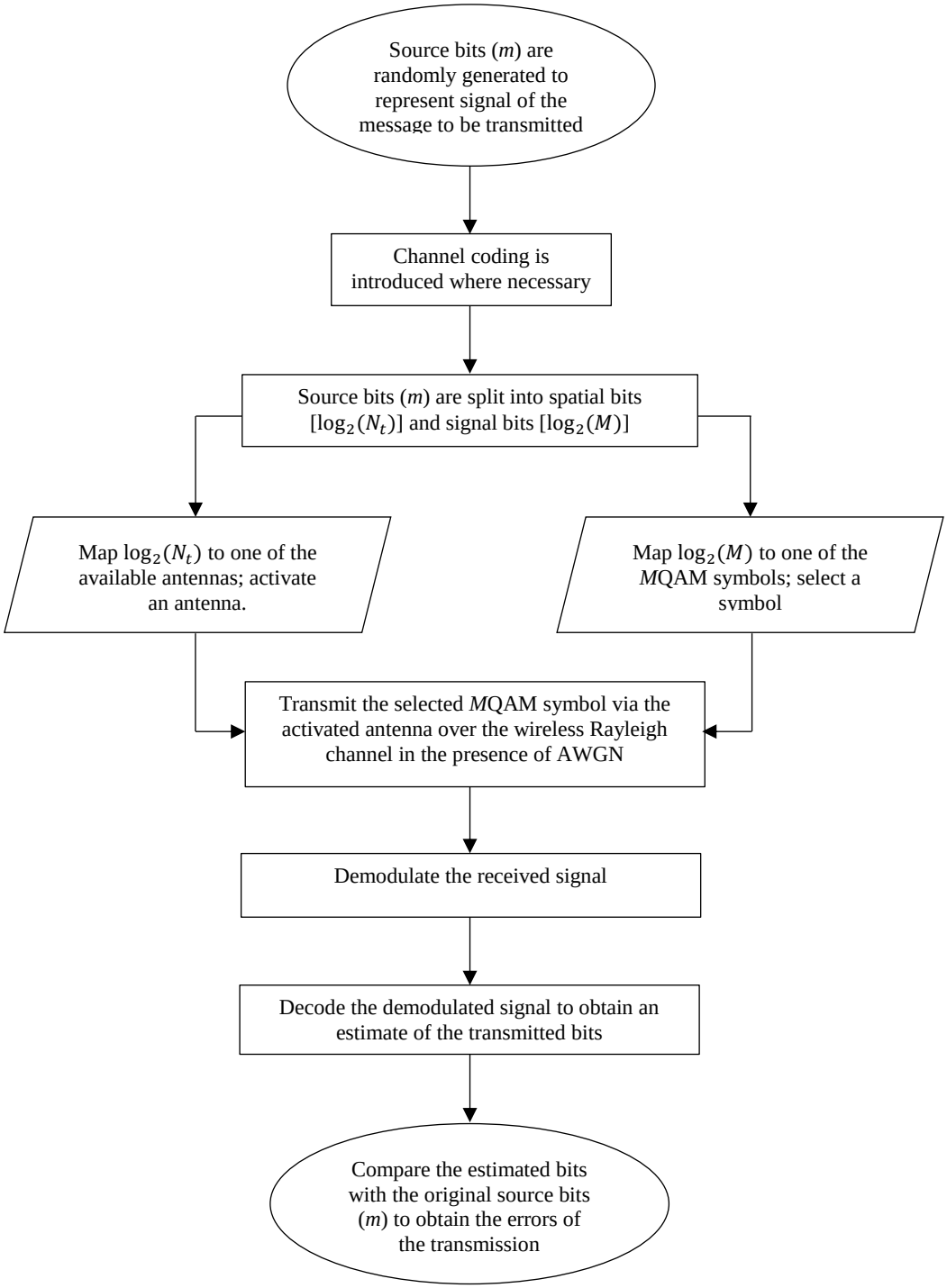

Figure 2.3: A flowchart depicting the MATLAB simulation process of SM system

In Figure 2.4, the results shown are the error performances of two different SM systems configured with N_t = 4 and N_t = 16, while M = 4 and N_r = 4 are kept constant in both setups. This demonstrates the effect of increase in the number of transmit antenna in SM system. Our simulation results, which has been validated with the theoretical analysis of Section 2.4, show that spectral efficiency of SM systems can be enhanced by increasing N_t. For example, the 16×4 4QAM system has a spectral efficiency of 6 b/s/Hz while the 4×4 4QAM system achieves 4 b/s/Hz. We note also that achieving higher spectral efficiency in SM results in hardware complexity at the transmitter. Nevertheless, the 4 bits SM system has a better performance in terms of BER compared to the 6 bits SM. For instance, at a BER of 10^{-6}, the 4 bits SM system has an SNR gain of approximately 1.9 dB over its 6 bits SM counterpart. In other words, it can be said that the low spectral efficient system is more energy efficient.

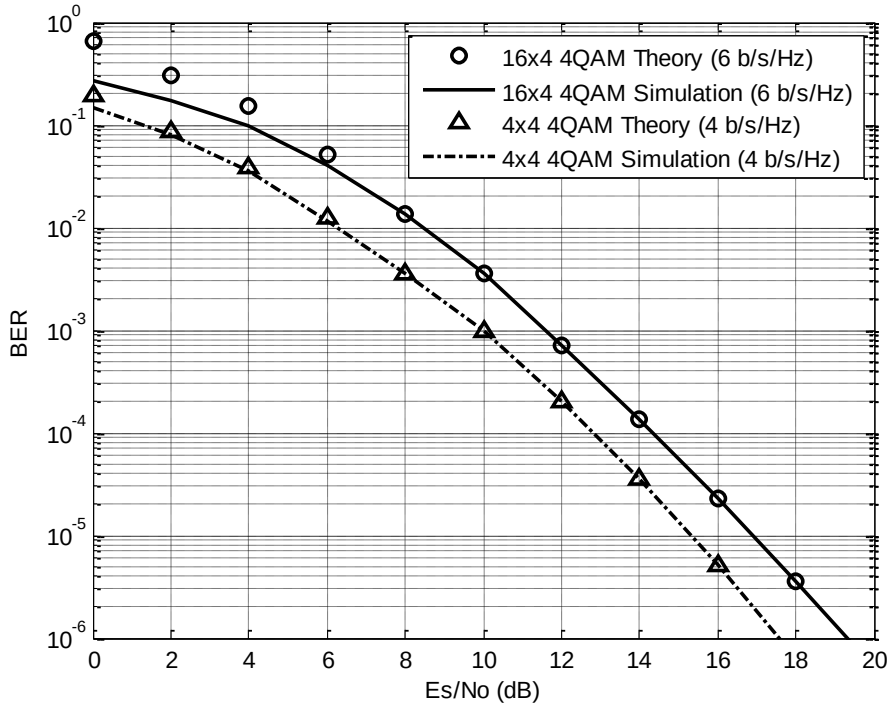

Figure 2.4: BER performance of SM (simulation and theory) for 4 b/s/Hz and 6 b/s/Hz (M = 4, N_r = 4)

Figure 2.5, shows a 4×4 4QAM V-BLAST system with spectral efficiency of 8 b/s/Hz, 16×4 16QAM SM with spectral efficiency of 8 b/s/Hz and a 4×4 4QAM SM with spectral efficiency of 4 b/s/Hz. Considering systems with 4×4 antenna configurations, we observe

that the SM-OD has a major SNR gain over the MMSE V-BLAST system. It is shown that, at a BER of 10^{-6}, an impressive performance improvement of approximately 14.0 dB can be achieved in SM-OD over the V-BLAST system. Meanwhile, it is worthy of note that the V-BLAST system transmitted twice the data of the SM system under this transceiver configurations.

Figure 2.5 still compares the SM to V-BLAST system under the same spectral efficiency of 8 b/s/Hz. We realised that the SM still performs better. At 10^{-6} BER, approximately 7.0 dB SNR gain is achieved over V-BLAST, even though the systems' performances are closely matching at lower SNR until around 16.0 dB. Meanwhile, it is evident that SM shows a significant reduction in receiver complexity compared to V-BLAST. To the SM advantage, only one RF chain is required and one antenna is active at any transmission time, thereby suggesting no need for transmit antenna synchronization.

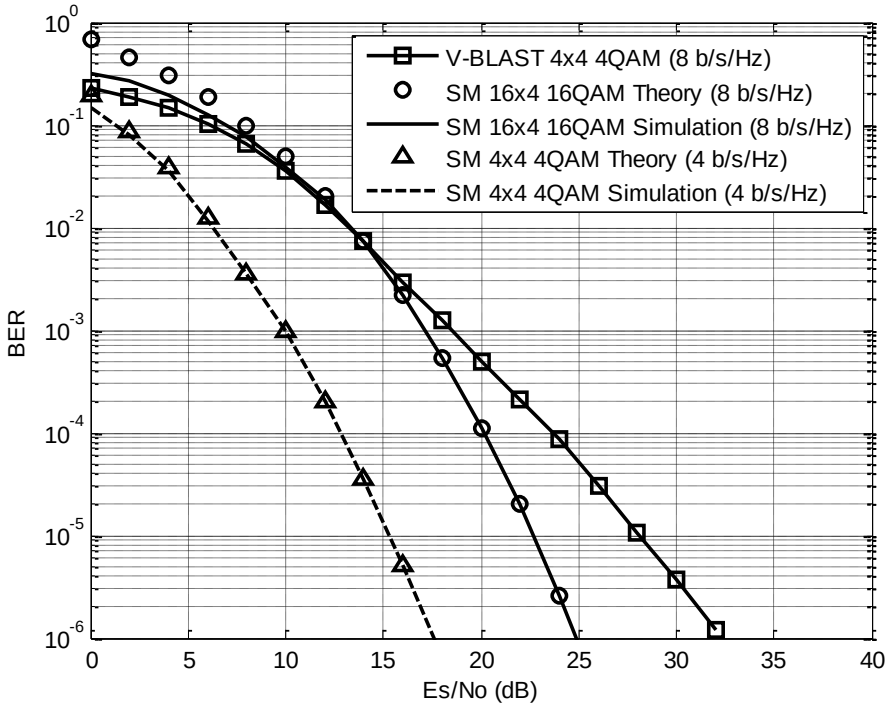

Figure 2.5: Comparison of BER performances of SM and V-BLAST systems for 4 b/s/Hz and 8 b/s/Hz

In Figure 2.6, we employ different transmit antenna number together with *M*-ary symbol constellation to achieve different spectral efficiencies in SM, while the number of receive antenna is kept constant at N_r = 4. From the figure, we observe that higher spectral efficiency can be achieve by increasing either N_t or *M*. It can also be inferred that the higher the spectral efficiency of SM systems, the lower it error performance becomes. However, a special case to be noted is that of the 4×4 16QAM and 16×4 4QAM systems both of which has the same spectral efficiencies but different error performances. We observe that the 16×4 4QAM SM system has a superior error performance of approximately 3.5 dB over the 4×4 16QAM. This is however achieved at the expense of increased number of transmit antennas from $N_t = 4$ to $N_t = 16$.

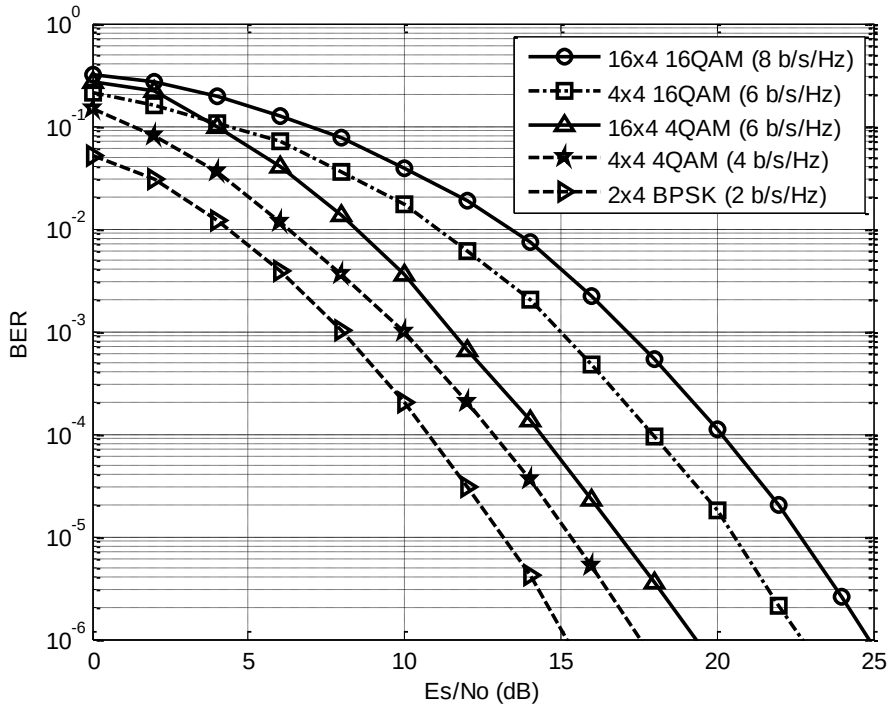

Figure 2.6: Comparison of BER performances of SM systems for 2, 4, 6 and 8 b/s/Hz using varying N_t and *M*

The error performances of the SM-HDMLD (2.13) and SM-SOMLD detectors (2.14) - (2.15) are evaluated for uncoded and coded channels and the results are presented in Figure 2.7. The simulation results show that the SOMLD schemes matches closely with the HDMLD in uncoded channels. However, the coded SM-SOMLD yields significant SNR gains over coded and uncoded SM-HDMLD. For example, at a BER of 10^{-6}, approximately

6.5 dB SNR gain is achieved by the coded SOMLD over the coded HDMLD while it achieved 8.8 dB SNR gain against the uncoded HDMLD.

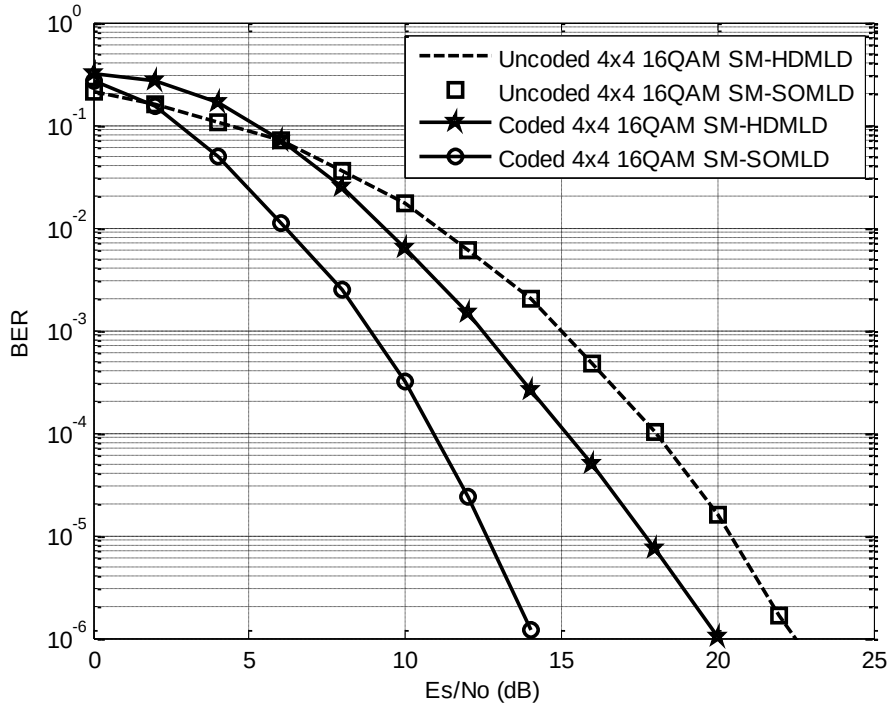

Figure 2.7: Comparison of BER performances of SM systems in coded and uncoded channels for a 6 b/s/Hz using 4×4 16QAM MIMO configurations

Note that, for channel coding, we consider a rate $1/2$ convolutional encoder with constraint length 9 and code generating matrices $[g_1, g_2] = [(561)_o, (753)_o]$, where '$o$' represents an octal number.

In [55], a look-up table (LUT) based method [56] was used to compute the logarithm function present in the SOMLD-SM detector given in (2.14) - (2.15). According to the LUT, the logarithm function was found to have imposed no additional complexity on the detection process of the SOMLD-SM; therefore its CC is given similar to (2.20) as $CC_{\mathrm{SM-SOMLD}} = 2N_rN_t + N_tM + M$

2.7. Conclusion

In this chapter, we have investigated the error performances of SM scheme and our simulation results are validated using the analytical performance bounds presented in Section 2.4. It was confirmed that an increase in N_t leads to enhanced spectral efficiency. Furthermore, SM systems are compared to the V-BLAST and the former was found to be better than the latter, both in error performance and spectral efficiency. We also investigated SM system, operated by SOMLD, in coded and uncoded channels. Results presented confirm that coded SM-SOMLD have a superior error performance compared to coded and uncoded SM-HDMLD. Meanwhile, the SOMLD matches closely with the HDMLD in uncoded channels.

Chapter 3

SSK and Bi-SSK Modulations

3.1. Introduction

In [34] and [35], SSK and Bi-SSK modulations schemes are introduced, respectively. In both schemes, only spatial domains are employed for transmission with no APM symbols. That is; only antenna indices are used to transmit information. Findings show that system hardware complexity is reduced, in both schemes, as a result of APM removal from the transmission. Although, this is at the expense of some degradation in the spectral efficiency of the system, as compared to the SM scheme; but SKK and Bi-SSK modulations, aside having the advantages of SM, possess other advantages such as lesser transceiver hardware requirements, lowered detection complexities and simple structures. No doubt, these are very much desired in the next generation communication systems.

In this chapter, therefore, we take a detailed look at the SSK and Bi-SSK schemes as two important members of the transmit antenna index modulation-based schemes which are being investigated in this dissertation. For both schemes, the succeeding subsections of the chapter, give further explanations of the system models, transmission techniques, detection schemes and detailed analytical performance analyses, for SSK and Bi-SSK schemes, respectively. Results obtained from our investigations of the two schemes are presented and accordingly discussed at the end of the chapter.

3.2. Space Shift Keying Modulation

3.2.1. System Model for SSK Modulation

SSK exhibits the fundamental advantages of SM, in addition to; lesser transceiver hardware requirements, lowered detection complexity for identical performance to SM and a simple structure that provides easy integration with communication systems. The SSK system model is presented in Figure 3.1. We recall that SM discussed in Chapter 2, relays information by means of antenna index and an APM data symbol. Meanwhile, the system model for SSK clearly shows that the APM data symbols have been removed [34, 52].

Instead of splitting the incoming information bits into two (as in the case of SM for selecting one APM symbol and an antenna index, respectively), they are used for selecting only an antenna index. Information is therefore relayed in SSK by means of antenna indices only, which makes it a subclass of SM. Remarkable advantages and differences have therefore been observed between SM and SSK due to the absence of APM [34]. However, high order SSK correspondingly requires a large number of transmit antenna. On this note, a more flexible form of SSK called generalized SSK (GSSK) has been proposed to bypass this difficulty [57].

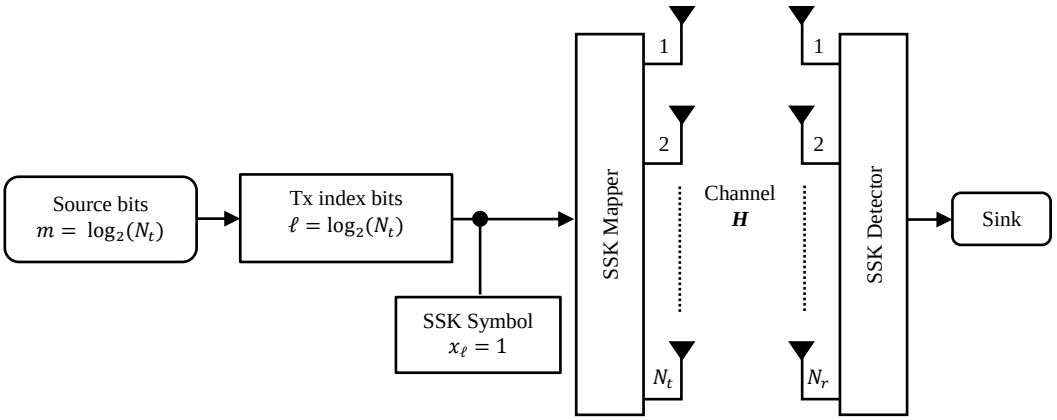

Figure 3.1: System model for SSK modulation

3.2.2. SSK Transmission and Detection

To form a symbol of SSK, a set of $m = \log_2(N_t)$ bits are mapped into a column vector, $\boldsymbol{x}_\ell$; where $\ell = 1, 2 \ldots N_t$ in $\boldsymbol{x}_\ell$ is nonzero and $\boldsymbol{x}_\ell = 1$ for all ℓ. This means that only one of the transmit antennas (ℓ^{th} antenna) is active during transmission. It is noted that even though the symbol itself does not contain any information, its location does and so it might be designed for optimal transmission [34]. A typical SSK symbol can be written as:

$$\boldsymbol{x}_\ell \triangleq [\,0\;0 \ldots \underbrace{\boldsymbol{x}_\ell = 1}_{\ell^{th}\ position} \quad 0 \ldots 0]^T \tag{3.1}$$

The channel output, in the presence of noise, is given as:

$$\boldsymbol{y} = \sqrt{\rho}\boldsymbol{H}\boldsymbol{x}_\ell + \boldsymbol{w} = \sqrt{\rho}\boldsymbol{h}_\ell + \boldsymbol{w} \tag{3.2}$$

where $\boldsymbol{H}$ and $\boldsymbol{w}$ are complex and assumed to be i.i.d as $CN(\mu = 0, \sigma^2 = 1)$. ρ is the average SNR at each receive antenna and $\boldsymbol{x}_\ell = 1$represents the chosen SSK symbol that is transmitted via the ℓ^{th} antenna.

From (3.2), it is observable that the effective constellations of SSK are contained in the scaled version of the columns of $\boldsymbol{H}$ (i.e. $\boldsymbol{h}_\ell$). That is, the column indices of $\boldsymbol{H}$ are used as sources of information. We note that in SSK transmission, the effective constellations are contained in scaled versions of the vector $\boldsymbol{h}\boldsymbol{x}_\ell$; simply put, $\boldsymbol{x}_\ell = 1$ is fixed, while $\boldsymbol{h}_\ell$ changes according to the incoming bit streams. Whereas, $\boldsymbol{x}_\ell$ changes, and $\boldsymbol{h}_\ell$ remains constant in APM. Basically, the changing channel columns $\boldsymbol{h}_\ell$ act as SSK random constellation points. If both the antenna index, $\boldsymbol{h}_\ell$ and the transmit symbol, $\boldsymbol{x}_\ell$, are made to convey information, the modulation is neither APM nor SSK, but SM. An illustration of SSK modulation assuming $N_t = 4$ is given in Table 3.1.

Table 3.1: Mapping illustration for SSK modulation

Input Bits ($b_1\, b_0$)	**Antenna index** (ℓ)	**SSK signal vector** $\boldsymbol{x}_\ell$	**Effective constellation** ($\boldsymbol{h}_\ell = \boldsymbol{H}\boldsymbol{x}_\ell$)
[1 1]	4	$[\,0\ 0\ 0\ 1\,]^T$	$\boldsymbol{h}_4$
[1 0]	3	$[\,0\ 0\ 1\ 0\,]^T$	$\boldsymbol{h}_3$
[0 1]	2	$[\,0\ 1\ 0\ 0\,]^T$	$\boldsymbol{h}_2$
[0 0]	1	$[\,1\ 0\ 0\ 0\,]^T$	$\boldsymbol{h}_1$

In [34, 52], the optimal hard decision-based maximum-likelihood (ML) detector (HDMLD) for SSK obtains the antenna index that was used at the transmitter, which is given as:

$$\hat{\ell} = \arg\max_{\ell}(\boldsymbol{y} \mid \boldsymbol{x}_\ell, \boldsymbol{H}) \tag{3.3}$$

$$\hat{\ell} = \arg\min_{\ell}\left\|\boldsymbol{y} - \sqrt{\rho}\boldsymbol{h}_\ell\right\|_F^2 \tag{3.4}$$

$$\hat{\ell} = \arg\max_{\ell}\left\{\left(\boldsymbol{y} - \sqrt{\rho}\boldsymbol{h}_\ell\right)^H \boldsymbol{h}_\ell\right\} \tag{3.5}$$

where $p_Y(\boldsymbol{y}\,|\boldsymbol{x}_\ell, \boldsymbol{H}) = \pi^{-N_r}\exp\left(-\left\|\boldsymbol{y} - \sqrt{\rho}\,\boldsymbol{h}\boldsymbol{x}_\ell\right\|_F^2\right)$, and $\hat{\ell}$ is the estimated antenna for $1 \leq \ell \leq N_t$.

3.3. Performance Analysis of SSK

The analytical error performance of the SSK is derived using the union bounding technique [1] employed to derive the performance analysis of the SM in [29] and [52]. The average BER is bounded in [34] as:

$$P_{e,bit}^{SSK} \leq E_x\left[\sum_{\hat{\ell}\neq\ell} N_{SSK}\left(\ell, \hat{\ell}\right) P\left(\boldsymbol{x}_\ell \to \boldsymbol{x}_{\hat{\ell}}\right)\right] \tag{3.6}$$

$$= \sum_{\ell=1}^{N_t}\sum_{\hat{\ell}=1}^{N_t} \frac{2N_{SSK}\left(\ell, \hat{\ell}\right)P\left(\boldsymbol{x}_\ell \to \boldsymbol{x}_{\hat{\ell}}\right)}{N_t} \tag{3.7}$$

Using (3.5), the pairwise error probability, (PEP), conditioned on $\boldsymbol{H}$ is given as:

$$P_{SSK}(\boldsymbol{x}_\ell \rightarrow \boldsymbol{x}_{\hat{\ell}} \mid \boldsymbol{H}) = P(d_\ell > d_{\hat{\ell}} \mid \boldsymbol{H}) = Q(\sqrt{k_{SSK}}) \tag{3.8}$$

where $Q(\beta)$ is the Q-function given as $Q(\beta) = \int_\beta^\infty \frac{1}{2\pi} e^{-\frac{t^2}{2}} dt$ and $d_\ell = 2\Re\{\boldsymbol{y}^H \boldsymbol{g}_{\ell q}\}$.

$$k_{SSK} \triangleq \frac{\rho}{2} \left\| \boldsymbol{h}_\ell - \boldsymbol{h}_{\hat{\ell}} \right\|_F^2 = \sum_{n=1}^{2N_r} \sigma_{SSK}^2(n) \tag{3.9}$$

such that $\alpha_{SSK}(n) \sim \mathcal{N}(0, \alpha_{SSK}^2)$ and $\sigma_{SSK}^2 = \frac{\rho}{2}$. Therefore, k_{SSK} is a random variable of the chi-squared distribution with $2N_r$ degrees of freedom, and its PDF is given as:

$$p_k(v) = \frac{v^{\frac{S}{2}-1} \exp(-\frac{v}{2\sigma_{SM}^2})}{(2\sigma_{SSK}^2)^{\frac{S}{2}} \Gamma\left(\frac{S}{2}\right)}, v > 0 .$$

In a closed form expression, PEP is given as:

$$P(\boldsymbol{x}_\ell \rightarrow \boldsymbol{x}_{\hat{\ell}}) = \gamma_{SSK}^{N_r} \sum_{k=0}^{N_r-1} \binom{N_r - 1 + k}{k} [1 - \gamma_{SSK}]^k \tag{3.10}$$

where $\gamma_{SSK} = \frac{1}{2}\left(1 - \sqrt{\frac{\sigma_{SSK}^2}{1+\sigma_{SSK}^2}}\right)$.

Let $N_\Sigma = \sum_{\ell=1}^{N_t} \sum_{\hat{\ell}=\hat{\ell}+1}^{N_t} 2N_{SSK}(\ell, \hat{\ell})$, and putting (3.10) in (3.7), we have:

$$P_{e,bit} \leq \frac{N_\Sigma \gamma_{SSK}^{N_r}}{N_t} \sum_{k=0}^{N_r-1} \binom{N_r - 1 + k}{k} [1 - \gamma_{SM}]^k \tag{3.11}$$

3.4. Computational Complexity of SSK

In [34], the complexity of SSK was quantified by the number of complex multiplications required in the detection process. Similar to [28], (3.5) was analysed to obtain the complexity of SSK receiver, which is given in [34] as:

$$CC_{SSK} = N_r M \tag{3.12}$$

In [34], the complexity of SSK was compared to that of SM-OD, and it was noted that a straightforward comparison of complexities of both detectors cannot be made at first glance. However, SSK was shown to have lower complexity by more than 50% complex multiplications, for practical values of N_t, N_r and M.

The numerical results and discussion of performances of SSK systems, in terms of bit error rate, are presented in Section 3.8. These are also compared to SM and Bi-SSK systems for various transceiver configurations.

3.5. Bi-Space Shift Keying Modulation

3.5.1. System Model for Bi-SSK Modulation

The SSK scheme was found to be lacking in good spectral efficiency when compared to SM, as would later be seen in the presentation of our results. Achieving higher efficiency in SSK can only be made possible by employing high order SSK, which means that large number of transmit antennas would have to be employed unnecessarily [57]. On this note, as an extension to SSK, Bi-SSK was proposed in [35] to employ dual antenna indices to convey information from the source to destination. One of these antennas is associated with a real number and the other with an imaginary number. This arrangement results in twice the achievable data rate of SSK in addition to preserving the advantages of SSK. We note that Bi-SSK modulation, like SSK, is done without the inclusion of APM required in the transmission and detection components of schemes such as SM and other conventional MIMO systems.

Meanwhile, Bi-SSK scheme exhibits no IAI, even though two antennas are active at the same time. This is done by activating two different or similar, but orthogonal, antennas to carry the information. It also solves the problem of ICI, while creating no need for IAS. However, it requires double the amount of power needed for SSK transmission [35]. Figure 3.2 illustrates the system model for Bi-SSK equipped with N_t transmit antennas and N_r receive antennas.

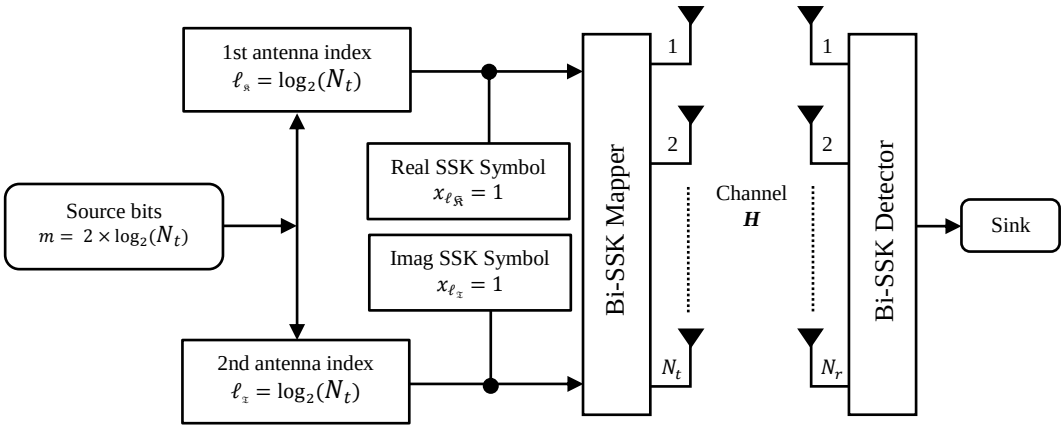

Figure 3.2: System model for Bi-SSK modulation

3.5.2. Bi-SSK Transmission and Detection

From Figure 3.2, the key idea of Bi-SSK transmission involves dividing the set of m information bits into two equal blocks of length $\log_2(N_t)$ bits. Each of the blocks are then mapped into an SSK transmit vector, and are represented as $\boldsymbol{x}_{\ell_{\Re}}$ and $\boldsymbol{x}_{\ell_{\Im}}$, where $\boldsymbol{x}_{\ell} = 1$ for both real and imaginary ℓ. The corresponding transmit antennas are then activated to transmit the vectors $\boldsymbol{x}_{\ell_{\Re}}$ and $\boldsymbol{x}_{\ell_{\Im}}$. It is noted that even though the symbols do not contain any information on both the real and imaginary antennas, their locations do and so they might be designed for optimal transmission [35]. An example of the mapping process for Bi-SSK modulation with $N_t = 4$ is tabulated in Table 3.2.

Table 3.2: Example of mapping rule for Bi-SSK modulation

Input Bits ($b_3b_2b_1b_0$)	**Real Bits** (b_3b_2)	**Imag. Bits** (b_1b_0)	**Real Tx Index**	**Real SSK Vector** $\boldsymbol{x}_{\ell_{\Re}}$	**Imag. Tx Index**	**Imag SSK Vector** $\boldsymbol{x}_{\ell_{\Im}}$	**Bi-SSK signal vector** $(\boldsymbol{x}_{\ell_{\Re}} + j\boldsymbol{x}_{\ell_{\Im}})$
[1 1 0 0]	1 1	0 0	4	$[0\ 0\ 0\ 1]^T$	1	$[1\ 0\ 0\ 0]^T$	$[j\ \ 0\ \ 0\ \ 1]^T$
[1 0 0 1]	1 0	0 1	3	$[0\ 0\ 1\ 0]^T$	2	$[0\ 1\ 0\ 0]^T$	$[0\ \ j\ \ 1\ \ 0]^T$
[0 0 1 0]	0 0	1 0	1	$[1\ 0\ 0\ 0]^T$	3	$[0\ 0\ 1\ 0]^T$	$[1\ \ 0\ \ j\ \ 0]^T$
[0 1 1 1]	0 1	1 1	2	$[0\ 1\ 0\ 0]^T$	4	$[0\ 0\ 0\ 1]^T$	$[0\ \ 1\ \ 0\ \ j]^T$
[0 0 0 0]	0 0	0 0	1	$[1\ 0\ 0\ 0]^T$	1	$[1\ 0\ 0\ 0]^T$	$[1+j\ 0\ \ 0\ \ 0\ ]^T$

In the example, the total number of transmitted information bits in one time slot can be calculated as $m = 2 \times \log_2(N_t) = 2 \times \log_2(4) = 4$ bits. In accordance with the mapping rules of Bi-SSK; the set of 4 bits (i.e. $b_3\, b_2\, b_1\, b_0$) are equally grouped into two (i.e. $b_3\, b_2$ and $b_1\, b_0$) and each group is used to select one of the $N_t = 4$ transmit antennas that are available for transmission: one for the real and the other for the imaginary number. In other words, it can be said that each group is used to modulate separate SSK symbols, which are added together in a complex manner to form the Bi-SSK symbol. Hence, only two of $\boldsymbol{x}_\ell,\ \ell = 1, 2 \ldots N_t$ in $\boldsymbol{x}_{\ell_{\text{Bi-SSK}}}$ are nonzero.

Hence, a set of $m = 2 \times \log_2(N_t)$ bits, is mapped into a Bi-SSK transmit vector $\boldsymbol{x}_{\ell_{\text{Bi-SSK}}}$, $\ell = 1, \cdots, N_t$, defined as:

$$\boldsymbol{x}_{\ell_{\text{Bi-SSK}}} = \boldsymbol{x}_{\ell_{\Re}} + j\boldsymbol{x}_{\ell_{\Im}} \tag{3.13}$$

where $\ell_{\Re}$ represents the active real transmit antenna and $\ell_{\Im}$ represents the active imaginary transmit antenna.

The received signal vector for Bi-SSK transmission may then be defined as [35]:

$$\boldsymbol{y} = \sqrt{\rho/\mu}\, \boldsymbol{H}\boldsymbol{x}_{\ell_{\text{Bi-SSK}}} + \boldsymbol{w} \tag{3.14}$$

where $\boldsymbol{H}$ and $\boldsymbol{w}$ are complex and assumed to be i.i.d as $CN(\mu = 0, \sigma^2 = 1)$. μ is a scaling factor for the average SNR, ρ at each receive antenna and $\boldsymbol{x}_{\ell_{\text{Bi-SSK}}}$ represents the Bi-SSK signal vector of size $N_t \times 1$.

For example, when the indices result in a single transmit antenna $\mu = 1$, and when the indices result in two antennas we employ $\mu = 2$. Since $\boldsymbol{x}_\ell = 1$ for both real and imaginary ℓ, (3.14) can further be simplified to yield:

$$\boldsymbol{y} = \sqrt{\rho/\mu}\, (\boldsymbol{h}_{\ell_{\Re}} + j\boldsymbol{h}_{\ell_{\Im}}) + \boldsymbol{w} \tag{3.15}$$

where $\boldsymbol{h}_{\ell_{\Re}}$ is the channel gain vector associated with the transmission of $\boldsymbol{x}_{\ell_{\Re}}$ and $\boldsymbol{h}_{\ell_{\Im}}$ is the channel gain vector associated with the transmission of $\boldsymbol{x}_{\ell_{\Im}}$.

From Table 3.2 and (3.14) - (3.15), it observable that the effective constellations of Bi-SSK are contained in the scaled version of the columns of $\boldsymbol{H}$ selected by the real and imaginary antenna indices, respectively. That is, the column indices of $\boldsymbol{H}$ are used as sources of information, i.e. both the real $\boldsymbol{x}_{\ell}$ and the imaginary $\boldsymbol{x}_{\ell}$ are fixed and equal to 1, while the real $\boldsymbol{h}_{\ell}$ and imaginary $\boldsymbol{h}_{\ell}$ change according to the incoming bit streams. Basically, the changing columns of the channel $\boldsymbol{H}$, act as the Bi-SSK random constellation points.

The optimal hard-decision maximum-likelihood detector/detection (HDMLD) for the Bi-SSK system is obtained and written in [35] as:

$$[\,\hat{\ell}_{\Re},\,\hat{\ell}_{\Im}] \;=\; \underset{\ell_{\Re},\ell_{\Im}\in[1:N_t]}{\operatorname{argmin}} \left\| \boldsymbol{y} - \sqrt{\rho/\mu}\left(\boldsymbol{h}_{\ell_{\Re}} + j\boldsymbol{h}_{\ell_{\Im}}\right)\right\|_F^2 \tag{3.16}$$

3.6. Performance Analysis of Bi-SSK

The analysis of error performance of the Bi-SSK system was given in [35]. The union bond technique was applied to the PEP of deciding $x_{\ell_{\Re}}$ given that $x_{\ell_{\Im}}$ is transmitted considering a Bi-SSK modulation system with ML detection at the receiver. The SER for Bi-SSK is derived from the total average of all possible transmitted symbols by separating all possible errors into non-overlapping subsets. According to [35], the SER is approximated as:

$$P_{sym} = \mathbb{E}_{\boldsymbol{x}_{\ell_{\Re}}}\left[\bigcup_{\boldsymbol{x}_{\ell_{\Im}}} P\left(\boldsymbol{x}_{\ell_{\Re}} \rightarrow \boldsymbol{x}_{\ell_{\Im}}\right)\right]$$

$$P_{sym} \leq \frac{1}{N_t^2}\sum_{\boldsymbol{x}_{\ell_{\Re}}}\sum_{\boldsymbol{x}_{\ell_{\Re}}\neq \boldsymbol{x}_{\ell_{\Im}}} P(\boldsymbol{x}_{\ell_{\Re}} \rightarrow \boldsymbol{x}_{\ell_{\Im}}) \tag{3.17}$$

$$P_{sym} \leq \sum_{\boldsymbol{x}_{\ell_{\Re}}\neq \boldsymbol{x}_{\ell_{\Im}}} P\left(\boldsymbol{x}_{\ell_{\Re}} \rightarrow \boldsymbol{x}_{\ell_{\Im}}\right)$$

$$= \sum_{\boldsymbol{x}_{\ell_{\Re}}\in k_1} P\left(\boldsymbol{x}_{\ell_{\Re}} \rightarrow \boldsymbol{x}_{\ell_{\Im}}\right) + \sum_{\boldsymbol{x}_{\ell_{\Re}}\in k_2} P(\boldsymbol{x}_{\ell_{\Re}} \rightarrow \boldsymbol{x}_{\ell_{\Im}}) \tag{3.18}$$

where

$$k_1 = \left\{\boldsymbol{x}_{\ell_{\Re}} \in \boldsymbol{x}_{\ell_{\mathrm{Bi-SSK}}} \setminus \boldsymbol{x}_{\ell_{\Re}} \,\middle|\, (c = d, a \neq b) or\ (c \neq d, a = b)\right\} \text{ and}$$

$$k_2 = \left\{ \boldsymbol{x}_{\ell_{\Re}} \in \boldsymbol{x}_{\ell_{\text{Bi-SSK}}} \setminus \boldsymbol{x}_{\ell_{\Re}} \,\middle|\, (c \neq d, a \neq b) \right\}$$

are the non-overlapping subsets of all possible errors such that a and b represent the antenna indices associated with real numbers and c and d represent the antenna indices associated with imaginary numbers.

In [34], the PEP conditioned on $\boldsymbol{H}$ was derived as:

$$\begin{aligned} & P\left(\boldsymbol{x}_{\ell_{\Re}} \to \boldsymbol{x}_{\ell_{\Im}} \middle| \boldsymbol{H}\right) \\ &= P\left(\left\| \boldsymbol{y} - \sqrt{\rho}\boldsymbol{H}\boldsymbol{x}_{\ell_{\Re}} \right\|^2 > \left\| \boldsymbol{y} - \sqrt{\rho}\boldsymbol{H}\boldsymbol{x}_{\ell_{\Im}} \right\|^2 \right) \end{aligned} \tag{3.19}$$

$$\begin{aligned} &= \left(\Re\left\{ n^H (\boldsymbol{H}\boldsymbol{x}_{\ell_{\Re}} - \boldsymbol{H}\boldsymbol{x}_{\ell_{\Im}}) \right\} > \frac{\sqrt{\rho}}{2} \left\| \boldsymbol{H}\boldsymbol{x}_{\ell_{\Re}} - \boldsymbol{H}\boldsymbol{x}_{\ell_{\Im}} \right\|^2 \right) \\ &= Q(\sqrt{\mu}) \end{aligned} \tag{3.20}$$

where $\Re\{\cdot\}$ is the real part of its argument, $Q(\beta) = \int_{\beta}^{\infty} \frac{1}{2\pi} e^{-\frac{t^2}{2}} dt$ and

$$\mu = \frac{\rho}{2N_0} \left\| \boldsymbol{H}\boldsymbol{x}_{\ell_{\Re}} - \boldsymbol{H}\boldsymbol{x}_{\ell_{\Im}} \right\|^2 \tag{3.21}$$

Note that $\boldsymbol{H}$ is of Gaussian distribution and as a result, $2N_r$ independent random variables can be summed up to μ and expressed as:

$$\mu = \sum_{i=1}^{2N_r} \alpha_i^2 \tag{3.22}$$

where $\alpha_i \backsim N(0, \sigma_\alpha^2)$ with $\sigma_\alpha^2 = \frac{\rho}{2N_0} \triangleq \sigma_{\alpha_1}^2$ for $\boldsymbol{x}_{\ell_{\Im}} \in k_1$ and $\sigma_\alpha^2 = \frac{\rho}{N_0} \triangleq \sigma_{\alpha_2}^2$ for $\boldsymbol{x}_{\ell_{\Im}} \in k_2$; hence the PDF of μ can be obtained since it is chi-squared distributed with 2N degrees of freedom.

Therefore, the PEP can be evaluated by finding the average of all channel realizations given as:

$$P\left(\boldsymbol{x}_{\ell_{\Re}} \rightarrow \boldsymbol{x}_{\ell_{\Im}}\right) = \mathbb{E}_{\mu}[P\left(\boldsymbol{x}_{\ell_{\Re}} \rightarrow \boldsymbol{x}_{\ell_{\Im}} \middle| \boldsymbol{H}\right)]$$
$$= \int_{v=0}^{\infty} Q\left(\sqrt{v}\right) p_{\mu}(v) dv \tag{3.23}$$

The closed form of (3.23) is given in [58] as:

$$P\left(\boldsymbol{x}_{\ell_{\Re}} \rightarrow \boldsymbol{x}_{\ell_{\Im}}\right) = \gamma_{\alpha}^{N_r} \sum_{t=0}^{N_r-1} \binom{N_r - 1 + k}{k} [1 - \gamma_{\alpha}]^k \tag{3.24}$$

where $\gamma_{\alpha} = \frac{1}{2}\left(1 - \sqrt{\frac{\sigma_{\alpha}^2}{1+\sigma_{\alpha}^2}}\right)$.

It is notable that the subsets $\left|k_1\right|$ and $\left|k_2\right|$ have the cardinalities of $2(N_t - 1)$ and $(N_t - 1)^2$. By using these cardinalities and replacing the two PEP in (3.17) and (3.24), the SER for Bi-SSK is obtained as:

$$P_{sym} \leq 2(N_t - 1)\gamma_{\alpha_1}^{N_r} \sum_{t=0}^{N_r-1} \binom{N_r - 1 + k}{k} [1 - \gamma_{\alpha_1}]^k$$
$$+ (N_t - 1)^2 \gamma_{\alpha_2}^{N_r} \sum_{t=0}^{N_r-1} \binom{N_r - 1 + k}{k} [1 - \gamma_{\alpha_2}]^k \tag{3.25}$$

and accordingly, $\gamma_{\alpha_1} = \frac{1}{2}\left(1 - \sqrt{\sigma_{\alpha_1}^2/1 + \sigma_{\alpha_1}^2}\right)$, and $\gamma_{\alpha_2} = \frac{1}{2}\left(1 - \sqrt{\sigma_{\alpha_2}^2/1 + \sigma_{\alpha_2}^2}\right)$.

3.7. Computational Complexity of Bi-SSK

In this section, the number of complex multiplications required in the detection process of Bi-SSK is used to quantify the computational complexity involved. The Bi-SSK optimal detector, given in (3.16), shows that the number of multiplications involved are twice of what is obtainable in the Section 3.4 for SSK optimal detector. Without any loss of generality, the total computational complexity imposed by the optimal Bi-SSK detector, in terms of complex multiplications, can be given as:

$$CC_{\text{Bi-SSK}} = 2N_r N_t \tag{3.26}$$

3.8. Simulation Results and Discussion

We present here, the simulation results of the error performances of SSK and Bi-SSK schemes and compare them to SM. For all simulations, we have considered a flat-fading MIMO channel with i.i.d. entries distributed according to *CN*(0,1), in the presence of AWGN. The results are obtained in terms of the BER as a function of the SNR. Different number of transmit antennas are employed to obtain different spectral efficiencies of 2, 4 and 6 bits/s/Hz. We also terminate all simulations at a BER of 10^{-6}.

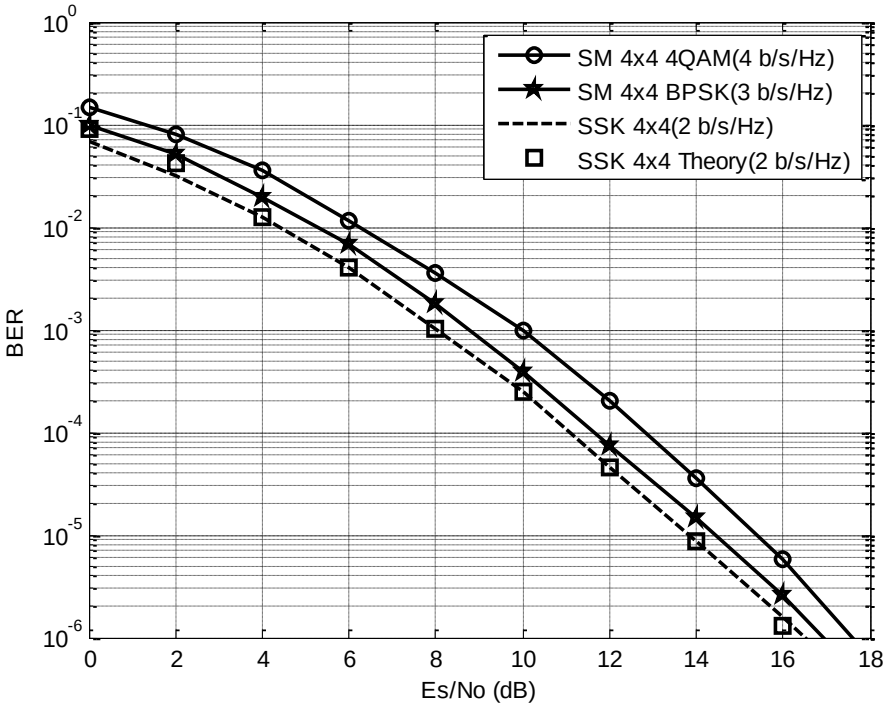

Figure 3.3: Comparison of BER performances of SSK and SM systems with 4×4 transceiver configurations

In Figure 3.3, the error performances of SM and SSK systems are evaluated using the optimal HDMLD given in (2.13) and (3.5) respectively. Under 4×4 transceiver configuration, a 4-ary SSK system is being compared to that of BPSK and 4QAM SM systems. The choice of BPSK and 4QAM modulation orders was to make a comparison in terms of the same antenna configurations. Even though the 4×4 BPSK and 4×4 4QAM SM

systems will give 3 and 4 b/s/Hz transmission rates respectively, they are still the least possible obtainable for 4×4 transceiver configuration. Meanwhile, we observe that the SSK outperforms SM systems in error performance. For example, at a BER of 10^{-6}, approximately 1.1 dB SNR gain is achieved by the SSK system compared to 4QAM SM system while the gain is reduced to about 0.5 dB in the case of BPSK SM system.

Under the same configuration as presented above, we note that SSK system has the least spectral efficiency of 2 b/s/Hz, followed by the BPSK SM with 3 b/s/Hz, while the 4QAM SM system possesses 4 b/s/Hz. On this note, the superiority of the SSK system to SM in terms of BER may be regarded as being insignificant, coupled with the fact that the dB gains appear small. Nevertheless, the advantage of the SSK lies in the lower complexity it possesses at the receiver. We recall that the task of SM receivers is doubled due to the detection of both the symbol and the antenna indices, but the SSK receiver estimates only the antenna index as no symbol was transmitted in the first instance.

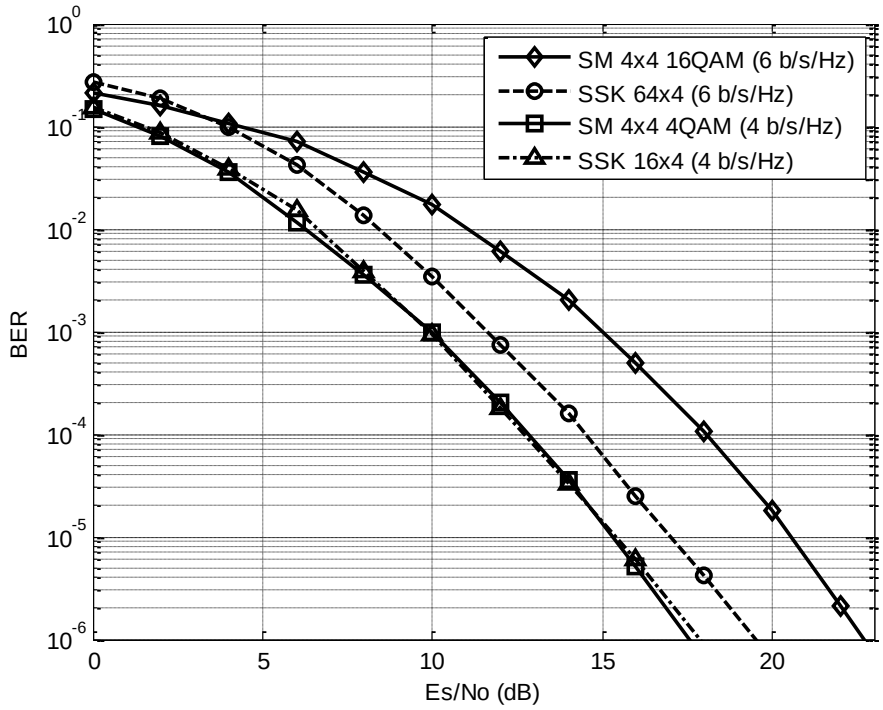

Figure 3.4: Comparison of BER performances of SSK and SM systems with spectral efficiencies of 4 and 6 b/s/Hz

Furthermore, Figure 3.4 shows the error performances of SM and SSK systems with the same spectral efficiency of 4 b/s/Hz and 6 b/s/Hz, respectively. Considering the 4 bit spectral efficient systems, both the 16×4 16-ary SSK and the 4×4 4QAM SM are almost matching each other in error performance showing insignificant or negligible difference. At a BER of 10^{-6}, both require approximately 17.6 dB SNR. Meanwhile, the 6 bits SSK system outperforms its SM counterpart by approximately 3.1 dB SNR gain, at a BER of 10^{-6}. Generally, we infer that SSK system truly outperforms the SM system in terms of error performance, especially at higher spectral efficiency; however, this is achieved at the expense of an exponentially increased number of transmit antennas.

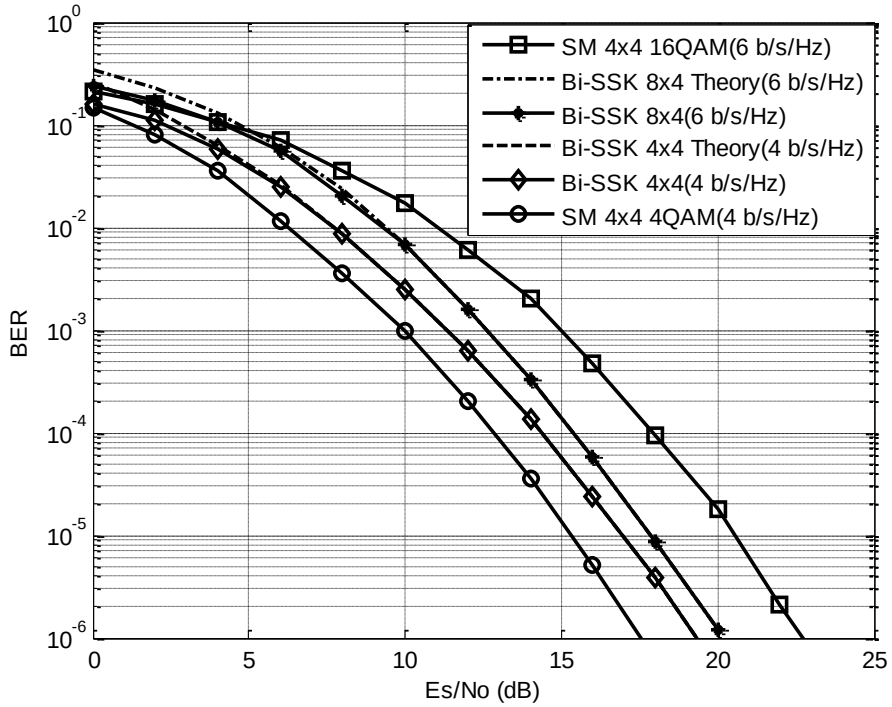

Figure 3.5: Comparison of BER performances of Bi-SSK and SM systems with spectral efficiencies of 4 and 6 b/s/Hz

The error performances of 4 bit/s/Hz and 6 bit/s/Hz transmissions for Bi-SSK and SM systems are presented in Figure 3.5. The same result also presents the error performance of Bi-SSK and SM systems being compared under similar antenna configuration. It is evident that the SM systems have better error performances compared to their Bi-SSK counterparts for lower spectral efficient transmission. For example, at a BER of 10^{-6}, the SM systems yield SNR gains of 2.1 dB over Bi-SSK systems for 4 b/s/Hz. Whereas, higher spectral

efficiency like 6 b/s/Hz Bi-SSK performs better by approximately 2.5 dB SNR gain over the SM at the same BER. Nonetheless, this is achieved at the expense of unnecessary requirement of large number of transmit antennas.

Meanwhile, another SM system configuration that achieves 6 bits spectral efficiency is 16×4 4QAM, apart from the 4×4 16QAM transceiver configuration. These two SM systems are compared to each other, and to SSK and Bi-SSK systems under the same spectral efficiencies. The results presented in Figure 3.6 show that the 16×4 4QAM SM system achieves an error performance that closely matches that of the SSK system. What makes this SM system better than the SSK is the reduced number of antennas employed in its transmitter. It also yields significant SNR gain compared to the Bi-SSK system. For example, at a BER of 10^{-6}, approximately 1.0 dB is its SNR gain over the Bi-SSK system.

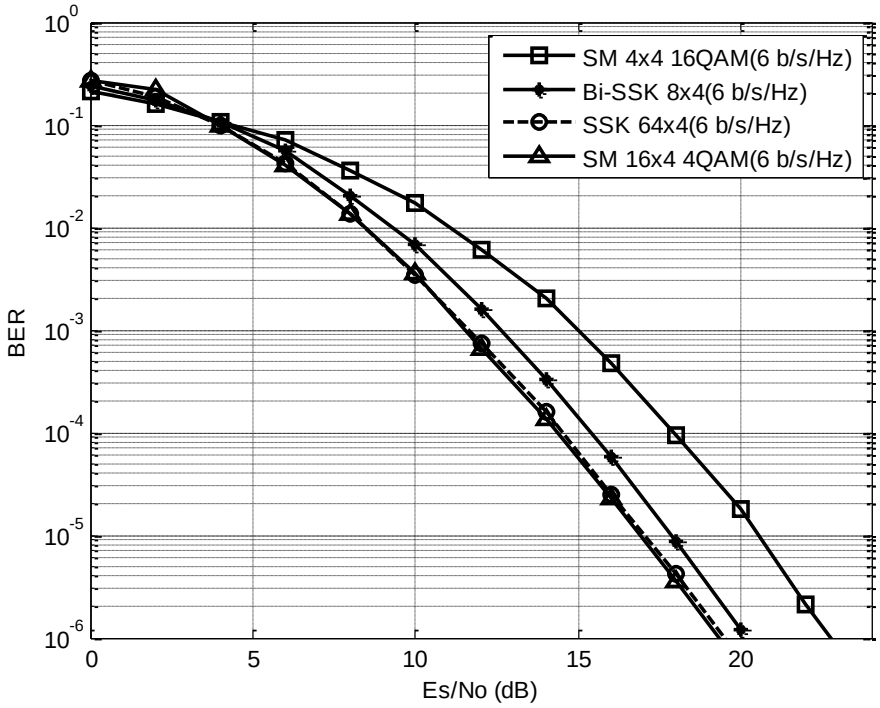

Figure 3.6: Comparison of BER performances of SM, SSK and Bi-SSK systems with spectral efficiency of 6 b/s/Hz

Meanwhile, with approximately 3.4 dB SNR gains possessed by the 16×4 4QAM SM system over the 4×4 16QAM, at a BER of 10^{-6}; it is evident that the lower *M*-ary order SM

system performs better than its higher *M*-ary order counterpart. We note, however, that this is done at the expense of an increased number of transmit antennas.

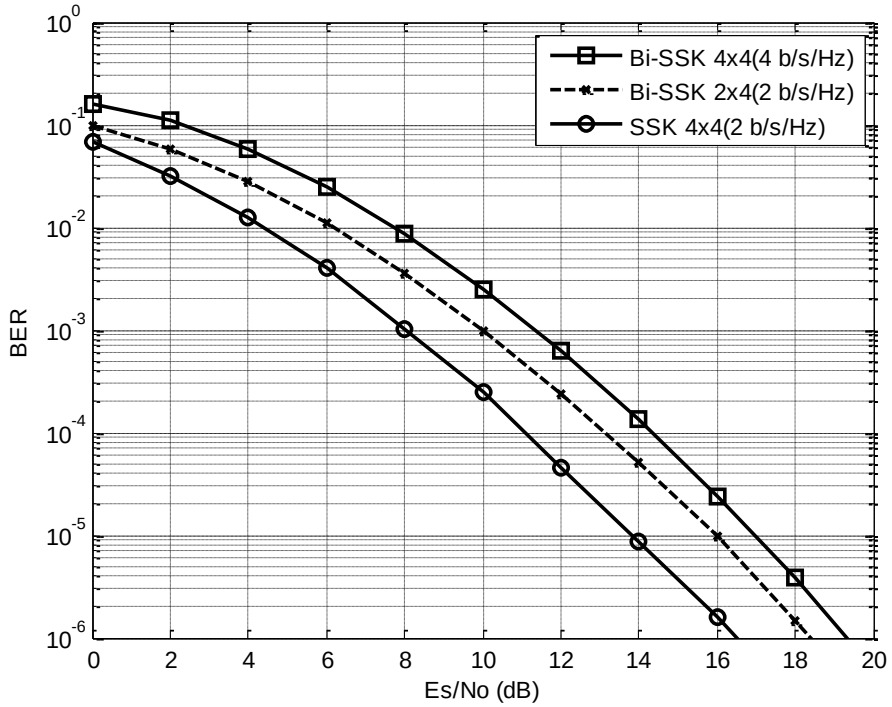

Figure 3.7: Comparison of BER performances of Bi-SSK and SSK systems

Figure 3.7 shows the results obtained for error performances of Bi-SSK and SSK systems for similar spectral efficiencies as well as similar antenna arrays. Considering the 4×4 transceiver configuration, it is evident that Bi-SSK system has twice the spectral efficiency of SSK system, but the latter is better in error performance. In one time slot, the Bi-SSK system transmits 4 bits while 2 bits is transmitted in SSK system. A degradation of 2.7 dB SNR is, however, observed in Bi-SSK with respect to SSK, under 4×4 transceiver configuration. For the fact that Bi-SSK transmit twice as much as the data of SSK, such error degradation may be considered insignificant. Again, the Bi-SSK scheme trades off error performance for fewer antenna requirement (low hardware complexity) when the same spectral efficiency is considered for both systems. For example, at a BER of 10^{-6}, approximately 2.1 dB SNR gain is achieved by SSK over the Bi-SSK; however, the Bi-SSK system requires N_t= 2 while N_t= 4 is required for SSK.

The summary of performances of SSK, Bi-SSK and SM are tabulated in Table 3.3. We observe that at a BER of 10^{-6} and N_t= 4, the SNR required is greatest in Bi-SSK with 19.2 dB, followed by SM with 17.6 dB and it is least in SSK with 16.4 dB. However, the spectral efficiencies involved are 4 b/s/Hz, 4 b/s/Hz and 2 b/s/Hz for Bi-SSK, SM and SSK systems, respectively. Given a target spectral efficiency of 6 b/s/Hz, Bi-SSK requires 8 N_t (and 20.1 dB SNR at 10^{-6}), SM requires 16 N_t (and 19.1 dB SNR at 10^{-6}) while 64 N_t (and 19.2 dB SNR at 10^{-6}) will be needed for SSK.

Table 3.3: Summary of performances of SM, SSK and Bi-SSK systems with $N_r = 4$

Scheme	**Transmit Antennas (N_t = 4)**		**Spectral efficiency = 6 b/s/Hz**	
	SNR at 10^{-6} BER	**Spectral Efficiency**	**SNR at 10^{-6} BER**	**N_t**
SSK	16.5 dB	2 b/s/Hz	19.2 dB	64
Bi-SSK	19.2 dB	4 b/s/Hz	20.1 dB	8
SM 4QAM	17.6 dB	4 b/s/Hz	19.1 dB	16

3.9. Conclusion

Generally, it can be concluded that: Bi-SSK is better in terms of reduced hardware complexity at the transceiver compared to SM and SSK for the same transmission rate, SSK is better in terms of power required for transmission but at the expense of a large array of antennas and reduced spectral efficiency compared to the SM and Bi-SSK system, and SM is always better in spectral efficiency compared to SSK and Bi-SSK systems.

Chapter 4

Quadrature Spatial Modulation

4.1. Introduction

Users of wireless communication systems continue to desire and demand higher data rates. The SM scheme, discussed in Chapter 2, demonstrates a simple and flexible transmission mechanism that achieves a high spectral efficiency as well as a relatively low receiver complexity [28], [30]. SM is such an indispensable scheme useful for integration in the next generation wireless communication systems. Nonetheless, its spectral efficiency is found to be proportional to base-two logarithm of the number of transmit antennas [36]. This forms a major criticism of the system because exponentially large number of transmit antennas would be needed if the promised higher spectral efficiency must be effectively realized. Motivated by this, a MIMO technique called quadrature spatial modulation (QSM) [36] was proposed. QSM aims at enhancing the overall spectral efficiency of the SM technique, while preserving its inherent advantages.

It must be noted that the novel idea of SM remains the basis for the proposed QSM. Basically, two major modifications are applied to the conventional SM to achieve QSM. We recall that, in SM, the combination of a spatial and signal constellation domain is employed for transmission; and clearly, only one spatial dimension (one antenna index) is used to convey one constellation symbol that contains both the real and imaginary parts. In QSM, the spatial domain is expanded to contain in-phase and quadrature-phase spatial dimensions. In addition to this, the complex constellation symbol of SM is further decomposed into its constituent real and imaginary parts. The in-phase and quadrature-phase spatial dimensions

are orthogonal cosine and sine carrier signals and are used, in a novel manner, for conveying the real and imaginary parts of the symbol, respectively, during transmission [36].

The advantages of QSM include that fact that the overall throughput of the SM system is enhanced by additional base-two logarithm of the number of transmit antennas bits. This is made possible, innovatively; by using the extra spatial dimension such that two transmit antennas are activated simultaneously. As noted earlier, other SM advantages, such as the usage of single RF chain at the transmitting end, avoidance of ICI, and low complexity receiver, are still well-preserved in the QSM scheme. The QSM system activates two transmit antennas at a time as spatial constellation points, and utilizes them to carry information, while still avoiding ICI. However, the complexity in the detection process if one disadvantage of QSM system.

Reported results of QSM demonstrate that the system requires 3 dB less signal power for the same error performance and spectral efficiency compared to its SM counterpart [36]. In this chapter, therefore, we present a detailed discussion of the QSM model, transmission and detection technique, its performance analysis as well a brief note on the computational complexity of its receiver. Simulation results, presented at the end of the chapter, are used to evaluate the QSM error performances compared to the SM system.

4.2. System Model and Transmission of QSM Signals

The rule governing the total number of information bits that can be transmitted in QSM stipulates that a group of $m = \log_2(N_t^2 M)$ data bits can be transmitted at once [36]. From this, it is evident that the choice of N_t and M determines m. Therefore, the vector of m data bits is grouped and mapped to form a constellation vector $\boldsymbol{x}_{\mathrm{QSM}}$ of size N_t. A model of the QSM system is depicted in Figure 4.1, considering a MIMO configuration with N_r receive antennas and N_t transmit antennas using well-known M-ary modulation order.

The source information bit sequence, m, is partitioned such that the first $\log_2(N_t)$ bits is used to select the real antenna index ($\ell_{\Re}$), and the second $\log_2(N_t)$ bits is used to select the imaginary antenna index ($\ell_{\Im}$) where $\ell_{\Re}, \ell_{\Im} \in [1, 2, \ldots, N_t]$. The remaining $\log_2(M)$ bits is used to select a constellation symbol $\boldsymbol{x}^q$ where $q \in [1, 2, \ldots, M]$. The selected symbol of the complex constellation $\boldsymbol{x}^q$ is further decomposed into its constituent real and imaginary parts.

These can be identified as $\boldsymbol{x}^{q\Re}$ and $\boldsymbol{x}^{q\Im}$, respectively. We note that the vector $\boldsymbol{x}_{\text{QSM}}$, which represents the QSM signal can also be written as $\boldsymbol{x}_{\ell}^{q}$, such that q denotes the index of the decomposed symbol and ℓ represents the two transmit antenna indices.

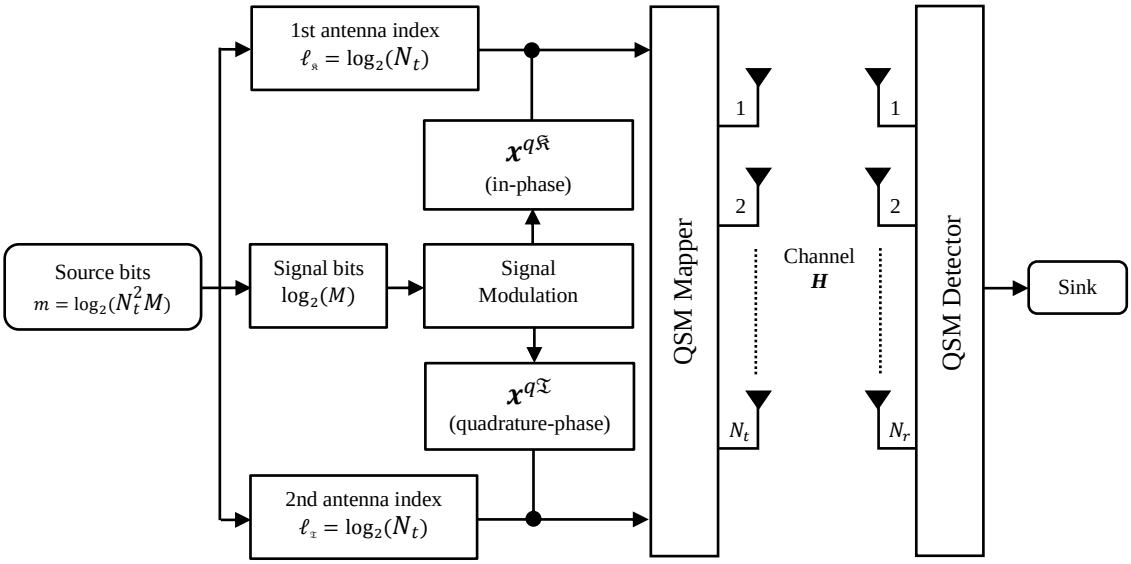

Figure 4.1: System model for QSM modulation

Table 4.1: Mapping rules for QSM modulation

Information Bits	**Symbol bits ($b_1 b_0$)**		**Transmit Antenna Pairs**		**QSM signal vector**
	$x^q = \log_2(M)$		($b_5 b_4$)	($b_3 b_2$)	
($b_5\, b_4\, b_3\, b_2\, b_1\, b_0$)	q ($b_1\, b_0$)	$x^{q\Re} + jx^{q\Im}$	$\ell_{\Re} = \log_2(N_t)$	$\ell_{\Im} = \log_2(N_t)$	$\left(\boldsymbol{x}_{\ell_{\Re}}^{q\Re} + j\boldsymbol{x}_{\ell_{\Im}}^{q\Im}\right)$
[1 0 1 1 0 0]	1	$+1+j$	3	4	$[\ 0 \quad 0 \quad +1 \quad +j\ ]^T$
[0 0 1 0 0 1]	2	$-1+j$	1	3	$[-1 \quad 0 \quad +j \quad 0\ ]^T$
[1 1 0 0 1 0]	3	$+1-j$	4	1	$[-j \quad 0 \quad 0 \quad +1]^T$
[0 1 1 0 1 1]	4	$-1-j$	2	3	$[\ 0 \quad -1 \quad -j \quad 0\ ]^T$
[0 1 0 0 1 0]	3	$+1-j$	2	1	$[-j \quad +1 \quad 0 \quad 0\ ]^T$
[0 0 1 1 0 1]	2	$-1+j$	1	4	$[-1 \quad 0 \quad 0 \quad +j\ ]^T$
[1 1 0 1 1 1]	4	$-1-j$	4	2	$[\ 0 \quad -j \quad 0 \quad -1]^T$
[1 0 1 0 0 0]	1	$+1+j$	3	3	$[\ 0 \quad 0 \quad +1+j \quad 0\ ]^T$

Table 4.1 illustrates a typical mapper for the 6 b/s/Hz QSM transmission with N_t = 4 and M = 4 or 4QAM (whose constellation diagram is shown in Figure (2.2)). The $\log_2(M)$ bits are mapped to one of the MQAM Gray code complex constellation symbol $\boldsymbol{x}^q$ selected by q according ($b_1\, b_0$). The complex form of x^q can be represented as:

$$\boldsymbol{x}^q = \Re\left[\boldsymbol{x}^q e^{-j2\pi f_c t}\right] \tag{4.1}$$

According to [36], a single RF chain can be used to decompose the complex symbol (4.1) to yield:

$$\boldsymbol{x}^q = \boldsymbol{x}^{q\Re}\cos(2\pi f_c t) + \boldsymbol{x}^{q\Im}\sin(2\pi f_c t) \tag{4.2}$$

$$\boldsymbol{x}^q = \boldsymbol{x}^{q\Re} + j\boldsymbol{x}^{q\Im} \tag{4.3}$$

Hence, $\boldsymbol{x}^{q\Re}$ is associated with the cosine carrier (i.e. active real transmit antenna $\ell_{\Re}$) and $\boldsymbol{x}^{q\Im}$ is associated with the sine carrier (i.e. active imaginary transmit antenna $\ell_{\Im}$). Thus, the signal vector of QSM can be represented as:

$$\boldsymbol{x}_{\text{QSM}} = \boldsymbol{x}_{\ell}^{q} = \boldsymbol{x}_{\ell_{\Re}}^{q\Re} + j\boldsymbol{x}_{\ell_{\Im}}^{q\Im} \tag{4.4}$$

At the output of the channel, the received signal vector for QSM transmission may then be defined as [36]:

$$\boldsymbol{y} = \sqrt{\rho/\mu}\,\boldsymbol{H}\boldsymbol{x}_{\text{QSM}} + \boldsymbol{w} = \sqrt{\rho/\mu}\,\boldsymbol{H}\boldsymbol{x}_{\ell}^{q} + \boldsymbol{w} \tag{4.5}$$

where $\boldsymbol{H}$ and $\boldsymbol{w}$ are complex and assumed to be i.i.d as $CN(\mu = 0, \sigma^2 = 1)$, μ is the scaling factor for the average SNR, ρ, at each receive antenna. For example when $\ell_{\Re} = \ell_{\Im}$, $\mu = 1$, and when $\ell_{\Re} \neq \ell_{\Im}$, $\mu = 2$. $\boldsymbol{x}_{\text{QSM}}$ represents the complex signal of the ttransmitted QSM vector.

Substituting (4.4) in (4.5) yields:

$$\boldsymbol{y} = \sqrt{\rho/\mu}\,\boldsymbol{H}\left(\boldsymbol{x}_{\ell_{\Re}}^{q\Re} + j\boldsymbol{x}_{\ell_{\Im}}^{q\Im}\right) + \boldsymbol{w} \tag{4.6}$$

This can further be simplified as:

$$\boldsymbol{y} = \sqrt{\rho/\mu}\left(\boldsymbol{h}_{\ell_{\Re}}\boldsymbol{x}_{\ell_{\Re}}^{q\Re} + j\boldsymbol{h}_{\ell_{\Im}}\boldsymbol{x}_{\ell_{\Im}}^{q\Im}\right) + \boldsymbol{w} \tag{4.7}$$

where $\boldsymbol{h}_{\ell_{\Re}}$ represents the ${\ell_{\Re}}^{th}$ column of $\boldsymbol{H}$, i.e $\boldsymbol{h}_{\ell_{\Re}} = [\boldsymbol{h}_{1,\ell_{\Re}}, \ldots \boldsymbol{h}_{Nr,\ell_{\Re}}]^T$ and $\boldsymbol{h}_{\ell_{\Im}}$ represents the ${\ell_{\Im}}^{th}$ column of $\boldsymbol{H}$, i.e $\boldsymbol{h}_{\ell_{\Im}} = [\boldsymbol{h}_{1,\ell_{\Im}}, \ldots \boldsymbol{h}_{Nr,\ell_{\Im}}]^T$. $\boldsymbol{x}_{\ell_{\Re}}^{q\Re}$ and $\boldsymbol{x}_{\ell_{\Im}}^{q\Im}$ represent the decomposed symbol of q index on real and imaginary antennas respectively.

4.3. QSM Detection Scheme

Assuming a perfect knowledge of the channel at the receiver, the received signals are processed by the optimum ML detector derived for QSM given in [59]. The detector does this by searching through all the available antennas as well as through all the possible data symbols. Joint estimation of $\hat{\ell}_{\Re}, \hat{\ell}_{\Im}$ (i.e. detected antenna indices for real and imaginary components) and $\boldsymbol{x}^{q\Re}$, $\boldsymbol{x}^{q\Im}$ (i.e. detected data symbols for real and imaginary components) are used to recover the original message. This is given in [59] as:

$$\left[\hat{\ell}_{\Re}, \hat{\ell}_{\Im}, \hat{x}^{q\Re}, \hat{x}^{q\Im}\right] = \underset{\ell_{\Re}, \ell_{\Im}, x^{q\Re}, x^{q\Im}}{\operatorname{argmin}} \left\| \boldsymbol{y} - \sqrt{\rho/\mu}\left(\boldsymbol{h}_{\ell_{\Re}}\boldsymbol{x}_{\ell_{\Re}}^{q\Re} + j\boldsymbol{h}_{\ell_{\Im}}\boldsymbol{x}_{\ell_{\Im}}^{q\Im}\right)\right\|_F^2 \tag{4.8}$$

If

$$\boldsymbol{g} = \sqrt{\rho/\mu}\left(\boldsymbol{h}_{\ell_{\Re}}\boldsymbol{x}_{\ell_{\Re}}^{q\Re} + j\boldsymbol{h}_{\ell_{\Im}}\boldsymbol{x}_{\ell_{\Im}}^{q\Im}\right) \tag{4.9}$$

then, expanding the Frobenious norm will simplify (4.8) to yield:

$$\left[\hat{\ell}_{\Re}, \hat{\ell}_{\Im}, \hat{\boldsymbol{x}}^{q\Re}, \hat{\boldsymbol{x}}^{q\Im}\right] = \underset{\ell_{\Re}, \ell_{\Im}, \boldsymbol{x}^{q\Re}, \boldsymbol{x}^{q\Im}}{\operatorname{argmin}} \|\boldsymbol{g}\|_F^2 - 2\Re\{\boldsymbol{y}^H\boldsymbol{g}\} \tag{4.10}$$

The expression in (4.10) is regarded as the optimum receiver for the QSM scheme.

4.4. Performance Analysis of QSM

A detailed analysis error performance for the QSM system has been given in [36, 59]. The analysis is computed with an upper bound approach following a tight union bound. The case of $N_r = 1$ is presented to make it simple and can be generalized for an arbitrary number of receive antennas. From (4.9) and (4.10) then:

$$P_{QSM}(\boldsymbol{g} \rightarrow \widehat{\boldsymbol{g}} \mid \boldsymbol{H}) \tag{4.11}$$

$$P_{QSM}(d_g \rightarrow d_{\hat{g}} \mid \boldsymbol{H}) = Q(\sqrt{\zeta}) \tag{4.12}$$

where $Q(\beta)$ denotes the Q-function given as $Q(\beta) = \int_{\beta}^{\infty} \frac{1}{2\pi} e^{-\frac{t^2}{2}} dt$,

$$d_g = \|\boldsymbol{g}\|_F^2 - 2\Re\{\boldsymbol{y}^H \boldsymbol{g}\} \tag{4.13}$$

and ζ is an exponential random variable given by:

$$\zeta = \frac{1}{2N_o} \|\boldsymbol{g} - \widehat{\boldsymbol{g}}\|_F^2 \tag{4.14}$$

Let

$$A = \sqrt{\rho}\ \left[\ \Re(\boldsymbol{h}_{\ell_\Re} \widehat{\boldsymbol{x}}_\Re) - \Im(\boldsymbol{h}_{\ell_\Im} \widehat{\boldsymbol{x}}_\Im) - \Re(\widehat{\boldsymbol{h}}_{\ell_\Re} \widehat{\boldsymbol{x}}_\Re) + \Im(\widehat{\boldsymbol{h}}_{\ell_\Im} \widehat{\boldsymbol{x}}_\Im)\ \right]$$

$$B = \sqrt{\rho}\ \left[\ \Im(\boldsymbol{h}_{\ell_\Re} \widehat{\boldsymbol{x}}_\Re) + \Re(\boldsymbol{h}_{\ell_\Im} \widehat{\boldsymbol{x}}_\Im) - \Im(\widehat{\boldsymbol{h}}_{\ell_\Re} \widehat{\boldsymbol{x}}_\Re) - \Re(\widehat{\boldsymbol{h}}_{\ell_\Im} \widehat{\boldsymbol{x}}_\Im)\ \right]$$

such that (4.14) can be written as:

$$\zeta = \frac{1}{2N_o} |A + jB|^2 \tag{4.15}$$

Therefore, the average PEP for just one receive antenna (N_r = 1) is written as [59]:

$$\bar{P}_e(\boldsymbol{g}_n \rightarrow \widehat{\boldsymbol{g}}_n) = \frac{1}{2}\left(1 - \sqrt{\frac{\zeta}{2}\Big/1 + \frac{\zeta}{2}}\right) \tag{4.16}$$

To evaluate the average bit error probability (ABEP) of the QSM system, the asymptotic tight union bound given in (4.17) is used on assumption that $e_{n,k}$ is the number of bit errors associated with the corresponding PEP events.

$$P_b = \frac{1}{2^m}\sum_{n=1}^{2^m}\sum_{k=1}^{2^m}\frac{1}{m}\bar{P}_e(\boldsymbol{g}_n \rightarrow \widehat{\boldsymbol{g}}_k)e_{n,k} \tag{4.17}$$

Therefore, the average bit error rate (ABER) of QSM system can be written as:

$$\text{ABER} = \frac{1}{N_t^2 M}\sum_{n=1}^{2^m}\sum_{k=1}^{2^m}\frac{1}{m}e_{n,k} \times P_b \tag{4.18}$$

For N_r receive antennas, the instantaneous PEP is given by [59]:

$$P_e(\boldsymbol{g}_n \rightarrow \widehat{\boldsymbol{g}}_k) = Q\left(\sqrt{\sum_{k=1}^{N_r}\zeta_k}\right) \tag{4.19}$$

The average PEP can be written as [59]:

$$P_e(\boldsymbol{g}_n \rightarrow \widehat{\boldsymbol{g}}_k) = \gamma_\lambda^{N_r}\sum_{k=0}^{N_r-1}\binom{N_r-1+k}{k}[1-\gamma_\lambda]^k \tag{4.20}$$

where γ_λ is equivalent to $\bar{P}_e(\boldsymbol{g}_n \rightarrow \widehat{\boldsymbol{g}}_n)$ in (4.16).

Ignoring the higher order terms of the Taylor series of (4.20) will give the asymptotic average PEP of the QSM system from which diversity gain of N_r is clearly obvious; and from this, we arrive at [59]:

$$\bar{P}_e(\boldsymbol{g}_n \rightarrow \widehat{\boldsymbol{g}}_k) = \frac{2^{N_r-1}\Gamma(N_r+0.5)}{\sqrt{\pi(N_r)!}}\left(\frac{1}{\bar{\zeta}}\right)^{N_r} \tag{4.21}$$

where Γ represents the incomplete gamma function.

4.5. Computational Analysis of QSM Receiver

The computational complexity of the QSM can be formulated in terms of complex multiplications involved in the detection process. To formulate the computational complexity of the QSM optimal detector, the complexity imposed by jointly detecting $\hat{\ell}_{\Re}, \hat{\ell}_{\Im}, \hat{\boldsymbol{x}}^{q\Re}$ and $\hat{\boldsymbol{x}}^{q\Im}$ is analysed. Upon inspection, (4.9) can further be simplified and expressed as $\boldsymbol{G}$, given in (4.22) as:

$$\boldsymbol{G} = \sqrt{\rho/\mu}\left(\left(\boldsymbol{h}_{\ell_{\Re}}\boldsymbol{x}_{\ell_{\Re}}^{q\Re}\right) - j\left(\boldsymbol{h}_{\ell_{\Im}}\boldsymbol{x}_{\ell_{\Im}}^{q\Im}\right)\right) \tag{4.22}$$

putting (4.22) in (4.10) yields:

$$\left[\hat{\ell}_{\Re}, \hat{\ell}_{\Im}, \hat{x}^{q\Re}, \hat{x}^{q\Im}\right] = \underset{\ell_{\Re},\ell_{\Im},\boldsymbol{x}^{q\Re},\boldsymbol{x}^{q\Im}}{\operatorname{argmin}} \|\boldsymbol{G}\|_F^2 - 2\Re\{\boldsymbol{y}^H\boldsymbol{G}\} \tag{4.23}$$

Such that $\|\boldsymbol{G}\|_F^2$ in (4.23) can be expanded to yield:

$$\|\boldsymbol{G}\|_F^2 = \sqrt{\rho/\mu}\left\|\boldsymbol{h}_{\ell_{\Re}}\right\|_F^2\left|x_{\ell_{\Re}}^{q\Re}\right|^2 + \sqrt{\rho/\mu}\left\|\boldsymbol{h}_{\ell_{\Im}}\right\|_F^2\left|x_{\ell_{\Im}}^{q\Im}\right|^2 \tag{4.24}$$

Putting (2.22) and (2.24) back in (2.23), we obtain;

$$\left[\hat{\ell}_{\Re}, \hat{\ell}_{\Im}, \hat{x}^{q\Re}, \hat{x}^{q\Im}\right] = \underset{\ell_{\Re},\ell_{\Im},x^{q\Re},x^{q\Im}}{\operatorname{argmin}} [K] \tag{4.25}$$

where

$$K = \sqrt{\rho/\mu}\left\|\boldsymbol{h}_{\ell_{\Re}}\right\|_F^2\left|x_{\ell_{\Re}}^{q\Re}\right|^2 + \sqrt{\rho/\mu}\left\|\boldsymbol{h}_{\ell_{\Im}}\right\|_F^2\left|x_{\ell_{\Im}}^{q\Im}\right|^2 - 2\Re\left\{\boldsymbol{y}^{\mathrm{H}}\boldsymbol{h}_{\ell_{\Re}}x_{\ell_{\Re}}^{q\Re}\right\} - 2\Re\left\{\boldsymbol{y}^{\mathrm{H}}\boldsymbol{h}_{\ell_{\Im}}x_{\ell_{\Im}}^{q\Im}\right\}$$

The computational complexity of the QSM detector is evaluated based on (4.25) as the total complexities imposed by the joint detection of $\hat{\ell}_{\Re}, \hat{\ell}_{\Im}, \hat{x}^{q\Re}$ and $\hat{x}^{q\Im}$, in terms of complex multiplications and the overall computational complexity is estimated and given as:

$$CC_{\mathrm{QSM}} = c(6N_r + 2M) + 2M \tag{4.26}$$

We note that in [36], the estimation of the overall number of real multiplications and divisions needed for the joint detection of $\hat{\ell}_{\Re}, \hat{\ell}_{\Im}, \hat{x}^{q\Re}$ and $\hat{x}^{q\Im}$ in QSM was given as $CC_{\text{QSM}} = 8N_r 2^m$. It was thereafter noted that the receiver complexity of QSM is equivalent to that of SM as presented in [29], [33] and [43]. The improvements observed in QSM in terms of spectral efficiency and error performance are therefore achieved at almost no cost.

4.6. Simulation Results and Discussion

Simulation results of the error performances of QSM are presented in this section. Comparisons of its error performances are made with SM system, under the same/different spectral efficiencies and similar/different antenna configurations. For all results, simulations have been made under a Rayleigh flat-fading MIMO channels with i.i.d. entries distributed according to *CN*(0,1), and in the presence of AWGN. The results are therefore presented in terms of BER as a function of the SNR. While all simulations are terminated at a BER of 10^{-6}, we have carefully employed 2 and 4 antennas at the receiver and different numbers of transmit antennas are used to obtain different spectral efficiencies of 6 and 8 bits/s/Hz.

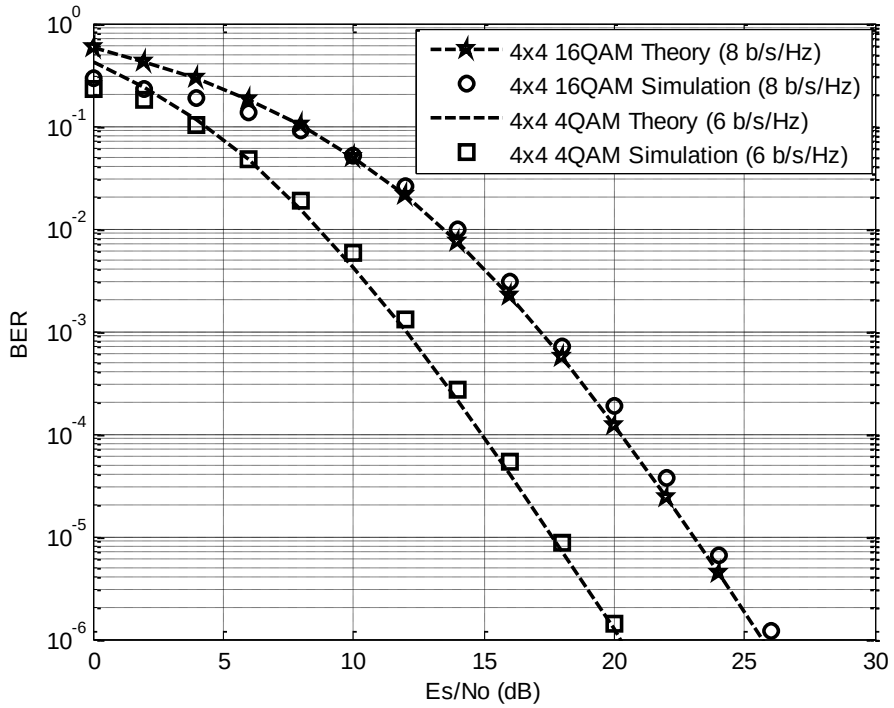

Figure 4.2: Comparison of BER performance of QSM systems with spectral efficiencies of 6 and 8 b/s/Hz using 4×4 MIMO configurations

In Figure 4.2., we present the simulation results for error performance of QSM systems with spectral efficiencies of 6 and 8 b/s/Hz together with their theoretical/analytical results. It was confirmed that a 4×4 4QAM and 4×4 16QAM QSM system configurations would transmit 6 and 8 b/s/Hz, respectively. This is in accordance with the QSM mapping rule given in Section 4.2. The computed upper bound approach of the performance analysis presented in Section 4.4 was used to validate the simulation results of the QSM system which shows little variations at lower SNR.

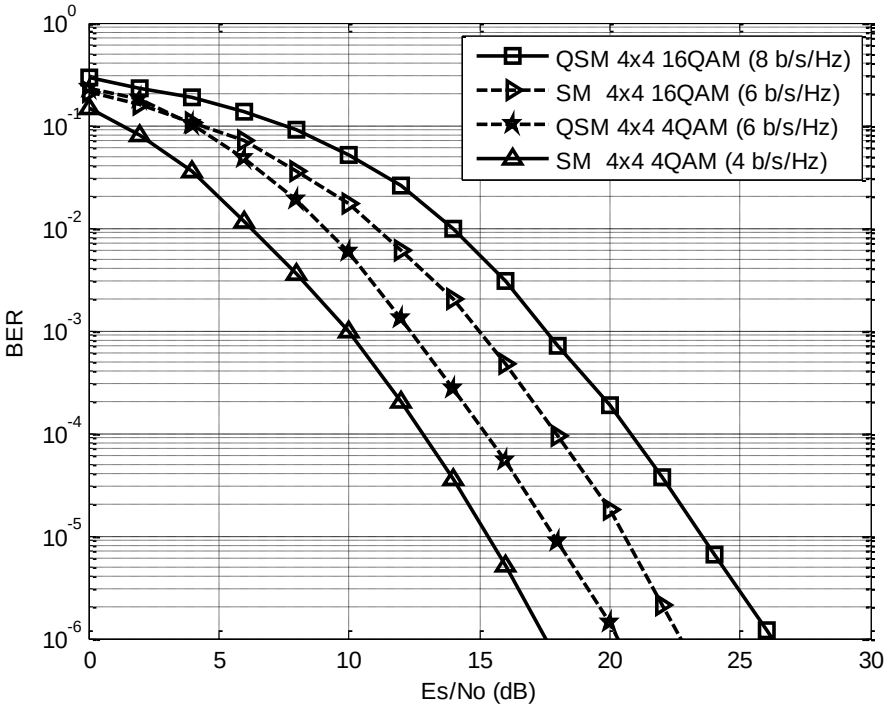

Figure 4.3.: Comparison of BER performances of QSM and SM systems with 4×4 transceiver using M = 4 and M = 16, using 4×4 MIMO configurations

Figure 4.3 aims to compare the error performances of QSM and SM using 4×4 transceiver configurations with the modulation order M = 4 and M = 16. In both cases, the SM systems outperform their QSM counterparts, with approximately 2.6 dB and 3.5 dB SNR gains for M = 4 and M = 16, respectively, at a BER of 10^{-6}. However, it is evident that these SM systems lack good spectral efficiencies compared to their QSM counterparts, when the same hardware configurations are employed. For example, with 4×4 16QAM configurations, QSM system has a spectral efficiency of 8 b/s/Hz as against 6 b/s/Hz that is achievable in SM system. In a similar way, QSM system achieves a spectral efficiency of 6 b/s/Hz, while SM system has a spectral efficiency of 4 b/s/Hz with 4×4 4QAM configurations. It therefore

means that, given the same hardware/antenna configuration, the QSM scheme enhances the spectral efficiency of SM system, while the SM is superior in error performance.

Meanwhile, a second look at Figure 4.3 shows that, with 4×4 transceiver configuration, and at a target transmission rate of 6 b/s/Hz, the QSM system is better than the SM in error performance. For example, at a BER 10^{-6}, the 4×4 4QAM QSM achieves approximately 2.3 dB SNR gain over the 4×4 16QAM SM system. In addition, the modulation order involved in the SM is higher than in QSM, resulting in relatively higher complexity at the SM receiver. It is therefore appropriate to say that, under the conditions of the same spectral efficiencies and same transceiver configurations, the QSM is better than the SM system both in error performance and receiver complexity.

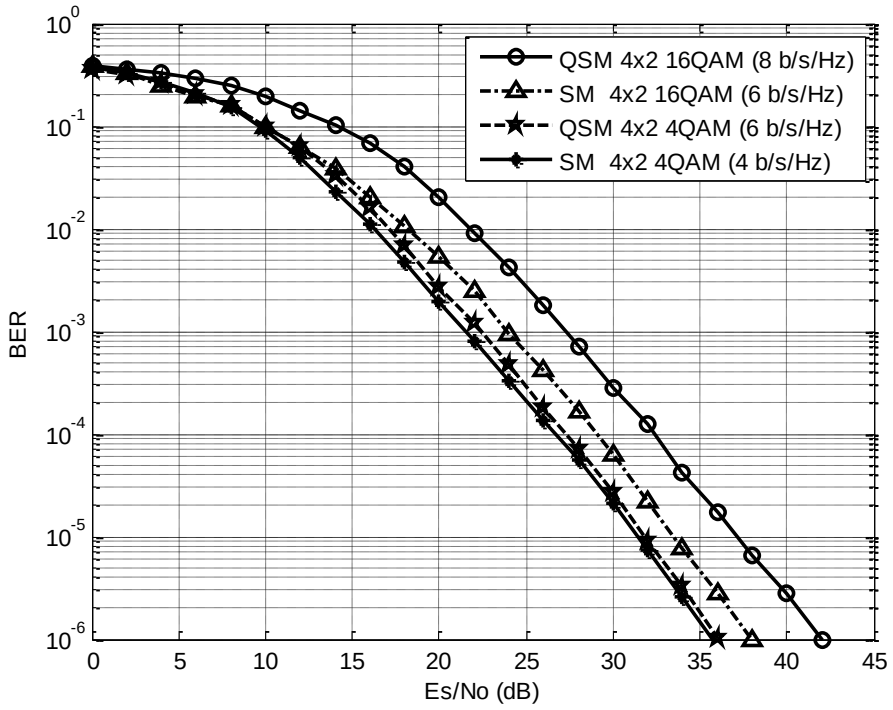

Figure 4.4: Comparison of BER performances of QSM and SM systems with 4×2 transceiver using M = 4 and M = 16

Again, we present the error performances of SM and QSM systems in Figure 4.4. Like what we obtained in Figure 4.3., 4QAM and 16QAM are employed, but this time with N_r = 2. Under these configurations, once again, the SM systems outperform the QSM systems. At a BER of 10^{-6}, the 6 bits SM system achieved the 4.0 dB over 8 bits QSM system. Furthermore, the 4 bits SM achieved 0.5 dB compared to the 6 bits QSM system at the same

BER. We infer therefore that, given the same antenna configuration, the QSM scheme has improved spectral efficiency compared to SM system. Meanwhile, with N_r = 2, both systems show worse error performances compared to N_r = 4 (as obtained in Figure 4.3).

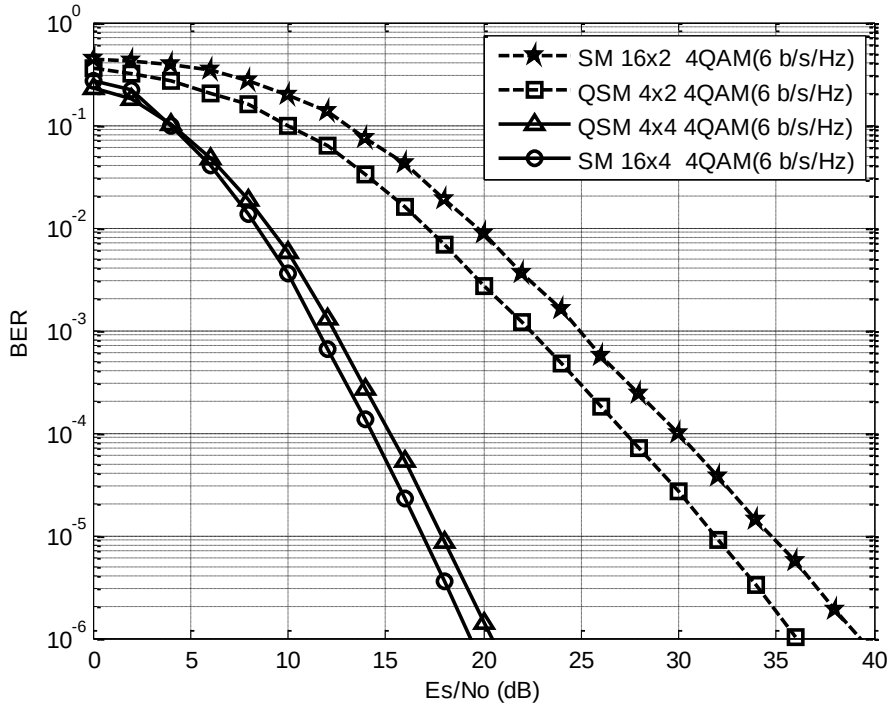

Figure 4.5: Comparison of BER performances of 6 b/s/Hz systems
for QSM and SM with M = 4 using N_r = 2 and N_r = 4

In Figure 4.5., we target a 6 b/s/Hz transmission rate using 4QAM for both QSM and SM systems with N_r = 2 and N_r = 4. With N_r = 4, the error superiority of SM over QSM system is about 1.0 dB SNR gain at a BER of 10^{-6}. However, the SM system would require N_t= 16 to achieve an SNR gain that is as small as 1.0 dB over the QSM system that requires N_t= 4. When N_r = 2, QSM system outperforms the SM system with approximately 3.0 dB SNR gain at a BER of 10^{-6}, even though the SM system still required N_t= 16 as against N_t= 4 in QSM. It, therefore, means that SM systems would require exponentially large number of transmit and receive antennas in order to compete with QSM system for the same error performances and spectral efficiencies.

Finally, the error performances of 4 b/s/Hz SM, SSK and Bi-SSK systems are compared to that of QAM system of the same spectral efficiency. Note that all of the systems are configured to employ N_r = 4 at the receiver. With the same spectral efficiency of 4 b/s/Hz,

the SM system outperformed the rest; requiring 17.6 dB SNR at a BER of 10^{-6}. This is just 0.2 dB better than the error performance of the SSK system. Again, the SM system outperform the QSM by approximately 1.6 dB SNR while it also has approximately 1.8 dB SNR gain over the Bi-SSK system. However, the QSM system would 2 transmit antennas, which happens to be the least required among the four systems. Both the SM and Bi-SSK system require 4 transmit antennas, while 16 antennas are required by the SSK system at the transmitter. Provided that all these systems are subjected to the same condition of transmitting at the rate of 4 b/s/Hz, we can conclude that the QSM system is economically more effective with the lowest cost of deploying transmit antenna array; while the SM and Bi-SSK systems will be suitable in terms of link reliability.

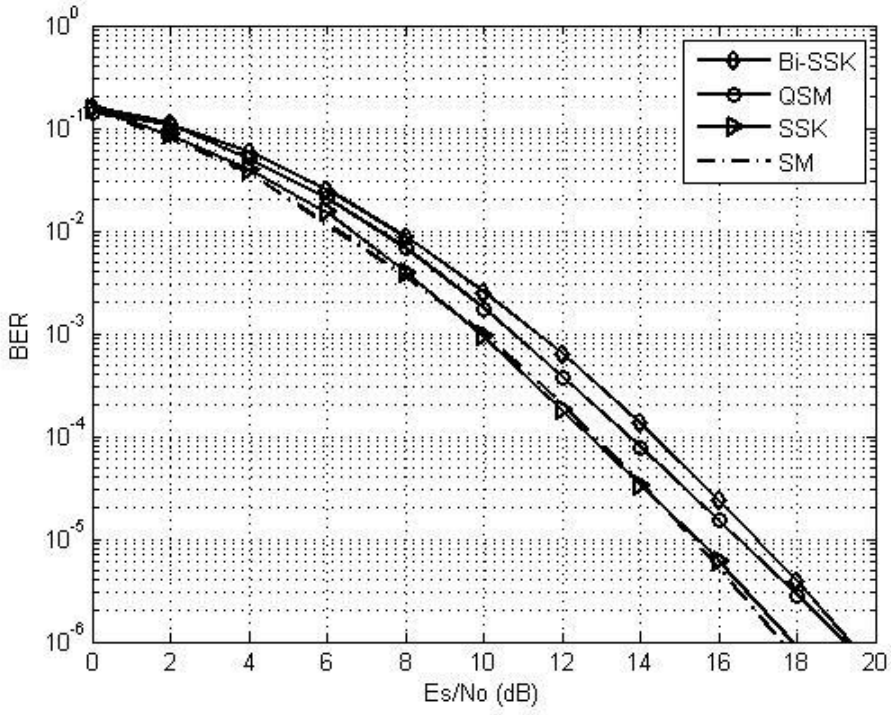

Figure 4.6: Comparison of BER performances of 4 b/s/Hz SM, SSK, Bi-SSK and QSM systems with N_r = 4

4.7. Conclusion

The QSM is able to improve on the overall spectral efficiency of the SM scheme. In addition, the QSM is better than the SM system both in error performance as well as in receiver complexity, under the conditions of the same spectral efficiencies. Meanwhile, to match the spectral efficiency of the QSM, SM system would need multiples of N_t required in QSM. It is noteworthy that these qualities are achieved in QSM at no additional computational complexity compared to SM.

Chapter 5

Soft-output Detection for SSK and Bi-SSK

5.1. Introduction

It is desired that the next generation communication systems provide users with high data rates, in addition to ensuring reliability and power efficiency. This is achievable, but with error control as a major challenge in the course of reproducing the transmitted information at the receiver [60]. Shannon provided a solution to this by properly encoding the information bits prior to transmission. Transmissions that strictly obey Shannon's Law can effectively reduce errors, induced by noise and unreliable channels, without any sacrifice of the transmission rate [10]. In practice, therefore, the majority of communication systems employ coding. Following the ground-breaking work of Shannon in [60], a number of encoding and decoding methods have evolved to control errors in noisy and unreliable communication channels.

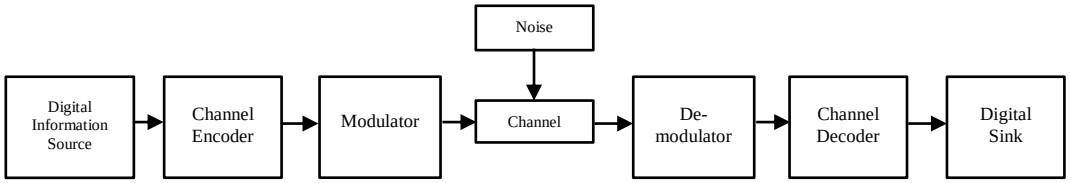

Figure 5.1: Basic block diagram of a typical coded system [10]

FEC codes, such as block codes and convolutional codes, are popular techniques used for channel coding. A typical coded system is illustrated in Figure 5.1. In this chapter of the dissertation, one of the objectives is to extend the FEC codes (as discussed in Sub-section 1.1.1.) to two of the transmit antenna index modulation-based schemes (i.e. SSK and Bi-

SSK) with an aim to achieve coding gains, in terms of error performance. However, achieving larger SNR gains would require a soft-output detector to be coupled with a soft-input decoder, for processing the signals at the receiver. Hence, another objective of this chapter is to develop receiver configurations for SSK and Bi-SSK that will perform soft-output ML detection (SOMLD).

Few authors, in literature, have employed the use of SOMLD in their works, over the years. One of the available ones (i.e SM-SOMLD scheme proposed in [37]) has already been studied in Chapter 2. In [55], SOMLD was extended to demodulate an hybrid system of SM and space-time block coding, STBC [61], called STBC-SM [62] that takes advantage of the benefits of both while avoiding their drawbacks. The SOMLD-STBC-SM [55], yields a significant improvement over the conventional STBC-SM [62]. Currently, there has been no literature which documents the SOMLD scheme for the SSK and Bi-SSK systems. Motivated by the good error performance of SM-SOMLD [37] under coded channel conditions and the superior performance of SOMLD-STBC-SM [55], we therefore extend the concept of SOMLD to SSK and Bi-SSK schemes.

5.2. Soft-Output ML Detection for SSK

In this section, we propose a SOMLD detector for SSK. It should be recalled that SSK scheme is discussed comprehensively in Chapter 3. Its key idea of transmission involves using the spatial dimension to convey information in the absence of an APM symbol. It was evidently confirmed that SSK exhibits the fundamental advantages of SM in addition to; lowered detection complexity for identical performance to SM, a simpler structure that provides easier integration with communication systems, and reduced hardware complexity. These qualities add to the motivation behind our proposal of a soft-output detector for SSK (i.e. SSK-SOMLD).

We employ a $1/2$ rate convolutional encoder with constraint length 9 and code generator matrixes [$g_1 = (561)_o$; $g_2 = (753)_o$], to encode the information bits. This is done to allow the proposed SSK-SMOLD obtain an improved error performance. The channel encoder is placed next to the source (refer to Figure 3.1) such that it accepts information bits from the source and gives codewords as output. The coded sequence is transmitted by SSK modulation such that the input to our proposed demodulator is given similar to (3.2) as:

$$\boldsymbol{y} = \sqrt{\rho}\boldsymbol{H}\boldsymbol{x}_{\ell} + \boldsymbol{w} = \sqrt{\rho}\boldsymbol{h}_{\ell} + \boldsymbol{w} \tag{5.1}$$

where $\boldsymbol{H}$ and $\boldsymbol{w}$ are as defined earlier; and ρ is the transmitted signal energy for each code bit.

The soft output detection is based on (5.1), by computing the a-posteriori log-likelihood ratio (LLR) for the transmit antenna index which we define as the logarithm of the joint probability of the received signal $\boldsymbol{y}$, conditioned on the transmitted bit sequences $\boldsymbol{x}_{\ell}$ (of paths with '1' and '0' bits respectively). The essence of making a decision between the two ('1' and '0') paths is to select the one with larger metric. This maximizes the probability of a correct decision, or, equivalently, minimizes the probability of error for the sequence of information bits.

The presence of (i) an uncorrelated and equally likely antenna indices (ii) an equally likely set of antenna bits, and (iii) N_t transmit antenna elements at the transmitter; are generally assumed. Hence, the a-posteriori LLR for the a$^{\text{th}}$ transmit antenna bit can be expressed as:

$$LLR(\ell^a) = \log\frac{P(\ell^a = 1 \,|\, \boldsymbol{y})}{P(\ell^a = 0 \,|\, \boldsymbol{y})} \tag{5.2}$$

$$= \log\left[\frac{\sum_{\hat{\ell}\in \ell_1^a} P(\boldsymbol{y} \,|\, \ell = \hat{\ell})}{\sum_{\hat{\ell}\in \ell_0^a} P(\boldsymbol{y} \,|\, \ell = \hat{\ell})}\right] \tag{5.3}$$

where ℓ_1^a and ℓ_0^a are vectors of the antenna indices with '1' and '0' at the a$^{\text{th}}$ antenna bit, respectively.

On application of the Bayes' theorem, the demodulator output in (5.3) can be described statistically by the PDF, such that the a$^{\text{th}}$ transmit antenna bit is expressed as:

$$LLR(\ell^a) = \log\left[\frac{\sum_{\hat{\ell}\,\epsilon\,\ell_1^a} \exp\frac{-\|\boldsymbol{y}-\sqrt{\rho}\boldsymbol{h}_{\ell}\|^2}{2\sigma^2}}{\sum_{\hat{\ell}\,\epsilon\,\ell_0^a} \exp\frac{-\|\boldsymbol{y}-\sqrt{\rho}\boldsymbol{h}_{\ell}\|^2}{2\sigma^2}}\right] \tag{5.4}$$

where σ^2 is the variance of the AWGN, $\boldsymbol{w}$.

As the name suggests, the outputs of the proposed detector are real (soft) numbers; unlike the optimal ML detector for SSK whose outputs are integers (1's and 0's). For the proposed detector to achieve the target improvement in error performance, it was earlier motivated that; in addition to channel coding, the proposed soft-output detector would require a soft-input decoder for processing the signals at the receiver. On this note, the soft output of our proposed demodulator, given in (5.4), is fed into a soft-input Viterbi channel decoder and an estimate of the transmitted message is obtained.

5.3. Computational Complexity of SSK-SOMLD

The computational complexity of the SSK-SOMLD may be formulated in terms of complex multiplications involved in the detection processes. Importantly, the computation of the logarithm functions present in the LLRs of the proposed soft-output detectors must be considered so as to determine their contributions to the total complexities of the detectors. In this dissertation, we assume that the computation of the logarithm functions are approximated via the use of LUT based method presented in [56], and therefore impose no additional complexity.

To formulate the computational complexity of the SSK-SOMLD, the complexity imposed by detecting the a$^{\text{th}}$ real antenna bit is analysed. Upon inspection, (5.4) can further be expressed as:

$$LLR(\ell^a) = \log\left[\frac{\sum_{\hat{\ell} \in \ell_1^a} \exp\frac{-\sqrt{\rho}\|\boldsymbol{h}_\ell\|_F^2 - 2\Re\{\boldsymbol{y}^{\mathrm{H}}\boldsymbol{h}_\ell\}}{2\sigma^2}}{\sum_{\hat{\ell} \in \ell_0^a} \exp\frac{-\sqrt{\rho}\|\boldsymbol{h}_\ell\|_F^2 - 2\Re\{\boldsymbol{y}^{\mathrm{H}}\boldsymbol{h}_\ell\}}{2\sigma^2}}\right] \tag{5.5}$$

The computation of $\|\boldsymbol{h}_\ell\|_F^2$ is equivalent to $\boldsymbol{h}_\ell{}^H\boldsymbol{h}_\ell$ and requires N_r complex multiplications for each $\hat{\ell}$. Considering the numerator of (5.5), $\|\boldsymbol{h}_\ell\|_F^2$ for $\hat{\ell} \in \ell_1^a$ requires a total of $N_r(\frac{N_t}{2})$ complex multiplications. It is evident that $\|\boldsymbol{h}_\ell\|_F^2$ would require $N_r(\frac{N_t}{2})$ complex multiplications at the denominator of (5.5) for $\hat{\ell} \in \ell_0^a$. As mentioned earlier, the computation of the logarithm functions present in the LLRs of the proposed soft-output

detectors can be ignored since a LUT-based method [56] has been assumed to approximate the functions. We also assume that computational results can be stored and reused in order to avoid redundancy.

On this note, the summation of complex multiplications at both numerator and denominator gives the total computational complexity of the SSK-SOMLD, which can be evaluated and expressed as:

$$CC_{\text{SSK-SOMLD}} = \; N_r N_t \tag{5.6}$$

By inspection, the computational complexity of the SSK-SOMLD given is (5.6) is similar to that of the SSK-HDMLD given in (3.12), as $N_t = M$ in the SSK scheme. On this note, we conclude that the proposed SSK-SOMLD detector imposes no additional complexity compared to the conventional SSK-HDMLD. In Section 5.6, we present the numerical evaluation and discussion of the error performance of the SSK-SOMLD detector in comparison to the SSK-HDMLD.

5.4. Soft-Output ML Detection for Bi-SSK

Bi-SSK, like the SSK, has been discussed in Chapter 3. It is an extension of the SSK, where dual antenna indices are employed to convey information from the source to destination. The Bi-SSK technique results in twice the achievable data rate of SSK, in addition to preserving major advantages of SSK. It must be recalled that the Bi-SSK modulation is also done without any APM symbol, and so, the task of the receiver is to detect only the two antenna indices. The numerous advantages of Bi-SSK as a modulation scheme add to our motivation of proposing a soft-output detector for it.

The source information stream is fed into a $1/2$ rate convolutional encoder with constraint length 9 and code generator matrixes $g_1 = (561)_o;\; g_2 = (753)_o$. This is done to allow the proposed Bi-SSK-SOMLD obtain an improved error performance. The channel encoder is placed next to the source (refer to Figure 3.2) and gives encoded bits as output. The encoded bits are mapped for Bi-SSK modulation and transmission occurs afterwards such that:

$$\boldsymbol{y} = \sqrt{\rho/\mu}\,\boldsymbol{x}_{\text{Bi-SSK}} + \boldsymbol{w} = \sqrt{\rho/\mu}\,(\boldsymbol{h}_{\ell_{\Re}} + j\boldsymbol{h}_{\ell_{\Im}}) + \boldsymbol{w} \tag{5.7}$$

where $\boldsymbol{H}$ and $\boldsymbol{w}$ are as defined earlier; and ρ/μ is the transmitted signal energy for each code bit.

At the receiver, the proposed demodulator independently calculates the LLR for the real and imaginary antenna indices bits using the received coded Bi-SSK signal of (5.7). The a-posteriori log-likelihood ratio (LLR), defined as the logarithm of the joint probability of the received signal $\boldsymbol{y}$, conditioned on the transmitted bit sequences $\boldsymbol{x}_{\text{Bi-SSK}}$ (of paths with '1' and '0' bits, respectively), is computed independently for a$^{\text{th}}$ real transmit antenna bits and a$^{\text{th}}$ imaginary transmit antenna bits. The reason for making the decision between two ('1' and '0') paths is to select the one with larger metric so as to maximize the probability of a correct decision, or, equivalently, minimize the probability of error for the sequence of information bits.

The presence of (i) an uncorrelated and equally likely antenna indices that consist of real and imaginary antenna bits (ii) an equally likely set of real antenna bits, and (iii) N_t transmit antenna elements at the transmitter, are generally assumed. Therefore, the a-posteriori LLR for the a$^{\text{th}}$ real transmit antenna bit can be expressed mathematically as:

$$LLR(\ell_{\Re}^{a}) = \log\frac{P(\ell_{\Re}^{a} = 1|y)}{P(\ell_{\Re}^{a} = 0|y)} \tag{5.8}$$

$$= \frac{\sum_{\hat{\ell}_{\Re}\in\ell_{1_{\Re}}^{a}} P(y \mid \ell_{\Re} = \hat{\ell}_{\Re}, \ell_{\Im} = \hat{\ell}_{\Im}) P(\ell_{\Re} = \hat{\ell}_{\Re})}{\sum_{\substack{\hat{\ell}_{\Re}\in\ell_{0_{\Re}}^{a} \\ \hat{\ell}_{\Im}\in\ell}} P(y \mid \ell_{\Re} = \hat{\ell}_{\Re}, \ell_{\Im} = \hat{\ell}_{\Im}) P(\ell_{\Re} = \hat{\ell}_{\Re})} \tag{5.9}$$

where $\ell_{0_{\Re}}^{\text{a}}$ and $\ell_{1_{\Re}}^{\text{a}}$are vectors of the real antenna indices with '0' and '1' at the a$^{\text{th}}$ antenna bits, respectively.

On application of the Bayes' theorem, the demodulator output in (5.9) can be described statistically by the PDF, such that the a$^{\text{th}}$ real transmit antenna bit is expressed as:

$$LLR(\ell_{\Re}^{a}) = \log\left[\frac{\sum_{\hat{\ell}_{\Re}\in\ell_{1_{\Re}}^{a},\hat{\ell}_{\Im}\in\ell}\exp(A)}{\sum_{\hat{\ell}_{\Re}\in\ell_{0_{\Re}}^{a},\hat{\ell}_{\Im}\in\ell}\exp(B)}\right] \tag{5.10}$$

where $A = B = \frac{-\|\boldsymbol{y}-\sqrt{\rho/\mu}(\boldsymbol{h}_{\ell_{\Re}}+j\boldsymbol{h}_{\ell_{\Im}})\|^{2}}{2\sigma^{2}}$ such that σ^{2} is the variance of the AWGN $\boldsymbol{w}$.

In the same vein, the a-posteriori LLR for the a$^{\text{th}}$ imaginary transmit antenna bit can be expressed mathematically as:

$$LLR(\ell_{\Im}^{a}) = \log\frac{P(\ell_{\Re}^{a}=1|\boldsymbol{y})}{P(\ell_{\Re}^{a}=0|\boldsymbol{y})} \tag{5.11}$$

$$LLR(\ell_{\Im}^{a}) = \frac{\sum_{\hat{\ell}_{\Im}\in\ell_{1_{\Im}}^{a}}\sum_{\hat{\ell}_{\Re}\in\ell} P\left(\boldsymbol{y}\,|\ell_{\Re}=\hat{\ell}_{\Re},\ell_{\Im}=\hat{\ell}_{\Im}\right)P\left(\ell_{\Im}=\hat{\ell}_{\Im}\right)}{\sum_{\hat{\ell}_{\Im}\in\ell_{0_{\Im}}^{a}}\sum_{\hat{\ell}_{\Re}\in\ell} P\left(\boldsymbol{y}\,|\ell_{\Re}=\hat{\ell}_{\Re},\ell_{\Im}=\hat{\ell}_{\Im}\right)P\left(\ell_{\Im}=\hat{\ell}_{\Im}\right)} \tag{5.12}$$

$$LLR(\ell_{\Im}^{a}) = \log\left[\frac{\sum_{\hat{\ell}_{\Im}\in\ell_{1_{\Im}}^{a},\hat{\ell}_{\Re}\in\ell}\exp(A)}{\sum_{\hat{\ell}_{\Im}\in\ell_{0_{\Im}}^{a},\hat{\ell}_{\Re}\in\ell}\exp(B)}\right] \tag{5.13}$$

where $\ell_{0_{\Im}}^{a}$ and $\ell_{1_{\Im}}^{a}$are vectors of the imaginary antenna indices with '0' and '1' at the a^{th} antenna bits, respectively.

In is noted that the outputs of (5.10) and (5.13) are real (soft) numbers; unlike the optimal ML detector for SSK (3.5) whose outputs are integers (1's and 0's). Again, detection is performed by our proposed Bi-SSK-SOMLD for one bit at a time as against the joint detection employed (3.5). It was motivated earlier that; in addition to channel coding, larger SNR gain is possible if a soft-input decoder is coupled with our soft-output detector for processing the signals at the receiver. Consequently, to achieve the target improvement in error performance, the outputs of our proposed demodulator (5.10) and (5.13) are fed into a soft-input Viterbi channel decoder and an estimate of the transmitted message is obtained.

5.5. Computational Complexity of Bi-SSK-SOMLD

We formulate the computational complexity of the Bi-SSK-SOMLD in terms of complex multiplications involved in the detection processes. We note that the computation of the logarithm functions present in the LLRs of the proposed soft-output detectors is considered

to have no addition complexities on the total complexities of the proposed detector. This is in line with the use of LUT based method presented in [56].

To formulate the computational complexity of the Bi-SSK-SOMLD, the individual complexity imposed by each of the two detection processes of detecting the ath real antenna bits, and ath imaginary antenna bits are analysed. It is evident that (5.10) and (5.13) can be written, on expansion of the Frobenious norms, and expressed as:

$$LLR(\ell_{\Re}^{a}) = \log\left[\frac{\sum_{\hat{\ell}_{\Re}\in\ell_{1_{\Re}}^{a},\hat{\ell}_{\Im}\in\ell}\exp(C)}{\sum_{\hat{\ell}_{\Re}\in\ell_{0_{\Re}}^{a},\hat{\ell}_{\Im}\in\ell}\exp(D)}\right] \tag{5.14}$$

$$LLR(\ell_{\Im}^{a}) = \log\left[\frac{\sum_{\hat{\ell}_{\Im}\in\ell_{1_{\Im}}^{a},\hat{\ell}_{\Re}\in\ell}\exp(C)}{\sum_{\hat{\ell}_{\Im}\in\ell_{0_{\Im}}^{a},\hat{\ell}_{\Re}\in\ell}\exp(D)}\right] \tag{5.15}$$

where $C = D = \frac{\sqrt{\rho/\mu}\left\|\boldsymbol{h}_{\ell_{\Re}}\right\|_F^2 + \sqrt{\rho/\mu}\left\|\boldsymbol{h}_{\ell_{\Im}}\right\|_F^2 - 2\Re\left\{\boldsymbol{y}^H\boldsymbol{h}_{\ell_{\Re}}\right\} - 2\Re\left\{\boldsymbol{y}^H\boldsymbol{h}_{\ell_{\Im}}\right\}}{2\sigma^2}$

Based on (5.14) and (5.15), we evaluate the complexity imposed by the B-SSK-SOMLD on assumption that results can be stored for reuse in future, so as to avoid redundant computations. Considering the numerator of (5.14), the computation of the first term $\left\|\boldsymbol{h}_{\ell_{\Re}}\right\|_F^2$, is equivalent to $\boldsymbol{h}_{\ell_{\Re}}{}^H\boldsymbol{h}_{\ell_{\Re}}$ and requires N_r complex multiplications for each $\hat{\ell}$, such that $\left\|\boldsymbol{h}_{\ell_{\Re}}\right\|_F^2$ for $\hat{\ell}\,\epsilon\,\ell_1^a$ requires a total of $N_r\frac{N_t}{2}$ complex multiplications.

The second term would also require $N_r\frac{N_t}{2}$. Since this has already been computed for the first term, we assume that the second term imposes no additional complexity and the result of the first term is reused. The third term $-2\Re\{\boldsymbol{y}^H\boldsymbol{h}_{\ell_{\Re}}\}$, requires $2N_r\frac{N_t}{2}$ complex multiplications for $\hat{\ell}\,\epsilon\,\ell_1^a$. Evidently, the computation of the forth term $-2\Re\{\boldsymbol{y}^H\boldsymbol{h}_{\ell_{\Im}}\}$, requires $2N_r\frac{N_t}{2}$. The summation of these gives the total computational complexity imposed by the computation of the numerator of (5.14), which is expressed as $\delta_{numerator} = 2N_rN_t$. A proper observation of the denominator of (5.14) reveals that the denominator would impose a total complexity of $2N_rN_t$ complex multiplication which can be ignored because it has been pre-computed for the numerator. This simply implies that the detection of the ath

real antenna bit, as given in (5.14), imposes a total complexity of $2N_rN_t$ complex multiplications on the SSK-SOMLD receiver.

Using a similar approach, it can be shown that the computational complexity imposed by the estimation of the a$^{\text{th}}$ imaginary antenna bit ($\ell_{\Im}^{a}$), in (5.17) will not impose any further complexities as stored results can be reused in order to avoid redundant computations. As mentioned earlier, the computation of the logarithm functions can be ignored since a LUT-based method [56] has been assumed for approximating the functions. Consequently, the total computation complexity of our proposed Bi-SSK-SOMLD detector is given as:

$$CC_{\text{Bi-SSK-SOMLD}} = 2N_rN_t \tag{5.16}$$

By inspection, (5.18) is similar to (3.26); we conclude, therefore, that the proposed QSM-SOMLD detector imposes no additional complexity compared to the conventional QSM-HDMLD.

5.6. Simulation Results and Discussion

Results of investigation of the error performances of the proposed soft-output detectors for SSK and Bi-SSK schemes are presented in this section. These detectors have been investigated under coded and uncoded channel conditions different configurations of SSK and Bi-SSK systems. For all simulations, Rayleigh flat-fading MIMO channels with i.i.d. entries distributed according $CN(0,1)$ are assumed. The presence of AWGN is also assumed, and simulations are terminated at a bit error rate (BER) of 10^{-6}. The results obtained are in terms of the BER as a function of the SNR. In both systems, different transmit antenna configurations are employed to obtain spectral efficiencies of 2, 4 and 6 b/s/Hz.

In Figure 5.2, the error performances of the SSK-HDMLD and our proposed SSK-SOMLD detectors are evaluated in uncoded channel conditions. The closely matching curves, in pairs, show the HDMLD and the proposed SOMLD for all configurations considered. This no gain scenario is much expected and hence, we affirm that the soft-output detector has no effect, unless coupled with a soft-input decoder at the receiver, when channel coding is employed.

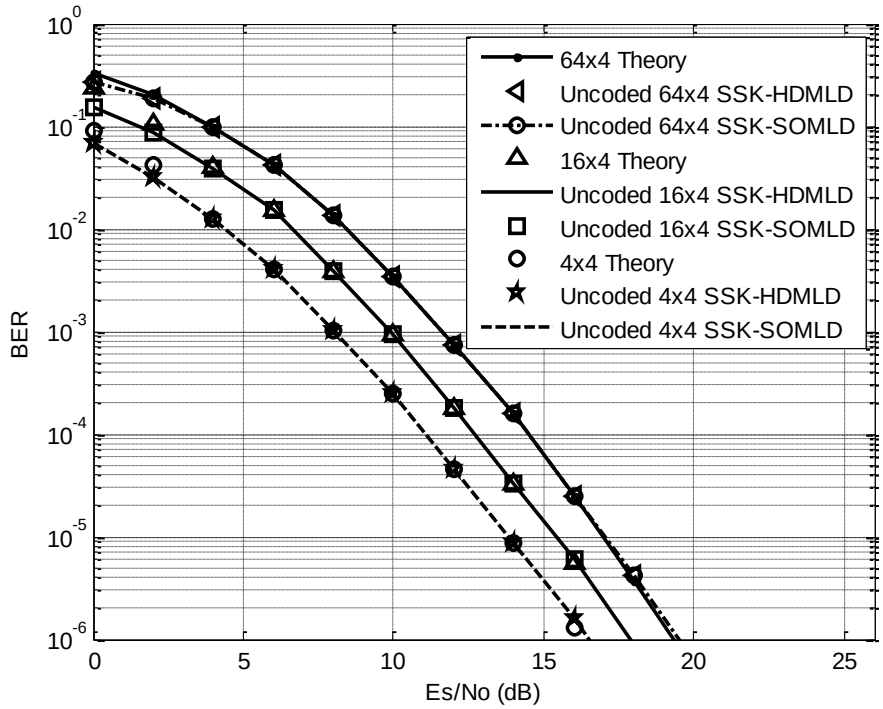

Figure 5.2: Comparison of BER performances of 2, 4 and 6 b/s/Hz SSK systems in uncoded channels using the proposed SOMLD and HDMLD (N_r = 4)

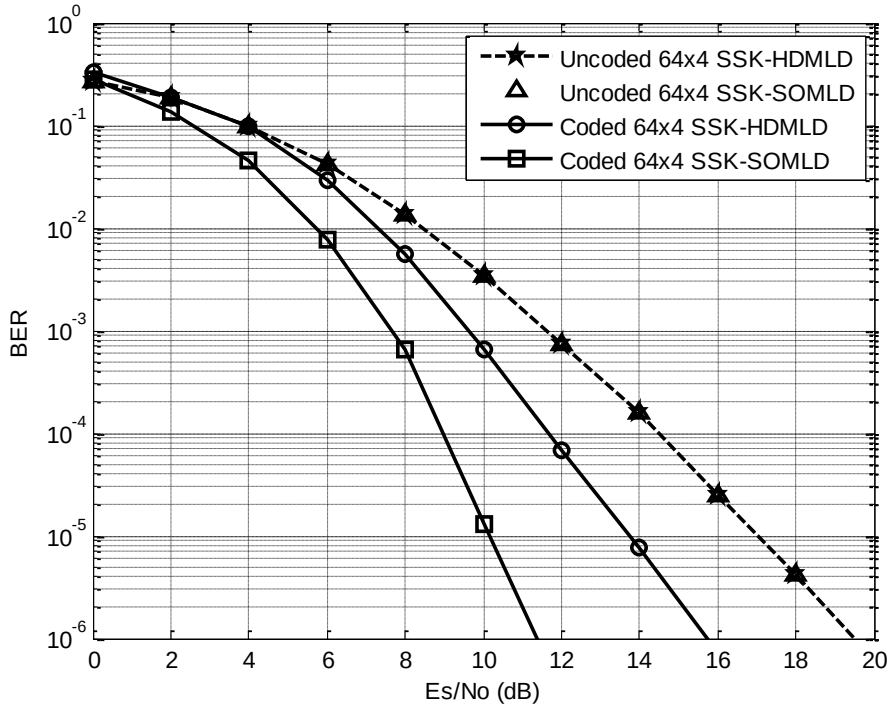

Figure 5.3: Comparison of BER performances for 6 b/s/Hz SSK system in coded and uncoded channels using 64×4 MIMO configuration

The error performances of a 6 bits/s/Hz 64×4 SSK systems with HDMLD and the proposed SOMLD detectors are depicted in Figure 5.3. We note quickly that, the SSK system with conventional HDMLD has been shown in Figure 5.2 to be closely matching the proposed SOMLD, in uncoded channels. Meanwhile, in coded channels, the proposed SOMLD for the 6 bits SSK system performs better than the HDMLD. For example at a BER of 10^{-6}, an SNR gain of approximately 4.3 dB is evident. Furthermore, the proposed coded SOMLD achieves 8.0 dB SNR gain over the uncoded conventional HDMLD scheme, at the same BER.

In Figure 5.4, we present the error performances for SSK of spectral efficiency of 4 b/s/Hz employing 16×4. It is evident that the coded SOMLD detector yields significant SNR gain. For example, at a BER of 10^{-6}, approximately 6.3 dB SNR gain is achieved by coded SOMLD compared to coded HDMLD. Furthermore, the coded SOMLD achieves 8.2 dB SNR gain over the uncoded HDMLD scheme, at the same BER.

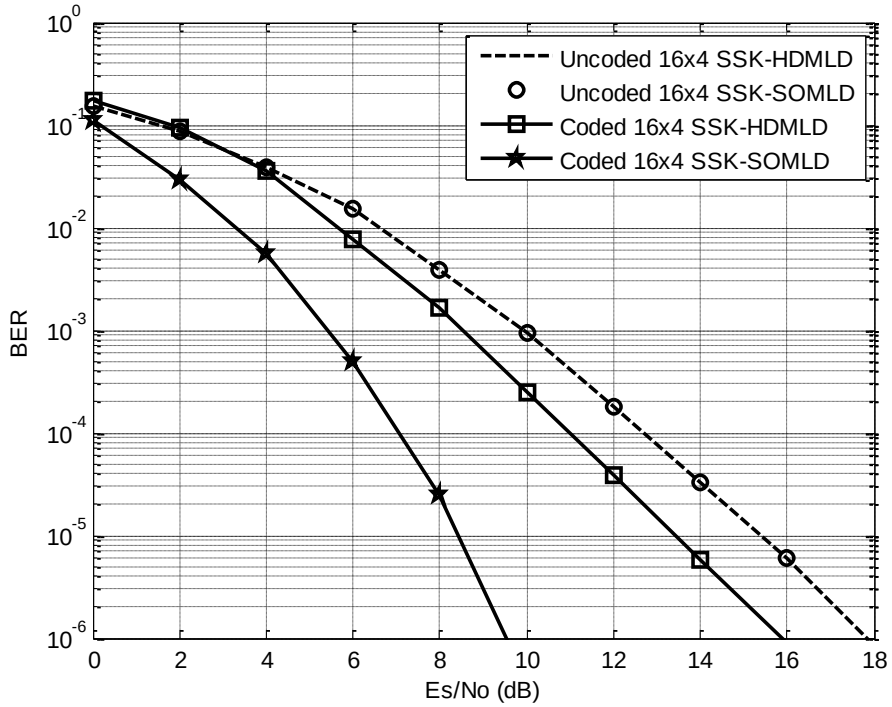

Figure 5.4: Comparison of BER performances for 4 b/s/Hz SSK system in coded and uncoded channels using 16×4 MIMO configuration

For Bi-SSK systems, the error performances of the HDMLD and SOMLD detectors are evaluated for uncoded channels, as depicted in Figure 5.5. As expected, the simulation results show that the proposed SOMLD scheme matches closely with the HDMLD for all the considered configurations. This means that the SOMLD has no effect under uncoded channel. Therefore, to achieve the target improvement, the soft-output detector, has to be coupled with a soft-input decoder at the receiver while channel coding is employed at the transmitter.

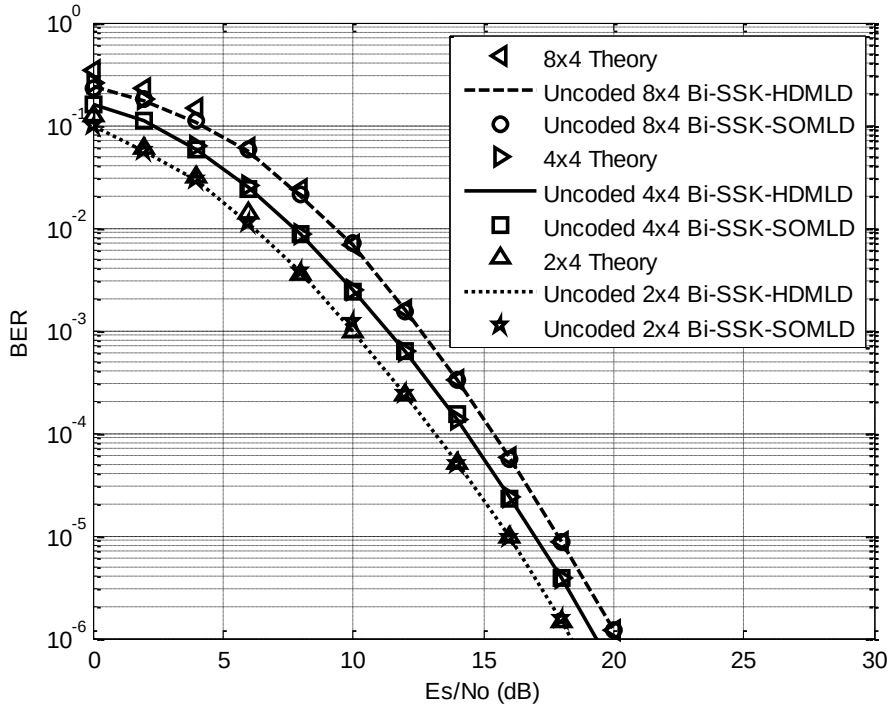

Figure 5.5: Comparison of BER performance of 2, 4 and 6 b/s/Hz Bi-SSK systems in uncoded channels using the proposed SOMLD and HDMLD (N_r = 4)

In Figure 5.6, the error performances of a 6 bits/s/Hz 8×4 Bi-SSK system with HDMLD and the proposed SOMLD schemes in uncoded and coded channels, are depicted. In coded channels, the SOMLD for Bi-SSK system performs better than the coded HDMLD. For example, at a BER of 10^{-6}, an SNR gain of approximately 4.2 dB is evident. Furthermore, the proposed SOMLD in coded channel achieves an SNR gain of 10.4 dB over the uncoded conventional HDMLD scheme, at the same BER.

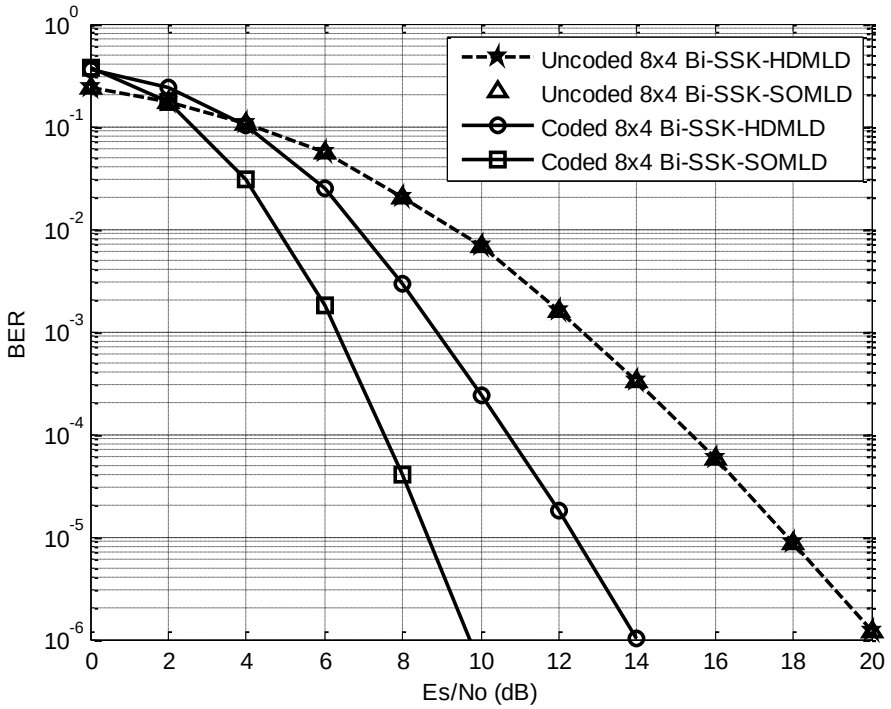

Figure 5.6: Comparison of BER performances for 6 b/s/Hz Bi-SSK system in coded and uncoded channels using 8×4 MIMO configuration

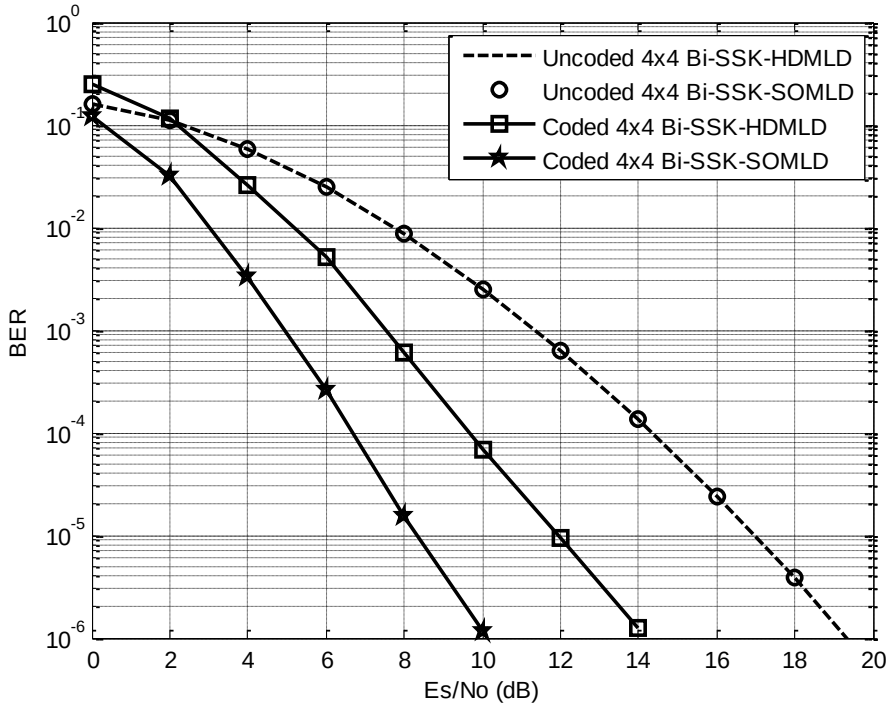

Figure 5.7: Comparison of BER performances for 4 b/s/Hz Bi-SSK system in coded and uncoded channels using 4×4 MIMO configuration

In Figure 5.7, we present the error performances for a spectral efficiency of 4 b/s/Hz employing 4×4, 4-ary Bi-SSK in coded and uncoded channels, using the proposed SOMLD and the HDMLD schemes. It is shown that the SOMLD detector yields significant SNR gain in coded channel by achieving approximately 4 dB SNR gain over HDMLD, at a BER of 10^{-6}. Furthermore, the proposed SOMLD in coded channel achieves an SNR gain of 9.2 dB over the uncoded HDMLD scheme, at a BER of 10^{-6}.

To summarize the improvements in error performances achieved by the proposed SOMLD detectors for SSK and Bi-SSK schemes, the SNRs gains for 4 and 6 b/s/Hz are tabulated in Table 5.1.

Table 5.1.: Summary of SNR gains of SOMLD compared to HDMLD for SSK and Bi-SSK schemes in coded channels

Detection Scheme	**SNR gains (at BER ≈ 10^{-6})**	
	4 bits/s/Hz	**6 bits/s/Hz**
Coded SSK-HDMLD	2.0 dB	4.3 dB
Coded Bi-SSK-HDMLD	5.1 dB	4.2 dB

5.7. Conclusion

In this chapter, we have proposed a SOMLD for SSK and Bi-SSK systems. For uncoded channels, the proposed detectors yield identical error performances as their respective HDMLD counterparts. However, when channel coding is employed, such that the soft-output detector is coupled with a soft-input channel decoder, significant SNR gains are achieved. The proposed soft-output detectors impose no additional computational complexity compared to the HDMLD.

Chapter 6

Soft-output Detection for QSM

6.1. Introduction

The QSM scheme has indeed demonstrated that high data transmission is achievable in wireless communication systems. It can be concluded, therefore, that QSM would be suitable for integration in the next generation communication systems. In addition to high data rate potential of QSM, the next generation communication systems aim at providing users with reliability and power efficiency. Research has shown that this is also achievable if errors, induced by noise and unreliable channels, can be controlled in the course of reproducing the transmitted information at the receiver [60]. To achieve this, in practice, the majority of communication systems employ channel coding. The basic block diagram of a typical coded system has been given in Figure 5.1.

In addition to channel coding, achieving larger SNR gain would require a soft-output detector coupled with a soft-input decoder, for processing the signals at the receiver. Such receivers have been identified in Chapter 5 as SOMLD. With an aim to achieve coding gains, in terms of error performance, the objectives of this chapter, therefore, are to extend the FEC codes (as discussed in Sub-section 1.1.1.) to QSM schemes as a member of the transmit antenna index modulation-based schemes, and also, develop a receiver configuration that will perform soft-output ML detection (SOMLD) on the coded QSM signal.

Few authors, [10], [37], and [55], have employed the use of SOMLD in their works, over the years. Currently, there has been no literature which documents the SOMLD scheme for the QSM system. Motivated by the good error performance of SM-SOMLD [37] under

coded channel conditions and the superior performance of SOMLD-STBC-SM [55], we hereby propose a soft-output ML detector (SOMLD) for the high spectral efficient QSM system (QSM-SOMLD).

6.2. Soft-Output ML Detection for QSM

QSM enhanced the overall throughput of SM, while the fundamental advantages of SM are retained. A detailed discussion of QSM has been presented in Chapter 4. In this section, we present a SOMLD for QSM. Before the QSM modulation, convolutional channel encoder, with constraint length 9 and code generator matrices $g_1 = (561)_o$; $g_2 = (753)_o$, is employed to encode the source information bits at the transmitter. The encoder is placed next to the source (refer to Figure 4.1) such that it accepts the source information bits as input and yields encoded bits as output, in accordance with the $1/2$ rate of the encoder. The encoded bits are then mapped for QSM modulation before transmission occurs over the wireless channel $\boldsymbol{H}$, whose entries are assumed to be i.i.d. with *CN*(0, 1) in the presence of AWGN $\boldsymbol{w}$.

This forms the input to our soft-output detector, which can be represented similar to (4.5) as:

$$\boldsymbol{y} = \sqrt{\rho/\mu}\left(\boldsymbol{h}_{\ell_{\Re}}\boldsymbol{x}_{\ell_{\Re}}^{q^{\Re}} + j\boldsymbol{h}_{\ell_{\Im}}\boldsymbol{x}_{\ell_{\Im}}^{q^{\Im}}\right) + \boldsymbol{w} \tag{6.1}$$

where $\boldsymbol{H}$ and $\boldsymbol{w}$ are as defined earlier; and ρ/μ is the transmitted signal energy for each code bit.

At the receiver, the proposed demodulator independently calculates the LLR for the a$^{\text{th}}$ real antenna bit (i.e. $\ell_{\Re}^{a}$), a$^{\text{th}}$ imaginary antenna bit (i.e. $\ell_{\Im}^{a}$), b$^{\text{th}}$ real symbol bit (i.e. $x_{\Re}^{b}$), and b$^{\text{th}}$ imaginary symbol bit (i.e. $x_{\Im}^{b}$), from the received coded QSM signals given in (6.1). The a-posteriori log-likelihood ratio (LLR) is defined as the as the logarithm of the joint probability of the received signal $\boldsymbol{y}$, conditioned on the transmitted bit sequences $\boldsymbol{x}_{\text{QSM}}$ (of paths with '1' and '0' bits, respectively). This is computed independently for $\ell_{\Re}^{a}$, $\ell_{\Im}^{a}$, $x_{\Re}^{b}$ and $x_{\Im}^{b}$, respectively. The reason for making the decision between two ('1' and '0') paths is to select the one with larger metric, which results in maximizing the probability of a correct decision, or, equivalently, minimizing the probability of error for the sequence of information bits.

Generally, the presence of (i) an uncorrelated and equally likely antenna indices that consist of real and imaginary antenna bits, (ii) an independent and uncorrelated data symbols that consist of real and imaginary data bits, and (iii) N_t transmit antenna elements at the transmitter, are assumed. Based on (6.1), the a-posteriori LLR for the a$^{\text{th}}$ real transmit antenna bit can be expressed mathematically as:

$$LLR(\ell_{\Re}^{a}) = \log \frac{P(\ell_{\Re}^{a} = 1|\boldsymbol{y})}{P(\ell_{\Re}^{a} = 0|\boldsymbol{y})} \tag{6.2}$$

$$= \log \left[\frac{\sum_{\substack{\hat{\ell}_{\Re} \in \ell_{1\Re}^{a} \\ \hat{\ell}_{\Im} \in \ell}} \sum_{\substack{\hat{x}_{\Re} \, \epsilon \, \chi \\ \hat{x}_{\Im} \, \epsilon \, \chi}} P(\boldsymbol{y} \mid \ell_{\Re} = \hat{\ell}_{\Re}, \ell_{\Im} = \hat{\ell}_{\Im}, x_{\Re} = \hat{x}_{\Re}, x_{\Im} = \hat{x}_{\Im}) \, P\left(\ell_{\Re} = \hat{\ell}_{\Re}\right)}{\sum_{\substack{\hat{\ell}_{\Re} \in \ell_{0\Re}^{a} \\ \hat{\ell}_{\Im} \in \ell}} \sum_{\substack{\hat{x}_{\Re} \, \epsilon \, \chi \\ \hat{x}_{\Im} \, \epsilon \, \chi}} P(\boldsymbol{y} \mid \ell_{\Re} = \hat{\ell}_{\Re}, \ell_{\Im} = \hat{\ell}_{\Im}, x_{\Re} = \hat{x}_{\Re}, x_{\Im} = \hat{x}_{\Im}) \, P\left(\ell_{\Re} = \hat{\ell}_{\Re}\right)} \right] \tag{6.3}$$

where $\ell_{0\,\Re}^{a}$ and $\ell_{1\,\Re}^{a}$are vectors of the real antenna indices with '0' and '1' at the a^{th} antenna bits, respectively.

On application of the Bayes' theorem, the demodulator output in (6.3) can be described statistically by the PDF, such that the a$^{\text{th}}$ real transmit antenna bit is expressed as:

$$LLR(\ell_{\Re}^{a}) = \log \left[\frac{\sum_{\hat{\ell}_{\Re} \in \ell_{1\,\Re}^{a}, \hat{\ell}_{\Im} \in \ell} \sum_{\hat{\boldsymbol{x}}_{\Re}, \hat{\boldsymbol{x}}_{\Im} \, \epsilon \, \chi} \exp(E)}{\sum_{\hat{\ell}_{\Re} \in \ell_{0\,\Re}^{a}, \hat{\ell}_{\Im} \in \ell} \sum_{\hat{\boldsymbol{x}}_{\Re}, \hat{\boldsymbol{x}}_{\Im} \, \epsilon \, \chi} \exp(F)} \right] \tag{6.4}$$

where $E = F = \frac{-\left\| \boldsymbol{y} - \sqrt{\rho/\mu} \left(\boldsymbol{h}_{\ell_{\Re}} \boldsymbol{x}_{\ell_{\Re}}^{q_{\Re}} + j \boldsymbol{h}_{\ell_{\Im}} \boldsymbol{x}_{\ell_{\Im}}^{q_{\Im}} \right) \right\|_F^2}{2\sigma^2}$ such that σ^2 is the variance of the AWGN $\boldsymbol{w}$.

In the same vein, the a$^{\text{th}}$ imaginary antenna bit is computed, and expressed as:

$$LLR(\ell_{\Im}^{a}) = \log \frac{P(\ell_{\Im}^{a} = 1|\boldsymbol{y})}{P(\ell_{\Im}^{a} = 0|\boldsymbol{y})} \tag{6.5}$$

$$= \log \left[\frac{\sum_{\substack{\hat{\ell}_{\Im} \in \ell_{1\Im}^{a} \\ \hat{\ell}_{\Re} \in \ell}} \sum_{\substack{\hat{x}_{\Re} \, \epsilon \, \chi \\ \hat{x}_{\Im} \, \epsilon \, \chi}} P(\boldsymbol{y} \mid \ell_{\Re} = \hat{\ell}_{\Re}, \ell_{\Im} = \hat{\ell}_{\Im}, x_{\Re} = \hat{x}_{\Re}, x_{\Im} = \hat{x}_{\Im}) \, P\left(\ell_{\Im} = \hat{\ell}_{\Im}\right)}{\sum_{\substack{\hat{\ell}_{\Im} \in \ell_{0\Im}^{a} \\ \hat{\ell}_{\Re} \in \ell}} \sum_{\substack{\hat{x}_{\Re} \, \epsilon \, \chi \\ \hat{x}_{\Im} \, \epsilon \, \chi}} P(\boldsymbol{y} \mid \ell_{\Re} = \hat{\ell}_{\Re}, \ell_{\Im} = \hat{\ell}_{\Im}, x_{\Re} = \hat{x}_{\Re}, x_{\Im} = \hat{x}_{\Im}) \, P\left(\ell_{\Im} = \hat{\ell}_{\Im}\right)} \right] \tag{6.6}$$

$$LLR(\ell_{\Im}^{a}) = \log \left[\frac{\sum_{\hat{\ell}_{\Im} \in \ell_{1\,\Im}^{a}, \hat{\ell}_{\Re} \in \ell} \sum_{\hat{\boldsymbol{x}}_{\Re}, \hat{\boldsymbol{x}}_{\Im} \, \epsilon \, \chi} \exp(E)}{\sum_{\hat{\ell}_{\Im} \in \ell_{0\,\Im}^{a}, \hat{\ell}_{\Re} \in \ell} \sum_{\hat{\boldsymbol{x}}_{\Re}, \hat{\boldsymbol{x}}_{\Im} \, \epsilon \, \chi} \exp(F)} \right] \tag{6.7}$$

where $\ell_{0_{\Im}}^{a}$ and $\ell_{1_{\Im}}^{a}$are vectors of the imaginary antenna indices with '0' and '1' at the a^{th} antenna bits, respectively.

Furthermore, the b$^{\text{th}}$ real symbol bit is computed and expressed mathematically as:

$$LLR\left(x_{\Re}^{b}\right) = \log\frac{P\left(x_{\Re}^{b}=1\middle|\boldsymbol{y}\right)}{P\left(x_{\Re}^{b}=0\middle|\boldsymbol{y}\right)} \tag{6.8}$$

$$= \log\left[\frac{\sum_{\substack{\hat{x}_{\Re}\,\epsilon\, x_{1_{\Re}}^{a} \\ \hat{x}_{\Im}\,\epsilon\,\chi}}\sum_{\substack{\hat{\ell}_{\Re}\in\ell \\ \hat{\ell}_{\Im}\in\ell}} P\left(\boldsymbol{y}\middle|\ell_{\Re}=\hat{\ell}_{\Re},\ell_{\Im}=\hat{\ell}_{\Im},x_{\Re}=\hat{x}_{\Re},x_{\Im}=\hat{x}_{\Im}\right)P(x_{\Re}=\hat{x}_{\Re})}{\sum_{\substack{\hat{x}_{\Re}\,\epsilon\, x_{0_{\Re}}^{a} \\ \hat{x}_{\Im}\,\epsilon\,\chi}}\sum_{\substack{\hat{\ell}_{\Re}\in\ell \\ \hat{\ell}_{\Im}\in\ell}} P\left(\boldsymbol{y}\middle|\ell_{\Re}=\hat{\ell}_{\Re},\ell_{\Im}=\hat{\ell}_{\Im},x_{\Re}=\hat{x}_{\Re},x_{\Im}=\hat{x}_{\Im}\right)P(x_{\Re}=\hat{x}_{\Re})}\right] \tag{6.9}$$

$$LLR\left(x_{\Re}^{b}\right) = \log\left[\frac{\sum_{\hat{x}_{\Re}\,\epsilon\, x_{1_{\Re}}^{a},\hat{x}_{\Im}\,\epsilon\,\chi}\sum_{\hat{\ell}_{\Re},\hat{\ell}_{\Im}\in\ell}\exp(E)}{\sum_{\hat{x}_{\Re}\,\epsilon\, x_{0_{\Re}}^{a},\hat{x}_{\Im}\,\epsilon\,\chi}\sum_{\hat{\ell}_{\Re},\hat{\ell}_{\Im}\in\ell}\exp(F)}\right] \tag{6.10}$$

where $x_{0_{\Re}}^{b}$ and $x_{1_{\Re}}^{b}$ are vectors of the real data symbols with '0' and '1' at the b^{th} data bit, respectively.

Finally, the b$^{\text{th}}$ imaginary symbol bit is can be written as:

$$LLR\left(x_{\Im}^{b}\right) = \log\frac{P\left(x_{\Im}^{b}=1\middle|\boldsymbol{y}\right)}{P\left(x_{\Im}^{b}=0\middle|\boldsymbol{y}\right)} \tag{6.11}$$

$$= \log\left[\frac{\sum_{\substack{\hat{x}_{\Im}\,\epsilon\, x_{1_{\Im}}^{a} \\ \hat{x}_{\Re}\,\epsilon\,\chi}}\sum_{\substack{\hat{\ell}_{\Re}\in\ell \\ \hat{\ell}_{\Im}\in\ell}} P\left(\boldsymbol{y}\middle|\ell_{\Re}=\hat{\ell}_{\Re},\ell_{\Im}=\hat{\ell}_{\Im},x_{\Re}=\hat{x}_{\Re},x_{\Im}=\hat{x}_{\Im}\right)P(x_{\Im}=\hat{x}_{\Im})}{\sum_{\substack{\hat{x}_{\Im}\,\epsilon\, x_{0_{\Im}}^{a} \\ \hat{x}_{\Re}\,\epsilon\,\chi}}\sum_{\substack{\hat{\ell}_{\Re}\in\ell \\ \hat{\ell}_{\Im}\in\ell}} P\left(\boldsymbol{y}\middle|\ell_{\Re}=\hat{\ell}_{\Re},\ell_{\Im}=\hat{\ell}_{\Im},x_{\Re}=\hat{x}_{\Re},x_{\Im}=\hat{x}_{\Im}\right)P(x_{\Im}=\hat{x}_{\Im})}\right] \tag{6.12}$$

$$LLR\left(x_{\Im}^{b}\right) = \log\left[\frac{\sum_{\hat{x}_{\Im}\,\epsilon\, x_{1_{\Im}}^{a},\hat{x}_{\Re}\,\epsilon\,\chi}\sum_{\hat{\ell}_{\Re},\hat{\ell}_{\Im}\in\ell}\exp(E)}{\sum_{\hat{x}_{\Im}\,\epsilon\, x_{0_{\Im}}^{a},\hat{x}_{\Re}\,\epsilon\,\chi}\sum_{\hat{\ell}_{\Re},\hat{\ell}_{\Im}\in\ell}\exp(F)}\right] \tag{6.13}$$

where $x_{0_{\Im}}^{b}$ and $x_{1_{\Im}}^{b}$ are vectors of the imaginary data symbols with '0' and '1' at the b^{th} data bit, respectively.

It is important to note that detection of the QSM signal with our proposed demodulator is done bit-by-bit (in terms of $\ell_{\Re}^{a}$, $\ell_{\Im}^{a}$, $x_{\Re}^{b}$, and $x_{\Im}^{b}$) as against the joint detection of the conventional optimal detector for QSM given in (4.10). As the name suggests, the outputs of

the proposed detector are real (soft) numbers; unlike the optimal ML detector whose outputs are integers (1's and 0's).

It was earlier motivated that; in addition to channel coding, achieving larger SNR gain with a soft-output detector would require a soft-input decoder for processing the signals at the receiver. On this note, the proposed detector would achieve the target improvement in error performance, as soft outputs from the proposed demodulator, given in (6.7), (6.10), (6.13) and (6.16), are fed into a soft-input Viterbi channel decoder and an estimate of the transmitted message is obtained.

6.3. Computational Complexity of QSM-SOMLD

The computational complexity of the proposed QSM-SOMLD detector is formulated in terms of complex multiplications involved in the detection processes. Importantly, the computation of the logarithm functions present in the LLRs of the proposed soft-output detector must be considered so as to determine their contributions to the total complexity of the detector. In this dissertation, we assume that the computation of the logarithm functions are approximated via the use of LUT based method presented in [56], and therefore impose no additional complexity.

To formulate the computational complexity of the QSM-SOMLD, the individual complexity imposed by each of the four detection processes of detecting the a^{th} real antenna bit, a^{th} imaginary antenna bit, b^{th} real symbol bit and b^{th} imaginary symbol bit, is analysed. On a general note, the Frobenious norm of the numerator of E and F can be expanded to yield:

$$c = d = -\left\|\boldsymbol{y} - \sqrt{\rho/\mu}\left(\boldsymbol{h}_{\ell_{\Re}}\boldsymbol{x}_{\ell_{\Re}}^{q\Re}\right)\right\|_F^2 - \left\|\boldsymbol{y} + j\sqrt{\rho/\mu}\left(\boldsymbol{h}_{\ell_{\Im}}\boldsymbol{x}_{\ell_{\Im}}^{q\Im}\right)\right\|_F^2$$

$$c = d = \sqrt{\rho/\mu}\left\|\boldsymbol{h}_{\ell_{\Re}}\right\|_F^2\left|\boldsymbol{x}_{\ell_{\Re}}^{q\Re}\right|^2 - 2\Re\left\{\boldsymbol{y}^H\boldsymbol{h}_{\ell_{\Re}}\boldsymbol{x}_{\ell_{\Re}}^{q\Re}\right\} + \sqrt{\rho/\mu}\left\|\boldsymbol{h}_{\ell_{\Im}}\right\|_F^2\left|\boldsymbol{x}_{\ell_{\Im}}^{q\Im}\right|^2 - 2\Re\left\{\boldsymbol{y}^H\boldsymbol{h}_{\ell_{\Im}}\boldsymbol{x}_{\ell_{\Im}}^{q\Im}\right\}$$

since $\boldsymbol{h}_{\ell_{\Re}}{}^H\boldsymbol{h}_{\ell_{\Re}}, \boldsymbol{h}_{\ell_{\Im}}{}^H\boldsymbol{h}_{\ell_{\Im}} = 0$. Hence;

$$c = d = \sqrt{\rho/\mu}\left\|\boldsymbol{h}_{\ell_{\Re}}\right\|_F^2\left|\boldsymbol{x}_{\ell_{\Re}}^{q\Re}\right|^2 + \sqrt{\rho/\mu}\left\|\boldsymbol{h}_{\ell_{\Im}}\right\|_F^2\left|\boldsymbol{x}_{\ell_{\Im}}^{q\Im}\right|^2 - 2\Re\left\{\boldsymbol{y}^H\boldsymbol{h}_{\ell_{\Re}}\boldsymbol{x}_{\ell_{\Re}}^{q\Re}\right\} - 2\Re\left\{\boldsymbol{y}^H\boldsymbol{h}_{\ell_{\Im}}\boldsymbol{x}_{\ell_{\Im}}^{q\Im}\right\} \quad (6.14)$$

Therefore,

$$E_1 = \frac{c}{2\sigma^2} = \ E_2 = \frac{d}{2\sigma^2} \tag{6.15}$$

Hence, by putting (6.19) in (6.7), (6.10), (6.13) and (6.16), the proposed QSM-SOMLD detectors can be re-expressed, respectively, as:

$$LLR(\ell_{\Re}^{a}) = \log\left[\frac{\sum_{\hat{\ell}_{\Re}\in\ell_{1\,\Re}^{a},\hat{\ell}_{\Im}\in\ell}\sum_{\hat{\boldsymbol{x}}_{\Re},\hat{\boldsymbol{x}}_{\Im}\,\epsilon\,\chi}\exp(E_1)}{\sum_{\hat{\ell}_{\Re}\in\ell_{0\,\Re}^{a},\hat{\ell}_{\Im}\in\ell}\sum_{\hat{\boldsymbol{x}}_{\Re},\hat{\boldsymbol{x}}_{\Im}\,\epsilon\,\chi}\exp(E_2)}\right] \tag{6.15}$$

$$LLR(\ell_{\Im}^{a}) = \log\left[\frac{\sum_{\hat{\ell}_{\Im}\in\ell_{1\,\Im}^{a},\hat{\ell}_{\Re}\in\ell}\sum_{\hat{\boldsymbol{x}}_{\Re},\hat{\boldsymbol{x}}_{\Im}\,\epsilon\,\chi}\exp(E_1)}{\sum_{\hat{\ell}_{\Im}\in\ell_{0\,\Im}^{a},\hat{\ell}_{\Re}\in\ell}\sum_{\hat{\boldsymbol{x}}_{\Re},\hat{\boldsymbol{x}}_{\Im}\,\epsilon\,\chi}\exp(E_2)}\right] \tag{6.16}$$

$$LLR\left(x_{\Re}^{b}\right) = \log\left[\frac{\sum_{\hat{x}_{\Re}\,\epsilon\,x_{1\,\Re}^{a},\hat{x}_{\Im}\,\epsilon\,\chi}\sum_{\hat{\ell}_{\Re},\hat{\ell}_{\Im}\in\ell}\exp(E_1)}{\sum_{\hat{x}_{\Re}\,\epsilon\,x_{0\,\Re}^{a},\hat{x}_{\Im}\,\epsilon\,\chi}\sum_{\hat{\ell}_{\Re},\hat{\ell}_{\Im}\in\ell}\exp(E_2)}\right] \tag{6.17}$$

$$LLR\left(x_{\Im}^{b}\right) = \log\left[\frac{\sum_{\hat{x}_{\Im}\,\epsilon\,x_{1\,\Im}^{a},\hat{x}_{\Re}\,\epsilon\,\chi}\sum_{\hat{\ell}_{\Re},\hat{\ell}_{\Im}\in\ell}\exp(E_1)}{\sum_{\hat{x}_{\Im}\,\epsilon\,x_{0\,\Im}^{a},\hat{x}_{\Re}\,\epsilon\,\chi}\sum_{\hat{\ell}_{\Re},\hat{\ell}_{\Im}\in\ell}\exp(E_2)}\right] \tag{6.18}$$

In this dissertation, the total computational complexity of the proposed QSM-SOMLD is evaluated by calculating the complex multiplications imposed by the computation of (6.15), (6.16), (6.17) and (6.18), respectively, in terms of complex multiplications. To avoid redundant computations, it is assumed that results can be stored and reused in future computations. Therefore, the computation complexity of the proposed QSM-SOMLD is calculated as follows:

Considering the first term of the numerator of (6.20), $\left\|\boldsymbol{h}_{\ell_{\Re}}\right\|_F^2$ is equivalent to $\boldsymbol{h}_{\ell_{\Re}}{}^{H}\boldsymbol{h}_{\ell_{\Re}}$ and requires $2N_r$ complex multiplications for each $\hat{\ell}_{\Re}$.Thus, computing $\left\|\boldsymbol{h}_{\ell_{\Re}}\right\|_F^2$ for $\hat{\ell}_{\Re} \in \ell_{1\,\Re}^{a}$ requires $2N_r(\frac{c}{2})$ complex multiplications, while the computation of $\left|\boldsymbol{x}_{\ell_{\Re}}^{q\Re}\right|^2$ requires only M complex multiplications. Therefore, the computational complexity imposed by the first term is given by $2N_r\left(\frac{c}{2}\right) + M$. A consideration of the second term shows that the computation of $\left\|\boldsymbol{h}_{\ell_{\Im}}\right\|_F^2 = \left\|\boldsymbol{h}_{\ell_{\Re}}\right\|_F^2$, therefore, we ignore the computation of $\left\|\boldsymbol{h}_{\ell_{\Im}}\right\|_F^2$ and use

the stored result. This means that the computation of the seconds term $\sqrt{\rho/\mu}\left\|\boldsymbol{h}_{\ell_{\Im}}\right\|_F^2\left|\boldsymbol{x}_{\ell_{\Im}}^{q\Im}\right|^2$ dependent only on the computation of $\left|\boldsymbol{x}_{\ell_{\Im}}^{q\Im}\right|^2$ which is given by M.

The computation of the third term $2\Re\left\{\boldsymbol{y}^H\boldsymbol{h}_{\ell_{\Re}}\boldsymbol{x}_{\ell_{\Re}}^{q\Re}\right\}$ requires $2N_r$ complex multiplications for $\boldsymbol{y}^H\boldsymbol{h}_{\ell_{\Re}}$ and a further M complex multiplications for $\boldsymbol{x}_{\ell_{\Re}}^{q\Re}$, for each of the $\frac{c}{2}$ antenna-pair combinations; making a total of $(2N_r + M)\left(\frac{c}{2}\right)$. Obviously, the computation of the forth term will be equivalent to $(2N_r + M)\left(\frac{c}{2}\right)$. Hence, the computational complexity imposed by the numerator is the sum of: $\left(2N_r\left(\frac{c}{2}\right) + M\right) + M + (2N_r + M)\left(\frac{c}{2}\right) + (2N_r + M)\left(\frac{c}{2}\right)$. This equivalent to: $(c)(3N_r + M) + 2M$.

$$\delta_{numerator} = (c)(3N_r + M) + 2M \tag{6.19}$$

Next, we consider the denominator of (6.20). It is evident that the computation of the first term depends only on $\left\|\boldsymbol{h}_{\ell_{\Re}}\right\|_F^2$ for $\hat{\ell}_{\Re} \in \ell_{0\,\Re}^{a}$ which requires $2N_r(\frac{c}{2})$ complex multiplications. This is in line with the assumption that results can be stored and reused in future computations so as to avoid redundant computations. For the same reason, the second term does not impose any further complexity. The third term imposes $(2N_r + M)\left(\frac{c}{2}\right)$ complex multiplications, while the forth term similarly requires $(2N_r + M)\left(\frac{c}{2}\right)$ complex multiplications. Therefore, the computational complexity of the denominator is given by:

$$\delta_{denominator} = (c)(3N_r + M) \tag{6.20}$$

As mentioned earlier, no additional complexity is imposed by the computation of the logarithm functions. On this note, the computational complexity imposed by estimating the a^{th} real antenna bit ($\ell_{\Re}^{a}$) in (6.15) is given by the addition of (6.19) and (6.20) as:

$$\delta_{\ell_{\Re}^{a}} = c(6N_r + 2M) + 2M \tag{6.21}$$

Using a similar approach, it can be shown that the computational complexity imposed by the estimation of the a^{th} imaginary antenna bit ($\ell_{\Im}^{a}$), b^{th} real symbol bit ($x_{\Re}^{b}$), and b^{th}

imaginary symbol bit ($x_{\Im}^{b}$) will not impose any further complexities as stored results can reused in order to avoid redundant computations. Hence, the computation complexity of our proposed detector, in terms of complex multiplications, can be written, similar to (4.26), as given in (6.21). It can be concluded that the proposed QSM-SOMLD detector, despite its impressive performances, imposes no additional complexity compared to the conventional QSM-HDMLD.

6.4. Simulation Results and Discussion

In this section, we present the error performances of the proposed soft-output detector for QSM and are compared to the existing HDMLD detector. For all results presented in this section, simulations have been made under a Rayleigh flat-fading MIMO channels with i.i.d. entries distributed according to *CN*(0,1), and in the presence of AWGN. All simulations are terminated at a BER of 10^{-6}, and results are presented in terms of BER as a function of the SNR. It should be noted different numbers of transmit antennas are used to obtain different spectral efficiencies of 4, 6 and 8 b/s/Hz.

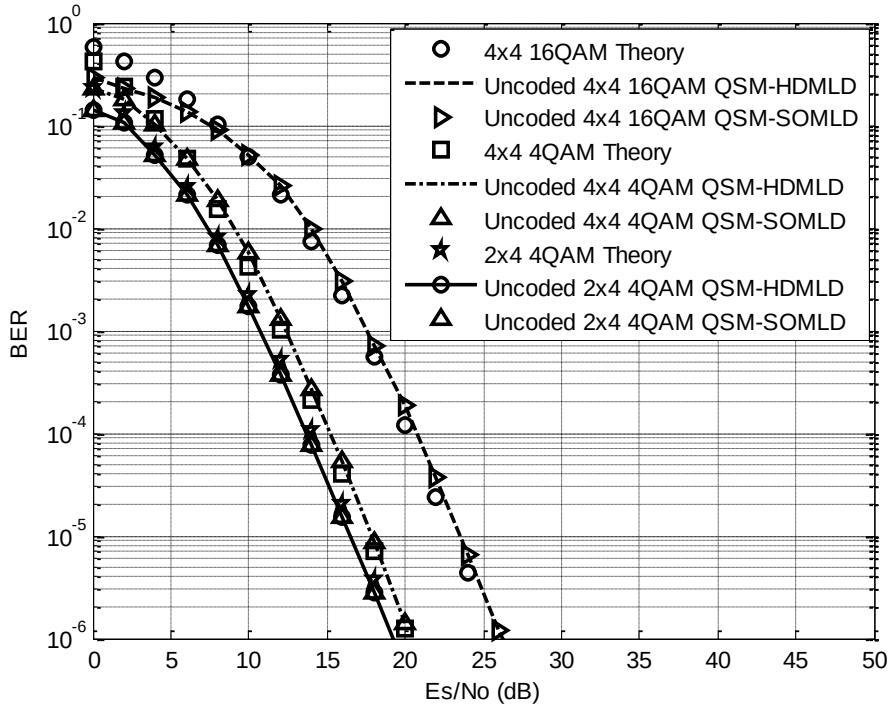

Figure 6.1: Comparison of BER performances for 4, 6 and 8 b/s/Hz QSM systems in uncoded channels using the proposed SOMLD and HDMLD (N_r = 4, M = 4)

In Figure 6.1, the error performances of the HDMLD and SOMLD detectors are evaluated for uncoded channel conditions. As expected, the simulation results show that the proposed SOMLD scheme is closely matching the HDMLD for all the configurations considered. Again, the BER performances of the respective QSM system configurations are validated by the theoretical performance bounds for *M*QAM QSM. Hence, the soft-output detector has no effect, unless coupled with a soft-input decoder at the receiver, in the presence of coded channels.

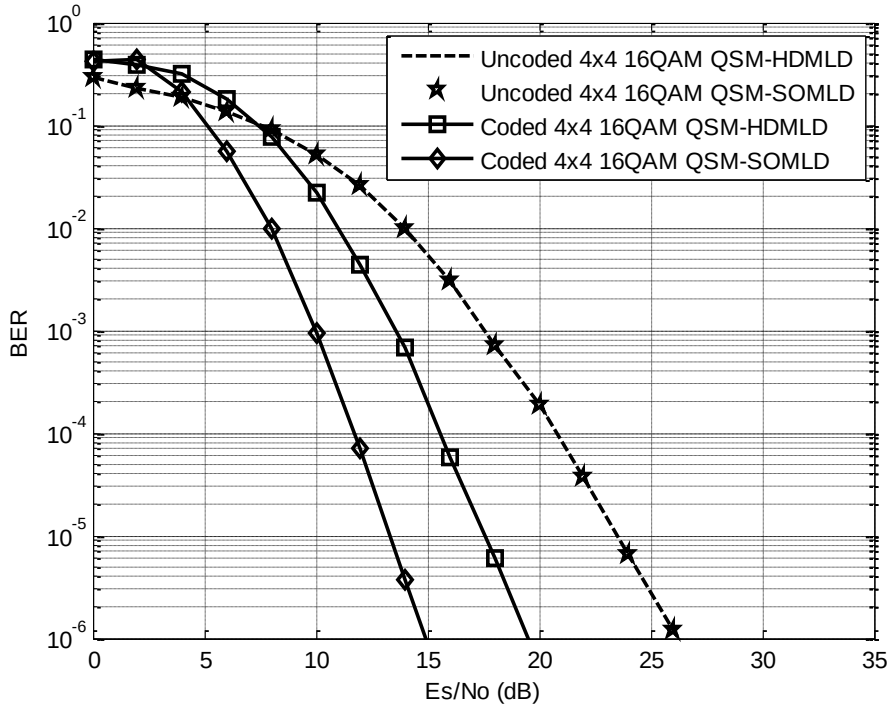

Figure 6.2: Comparison of BER performances for 8 b/s/Hz 16QAM QSM system in coded and uncoded channels using 4×4 MIMO configuration

In Figure 6.2, we present the error performances of 8 b/s/Hz 4×4 16QAM QSM system using the proposed SOMLD and the HDMLD detection schemes. It is evident that the coded SOMLD detector yields significant SNR gains over the coded and uncoded HDMLD detectors. For example, at a BER of 10^{-6}, it achieves approximately 6.5 dB SNR gain compared to coded HDMLD. Furthermore, the proposed SOMLD in coded channel achieves an SNR gain of 11 dB over the uncoded conventional HDMLD scheme, at the same BER.

Results of error performances for 6 bits 4×4 4QAM QSM system is presented in Figure 6.3. Recall that the QSM system with conventional HDMLD has been shown in Figure 6.1 to be matching closely with the proposed SOMLD, in uncoded channels. Meanwhile, in coded channels, the proposed QSM-SOMLD performs better than the coded HDMLD. For example at a BER of 10^{-6}, an SNR gain of approximately 5.1 dB is evidently achieved by the SOMLD over HDMLD. Furthermore, the proposed SOMLD in coded channel achieves an SNR gain of approximately 9.1 dB over the uncoded conventional HDMLD scheme, at the same BER.

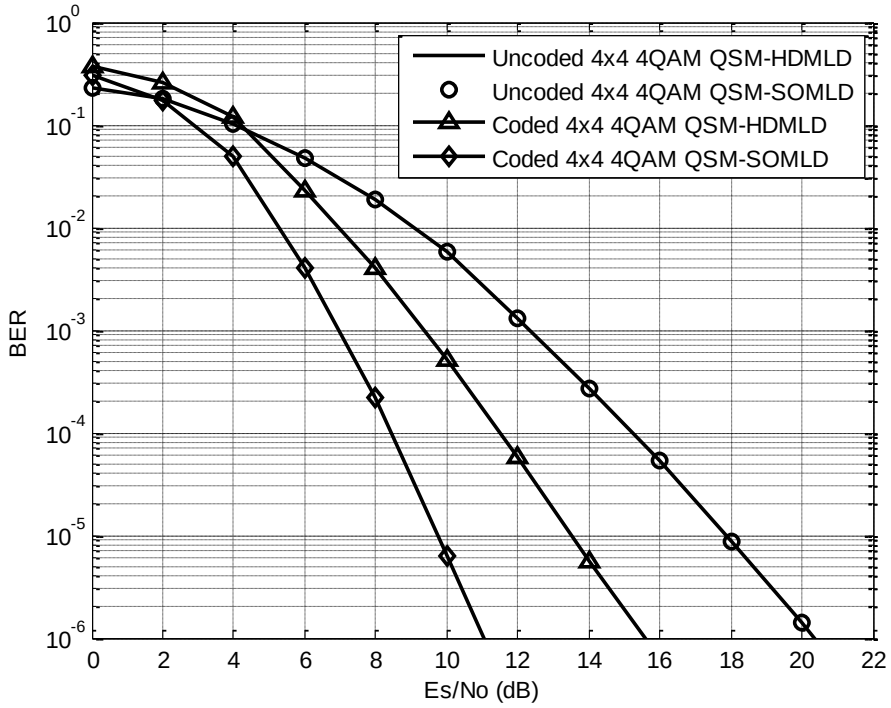

Figure 6.3: Comparison of BER performances of 6 b/s/Hz 4QAM QSM in coded and uncoded channels using 4×4 MIMO configuration

In Figure 6.4, a similar trend in error performance is observed for the 4 b/s/Hz 2×4 4QAM QSM system. At a BER of 10^{-6}, SOMLD achieves approximately 4 dB SNR gain over HDMLD in coded channels, while almost 6.5 dB SNR gain is achieved by the coded SOMLD over uncoded HDMLD, at the same BER.

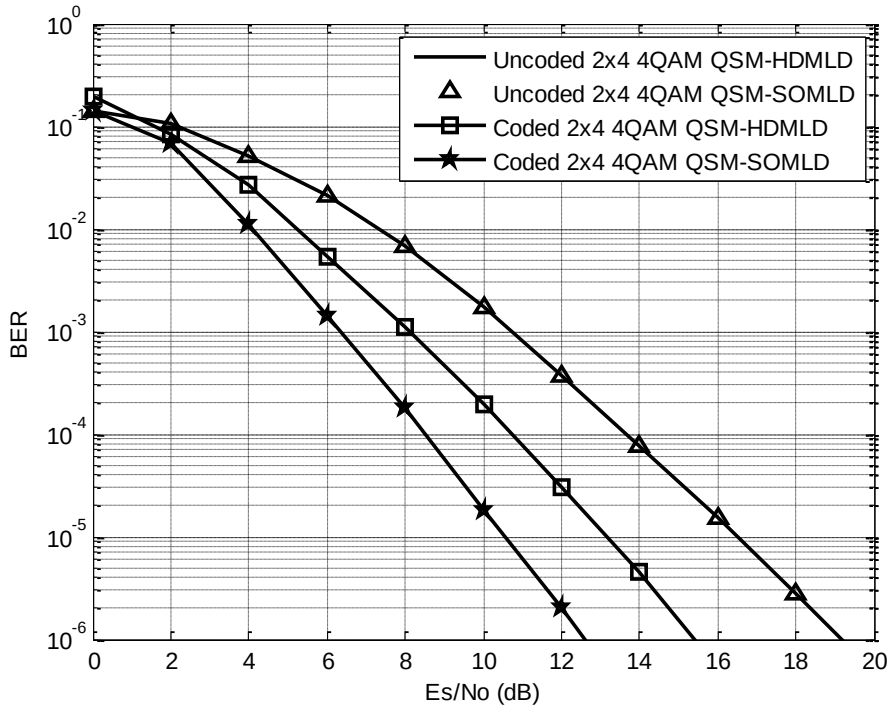

Figure 6.4: Comparison of BER performances of 4 b/s/Hz 4QAM QSM in coded and uncoded channels using 2×4 MIMO configuration

6.5. Conclusion

In this chapter, we have proposed a SOMLD detector for the QSM modulation scheme with the aim of further improving its error performances. Monte Carlo simulations are used to investigate the performance of the new detector in uncoded and coded channels. Results obtained from this demonstrate that the proposed SOMLD is able to match the performance of the existing optimal HDMLD detector for uncoded channels; while the coded SOMLD performs impressively better than the coded and uncoded HDMLD detectors.

Chapter 7

Conclusion

7.1. Research Achievements

This dissertation presented the soft detection techniques for transmit antenna index modulation-based schemes. First, the SM scheme was investigated as a fundamental on which others are based. Simulation results were presented as output of the investigation made into the error performances of SM, and its other inherent advantages were ascertained as well. As a way of verifying the simulated results, the evaluated analytical performance bounds were plotted, and found to closely match the error performance of optimal SM-OD. Secondly, it was verified that the soft-output ML detector (SM-SOMLD) closely matched the SM-HDMLD under uncoded channel conditions. However, the SM-SOMLD significantly outperformed the SM-HDMLD under coded channels as presented in Table 7.1.

Table 7.1: BER performance comparison of SM-HDMLD and SM-SOMLD under coded and uncoded channel conditions

MIMO configuration $[N_t, N_r, M]$	**Spectral length [b/s/Hz]**	**SNR of coded SM-SOMLD at 10^{-6} BER [dB]**	**SNR and gains of SM-HDMLD at 10^{-6} BER**			
			uncoded	**Gain**	**coded**	**Gain**
4, 4, 4	4	10.2 dB	17.5 dB	7.3 dB	14.1 dB	3.9 dB
4, 4, 16	6	13.7 dB	22.5 dB	8.8 dB	20.0 dB	6.3 dB
16, 4, 16	8	11.2 dB	25.0 dB	13.8 dB	15.4 dB	4.2 dB

Furthermore, investigations into the error performances for SSK, Bi-SSK and QSM schemes were conducted using Monte Carlo simulations. The analytical performance bounds of the respective schemes were evaluated and plotted to validate the simulation results. These systems were compared to SM in terms of error performances, spectral efficiencies and transceiver configurations. In this regard, the outcomes of the findings are presented in Table 7.2.

Table 7.2.: BER performances of SM, SSK, Bi-SSK and QSM with optimal HDMLD

Scheme	**Transmit Antenna (N_t = 4)**		**Spectral efficiency = 6 b/s/Hz**	
	SNR at 10^{-6} BER	**Spectral Efficiency**	**SNR at 10^{-6} BER**	**N_t**
SM 4QAM	17.6 dB	4 b/s/Hz	19.1 dB	16
SSK	16.5 dB	2 b/s/Hz	19.2 dB	64
Bi-SSK	19.2 dB	4 b/s/Hz	20.1 dB	8
QSM 4QAM	20.5 dB	6 b/s/Hz	20.5 dB	4

In line with the primary focus of this dissertation, the concept of soft-output detection was extended to SSK, Bi-SSK and QSM modulation schemes and consequently a soft-output ML demodulator each was proposed the systems. The error performances of the proposed SOMLD detectors were investigated and found to closely match the conventional HDMLD in uncoded channels. However, when channel coding was introduced, in the presence of a soft-input decoder at the receiver, the proposed SOMLD detectors achieved significant improvements in error performances as compared to HDMLD detectors of SSK, Bi-SSK and QSM systems. These improvements were noted and the corresponding SNR gains (in dB) are illustrated in Tables 7.3, 7.4 and 7.5 for SSK, Bi-SSK and QSM systems, respectively.

Table 7.3: BER performance comparison of SSK-HDMLD and SSK-SOMLD under coded and uncoded channel conditions

MIMO configuration $[N_t, N_r, M]$	**Spectral length [b/s/Hz]**	**SNR of coded SSK-SOMLD at 10^{-6} BER [dB]**	**SNR and gains of SSK-HDMLD at 10^{-6} BER**			
			Uncoded	**Gain**	**Coded**	**Gain**
4, 4, 4	2	10.2 dB	16.7 dB	6.5 dB	15.3 dB	5.1 dB
16, 4, 16	4	9.6 dB	17.8 dB	8.2 dB	15.9 dB	6.3 dB
64, 4, 64	6	11.4 dB	19.4 dB	8.0 dB	15.7 dB	4.3 dB

Table 7.4: BER performance comparison of Bi-SSK-HDMLD and Bi-SSK-SOMLD under coded and uncoded channel conditions

MIMO configuration $[N_t, N_r, M]$	**Spectral length [b/s/Hz]**	**SNR of coded Bi-SSK-SOMLD at 10^{-6} BER [dB]**	**SNR and gains of Bi-SSK-HDMLD at 10^{-6} BER**			
			Uncoded	**Gain**	**Coded**	**Gain**
2, 4, 2	2	12.0 dB	18.2 dB	6.2 dB	13.9 dB	1.9 dB
4, 4, 4	4	10.0 dB	19.2 dB	9.2 dB	14.1 dB	4.1 dB
8, 4, 8	6	9.7 dB	20.1 dB	10.4 dB	14.0 dB	4.3 dB

Table 7.5: BER performance comparison of QSM-HDMLD and QSM-SOMLD under coded and uncoded channel conditions

MIMO configuration $[N_t, N_r, M]$	**Spectral length [b/s/Hz]**	**SNR of coded QSM-SOMLD at 10^{-6} BER[dB]**	**SNR and gains of QSM-HDMLD at 10^{-6} BER**			
			Uncoded	**Gain**	**Coded**	**Gain**
2, 4, 4	4	12.7 dB	19.2 dB	6.5 dB	15.4 dB	2.7 dB
4, 4, 4	6	11.4 dB	20.5 dB	9.1 dB	15.6 dB	4.2 dB
4, 4, 16	8	15.0 dB	26.0 dB	11.0 dB	19.6 dB	4.6 dB

7.2. Future Work

The transmit antenna index modulation-based schemes have come with enticing properties such as improved BER performance, reduced hardware complexity and higher spectral efficiencies. In this dissertation, soft-output detections have been proposed and investigated for the SSK, Bi-SSK and QSM schemes. Motivated by the good performance of the soft-output detectors for SSK, Bi-SSK and QSM under convolutional coded channels, it may be beneficial to investigate the concept of soft-output detection under more robust codes, such as turbo codes. It may also be worthwhile to derive low complexity detection techniques for these schemes.

References

[1] J. G. Proakis. and M. Salehi., Digital Communications, 5th ed. New York: McGraw-Hill, 2008.

[2] A. J. Goldsmith, "Wireless Communications, 1st ed., New York: Cambridge University Press, 2005.

[3] W. Tranter, D. Taylor, R. Ziemer, N. Maxemchuk, and J. Mark, "Convolutional Codes and Their Performance in Communication Systems," *The Best of the Best: Fifty Years of Communications and Networking Research, Wiley-IEEE Press*, 1st ed, pp. 375-396, 2007

[4] S. Srinivasan and S. S. Pietrobon, "Decoding of High Rate Convolutional Codes Using the Dual Trellis," *IEEE Transactions on Information Theory*, vol. 56, no. 1, pp. 273-295, Jan. 2010.

[5] T. S. Rappaport, Wireless Communication: Principles and Practice, 2nd ed. New Jersey: Prentice Hall PTR, 1996.

[6] A. J. Viterbi, "Convolutional Codes and Their Performance in Communication Systems," *IEEE Transactions on Communications Technology*, vol. 19, no. 5, pp. 751-772, Oct. 1971.

[7] R. Fano, "A Heuristic Discussion of Probabilistic Decoding," *IEEE Transactions on Information Theory*, vol. 9, no 2, pp. 64-74, Apr. 1963.

[8] K. S. Zigangirov, "Some Sequential Decoding Procedures," *Journal of Problems on Information Transmission*, vol. 2, no. 4, pp.13-25, Mar. 1966.

[9] S. M. Reddy and J. P. Robinson, "A Decoding Algorithm for Some Convolutional Codes Constructed from Block Codes," *Information and Control*, vol. 13, no. 5, pp. 492-507, Nov. 1968.

[10] S. Lin and D. J. C. Jr., Error Control Coding, Upper Saddle River, New Jersey: Pearson Prentice Hall, 2004.

[11] R. Khanai and G. H. Kulkarni, "Performance Analysis of Conventional Crypto-Coding," *International Journal of Latest Trends in Computing*, vol. 2, no. 1, pp. 193-197, Mar. 2011.

[12] M. F. Mosleh and F. A. Abid, "Log-Likelihood Ratio to Improve Hard Decision Viterbi Algorithm," *Engineering and Technology Journal*, vol. 31, no. 9, pp. 1779-1790, Jan. 2013.

[13] G. D. Forney, "The Viterbi Algorithm," in *Proceedings of the IEEE International Conference on Communications*, vol. 61, no. 3, pp. 268-278, Mar. 1973.

[14] G. D. Forney, "Convolutional Codes I: Algebraic Structure," *IEEE Transactions on Information Theory*, vol. 16, no. 6, pp. 720-738, Nov. 1970.

[15] J. C. Dany, J. Antoine, L. Husson, A. Wautier, N. Paul, and J. Brouet, "Low Complexity Algorithm for the Decoding of Convolutional Codes of any Rate," in *Proceedings of the IEEE International Conference on Communications*, vol. 1, no. 1, pp. 547-551, Jun. 2004.

[16] T. M. Duman and A. Ghrayeb, Coding for MIMO Communication Systems: John Wiley & Sons Ltd, 2007.

[17] S. Schindler, Introduction to MIMO: Application Note, Rohde and Schwarz, Munich, Jul. 2009.

[18] I. E. Telatar, "Capacity of Multi-Antenna Gaussian Channels," *European Transactions on Telecommunications*, vol. 10, no. 6, pp. 585-595, Nov/Dec. 1999.

[19] A. U. H. Sheikh, "Principles of Transmission and Detection of Digital Signals," in *Digital Communication*, P. C. Palanisamy, ed: InTech Available: http://www.intechopen.com/books/digital-communication/principles-of-transmission-and-detection-of-digitalsignals, Mar. 2012.

[20] S. Catreux, P. F. Driessen, and L. J. Greenstein, "Simulation Results for an Interference-Limited Multiple-Input Multiple-Output Cellular System," *IEEE Communications Letters*, vol. 4, no. 11, pp. 334-336, Nov. 2000.

[21] S. Da-Shan, G. J. Foschini, M. J. Gans, and J. M. Kahn, "Fading Correlation and its Effect on the Capacity of Multi-Element Antenna Systems," *IEEE Transactions on Communications*, vol. 48, no. 3, pp. 502-513, Mar. 2000.

[22] S. Loyka and G. Tsoulos, "Estimating MIMO System Performance Using the Correlation Matrix Approach," *IEEE Communications Letters*, vol. 6, no. 1, pp. 19-21, Jan. 2002.

[23] M. Chiani, M. Z. Win, and A. Zanella, "On the Capacity of Spatially Correlated MIMO Rayleigh-Fading Channels," *IEEE Transactions on Information Theory*, vol. 49, no. 10, pp. 2363-2371, Oct. 2003.

[24] G. J. Foschini, "Layered Space-Time Architecture for Wireless Communication in a Fading Environment when using Multi-Element Antennas," *Bell Labs Technical Journal*, vol. 1, no. 2, pp. 41-59, Sep. 1996.

[25] P. W. Wolniansky, G. J. Foschini, G. D. Golden, and R. Valenzuela, "V-BLAST: An Architecture for Realizing Very High Data Rates over the Rich-Scattering Wireless Channel," in *Proceedings of the URSI International Symposium on Signals, Systems, and Electronics (ISSSE 98*), pp. 295-300, Sep-Oct. 1998.

[26] R. Y. Mesleh, H. Haas, L. Yeonwoo, and Y. Sangboh, "Interchannel Interference Avoidance in MIMO Transmission by Exploiting Spatial Information," in *Proceedings of the IEEE 16th International Symposium on Personal, Indoor and Mobile Radio Communications, (PIMRC 2005),* pp. 141-145, Sep. 2005.

[27] H. Haas, E. Costa, and E. Schulz, "Increasing Spectral Efficiency by Data Multiplexing using Antenna Arrays," in *Proceedings of the 13th IEEE International Symposium on Personal, Indoor and Mobile Radio Communications (PIMRC)*, vol 2., pp. 610-613, Sep. 2012.

[28] R. Y. Mesleh, H. Haas, A. Chang Wook, and Y. Sangboh, "Spatial Modulation - A New Low Complexity Spectral Efficiency Enhancing Technique," in *Proceedings of the 1st International Conference on Communications and Networking in China (ChinaCom '06*), pp. 1-5. Oct. 2006.

[29] R. Y. Mesleh, H. Haas, S. Sinanovic, C. W. Ahn, and S. Yun, "Spatial Modulation," *IEEE Transactions on Vehicular Technology*, vol. 57, no. 4, pp. 2228-2241, Jul. 2008.

[30] J. Jeganathan, A. Ghrayeb, and L. Szczecinski, "Spatial Modulation: Optimal Detection and Performance Analysis," *IEEE Communications Letters*, vol. 12, no. 8, pp. 545-547, Aug. 2008.

[31] N. R. Naidoo, H. J. Xu, and T. A. M. Quazi, "Spatial Modulation: Optimal Detector Asymptotic Performance and Multiple-Stage Detection," *IET Communications*, vol. 5, no. 10, pp. 1368-1376, Jul. 2011.

[32] J. Yang, W. Yuanlu, W. Jiejun, S. Mingxing, and L. Yibo, "Spatial Modulation Scheme with Low-Complexity Detection Algorithms," *IEEE Communications Letters*, vol. 19, no. 8, pp. 1422-1425, May. 2015.

[33] A. Younis, N. Serafimovski, R. Mesleh, and H. Haas, "Generalised Spatial Modulation," in *Proceedings of the 44th Asilomar Conference on Signals, Systems and Computers (ASILOMAR 2010)*, pp. 1498-1502., Nov. 2010.

[34] J. Jeganathan, A. Ghrayeb, L. Szczecinski, and A. Ceron, "Space Shift Keying Modulation for MIMO Channels," *IEEE Transactions on Wireless Communications*, vol. 8, no. 7, pp. 3692-3703, Jul. 2009.

[35] L. Han-Wen, R. Y. Chang, C. Wei-Ho, H. Zhang, and K. Sy-Yen, "Bi-Space Shift Keying Modulation for MIMO Systems," *IEEE Communications Letters*, vol. 16, no. 8, pp. 1161-1164, Aug. 2012.

[36] R. Y. Mesleh and S. S. Ikki, "A High Spectral Efficiency Spatial Modulation Technique," in *Proceedings of the IEEE 80th Vehicular Technology Conference (VTC Fall '14)* pp. 1-5, Sep. 2014.

[37] S. Soon Up Hwang, Sangjin Lee and Jongsco Seo, "Soft-output ML Detector for Spatial Modulation OFDM Systems," *IEICE Electronic Express*, vol. 6, no. 19, pp. 1426-1431, Oct. 2009.

[38] Y. Yang and B. Jiao, "Information-Guided Channel-Hopping for High Data Rate Wireless Communication," *IEEE Communications Letters*, vol. 12, no. 4, pp. 225-227, Apr. 2008.

[39] R. Rajashekar, K. V. S. Hari, and L. Hanzo, "Antenna Selection in Spatial Modulation Systems," *IEEE Communications Letters,* vol. 17, no. 3, pp. 521-524, Mar. 2013.

[40] Y. Zhang, C. Ji, W. Q. Malik, D. C. O. Brien, and D. J. Edwards, "Receive Antenna Selection for MIMO Systems over Correlated Fading Channels," *IEEE Transactions on Wireless Communications*, vol. 8, no. 9, pp. 4393-4399, Sep. 2009.

[41] M. Di Renzo, H. Haas, and P. M. Grant, "Spatial Modulation for Multiple-Antenna Wireless Systems: A Survey," *IEEE Communications Magazine*, vol. 49, no. 12, pp. 182-191, Dec. 2011.

[42] G. Mingxi, J. Ghong, and S. Yuehong, "Detection Algorithm for Spatial Modulation System under Unconstrained Channel," in *Proceedings of the IEEE International Conference on Communication Technology (ICCT)*, pp. 458-461, Nov. 2010.

[43] A. Younis, R. Y. Mesleh, H. Haas, and P. M. Grant, "Reduced Complexity Sphere Decoder for Spatial Modulation Detection Receivers," in *Proceedings of the IEEE Global Telecommunications Conference (GLOBECOM)*, pp. 1-5, Dec. 2010.

[44] A. Younis, M. Di Renzo, R. Y. Mesleh, and H. Haas, "Sphere Decoding for Spatial Modulation," in *Proceedings of the IEEE International Conference on Communications (ICC '11)*, pp. 1-6, Jun. 2011.

[45] H. J. Xu, "Simplified ML Based Detection Schemes for M-QAM Spatial Modulation," *IET Communications*, vol. 6, no. 11, pp. 1356-1363, Jul. 2012.

[46] J. Wang, S. Jia, and J. Song, "Signal Vector Based Detection Scheme for Spatial Modulation," *IEEE Communications Letters*, vol. 16, no. 1, pp. 19-21, Jan. 2012.

[47] N. Pillay and H. J. Xu, "Comments on "Signal Vector Based Detection Scheme for Spatial Modulation"," *IEEE Communications Letters*, vol. 17, no. 1, pp. 2-3, Jan. 2013.

[48] J. Zheng, "Signal Vector Based List Detection for Spatial Modulation," *IEEE Wireless Communications Letters*, vol. 1, no. 4, pp. 265-267, Aug. 2012.

[49] R. Rajashekar and K. V. S. Hari, "Low Complexity Maximum Likelihood Detection in Spatial Modulation Systems," Available: arXiv.1206.6190v1, Jun. 2012.

[50] C. Xu, S. X. N. Sugiura, and L. Hanzo, "Spatial Modulation and Space-Time Shift Keying: Optimal Performance at a Reduced Detection Complexity," *IEEE Transactions on Communications*, vol. 61, no. 1, pp. 206-216, Jan. 2013.

[51] Q. Tang, Y. Xiao, P. Yang, Q. Yu, and S. Li, "A New Low-Complexity Near-ML Detection Algorithm for Spatial Modulation," *IEEE Wireless Communications Letters*, vol. 2, no. 1, pp. 90-93, Dec. 2012.

[52] J. Jeganathan, "Space Shift Keying Modulation for MIMO Channels," MASc Thesis, Department of Electrical and Computer Engineering, Concordia University, Canada, Montreal, Quebec, Canada, Aug. 2008.

[53] R. Mesleh, S. Engelken, S. Sinanovic, and H. Haas, "Analytical SER Calculation of Spatial Modulation," in *Proceedings of the IEEE 10th International Symposium on Spread Spectrum techniques and Applications (ISSSTA '08)*, pp. 272-276, Aug. 2008.

[54] H. Xu, "Symbol Error Probability for Generalized Selection Combining Reception of M-QAM," *South African Institute of Electrical Engineers (SAIEEE) Africa Research Journal*, vol. 100, no. 3, pp. 68-71, Sep. 2009.

[55] R. Govender, N. Pillay, and X. HongJun, "Soft-output Space-Time Block Coded Spatial Modulation," *IET Communications*, vol. 8, no. 16, pp. 2786-2796, Jun. 2014.

[56] P. T. P. Tang, "Table-lookup Algorithms for Elementary Function and their Error Analysis," in *Proceedings of the 10th IEEE International Symposium on Computer Arithmetic*, pp. 232-236, Jun. 1991.

[57] J. Jeganathan, A. Ghrayeb, and L. Szczecinski, "Generalized Space Shift Keying Modulation for MIMO Channels," in *Proceedings of the IEEE 19th International Symposium on Personal, Indoor and Mobile Radio Communications (PIMRC 2008)*, pp. 1-5, Sep. 2008.

[58] M. S. Alouini and A. J. Goldsmith, "A Unified Approach for Calculating Error Rates of Linearly Modulated Signals over Generalized Fading Channels," *IEEE Transactions on Communications*, vol. 47, no. 9, pp. 1324-1334, Sep. 1999.

[59] R. Y. Mesleh, S. S. Ikki, and H. M. Aggoune, "Quadrature Spatial Modulation," *IEEE Transactions on Vehicular Technology*, vol. 64, no. 6, pp. 2738-2742, Jun. 2015.

[60] C. E. Shannon, "A Mathematical Theory of Communication," *Bell Labs Technical Journal*, vol. 27, pp. 623-656, Jul. 1948.

[61] A. Agrawal and T. Pangti, "Block Layered Space-Time Code Design," in *Proceedings of the 4th IEEE Workshop on Sensor Array and Multichannel Processing Waltham,* pp. 223-230, Sep. 2006.

[62] E. Basar, U. Aygolu, E. Panayirci, and H. V. Poor, "Space-Time Block Coded Spatial Modulation," *IEEE Transactions on Communications*, vol. 59, no. 3, pp. 823-832, Mar. 2011.

REFERENCES

[1] J. G. Proakis. and M. Salehi., *Digital Communications*, 5th ed. New York, NY 10020: McGraw-Hill, 2008.

[2] A. Goldsmith, "Wireless Communications," ed Salford University, 2004.

[3] W. Tranter, D. Taylor, R. Ziemer, N. Maxemchuk, and J. Mark, "Convolutional Codes and Their Performance in Communication Systems," in *The Best of the Best:Fifty Years of Communications and Networking Research*, ed: Wiley-IEEE Press, 2007, pp. 375-396.

[4] S. Srinivasan and S. S. Pietrobon, "Decoding of High Rate Convolutional Codes Using the Dual Trellis," *IEEE Transactions on Information Theory,* vol. 56, p. 22, January 2010.

[5] T. S. Rappaport, *Wireless Communication: Principles and Practice*, 2nd ed. New Jersy Prentice Hall PTR, 1996.

[6] A. J. Viterbi, "Convolutional Codes and Their Performance in Communication Systems," *Communication Technology, IEEE Transactions on,* vol. 19, pp. 751-772, 1971.

[7] R. Fano, "A heuristic discussion of probabilistic decoding," *IEEE Transactions on Information Theory,* vol. 9, pp. 64-74, 1963.

[8] K. S. Zigangirov, "Some Sequential Decoding Procedures," *jour Problems Inform. Transmission,* vol. 2, p. 13, 1966.

[9] S. M. Reddy and J. P. Robinson, "A decoding algorithm for some convolutional codes constructed from block codes," *Information and Control,* vol. 13, pp. 492-507, 1968/11/01 1968.

[10] S. D. Lin and J. Costello, *Error Control Coding*. USA: Pearson Prentice Hall, 2004.

[11] R. Khanai and G. H. Kulkarni, "Performance Analysis of Conventional Crypto-Coding," *International Journal of Latest Trends in Computing,* vol. 2, 2011.

[12] M. F. Mosleh and F. a. A. Abid, "Log-Likelihood ratio to Improve Hard Decission Viterbi Algorithm," *Engineering and Technology Journal,* vol. 31, p. 12, 2013.

[13] G. D. Forney, "The viterbi algorithm," *Proceedings of the IEEE,* vol. 61, pp. 268-278, 1973.

[14] G. Forney, "Convolutional codes I: Algebraic structure," *IEEE Transactions on Information Theory,* vol. 16, pp. 720-738, 1970.

[15] J. C. Dany, J. Antoine, L. Husson, A. Wautier, N. Paul, and J. Brouet, "Low complexity algorithm for the decoding of convolutional codes of any rate," in *Communications, 2004 IEEE International Conference on*, 2004, pp. 547-551 Vol.1.

[16] T. M. Duman. and A. Ghrayeb., *Coding for MIMO Communication Systems:* John Wiley & Sons Ltd, 2007.

[17] S. Schindler. (2009). *Introduction to MIMO: Application Note*.

[18] E. Telatar, "Capacity of Multi-Antenna Gaussian Channels," *European Transaction Telecommunication,* vol. 10, p. 37, November/December 1999.

[19] A. U. H. Sheikh, "Principles of Transmission and Detection of Digital Signals," in *Digital Communication*, P. C. Palanisamy, Ed., ed: InTech Available from: http://www.intechopen.com/books/digital-communication/principles-of-transmission-and-detection-of-digitalsignals, March, 2012.

[20] S. Catreux, P. F. Driessen, and L. J. Greenstein, "Simulation results for an interference-limited multiple input multiple output cellular system," in *Global Telecommunications Conference, 2000. GLOBECOM '00. IEEE*, 2000, pp. 1094-1096 vol.2.

[21] S. Da-Shan, G. J. Foschini, M. J. Gans, and J. M. Kahn, "Fading correlation and its effect on the capacity of multielement antenna systems," *IEEE Transactions on Communications,* vol. 48, pp. 502-513, 2000.

[22] S. Loyka and G. Tsoulos, "Estimating MIMO system performance using the correlation matrix approach," *IEEE Communications Letters,* vol. 6, pp. 19-21, 2002.

[23] M. Chiani, M. Z. Win, and A. Zanella, "On the capacity of spatially correlated MIMO Rayleigh-fading channels," *IEEE Transactions on Information Theory,* vol. 49, pp. 2363-2371, 2003.

[24] G. J. Foschini, "Layered space-time architecture for wireless communication in a fading environment when using multi-element antennas," *Bell Labs Technical Journal,* vol. 1, pp. 41-59, 1996.

[25] P. W. Wolniansky, G. J. Foschini, G. D. Golden, and R. Valenzuela, "V-BLAST: an architecture for realizing very high data rates over the rich-scattering wireless channel," in *Signals, Systems, and Electronics, 1998. ISSSE 98. 1998 URSI International Symposium on*, 1998, pp. 295-300.

[26] R. Mesleh, H. Haas, L. Yeonwoo, and Y. Sangboh, "Interchannel Interference Avoidance in MIMO Transmission by Exploiting Spatial Information," in *Personal, Indoor and Mobile Radio Communications, 2005. PIMRC 2005. IEEE 16th International Symposium on*, 2005, pp. 141-145.

[27] H. Haas, E. Costa, and E. Schulz, "Increasing spectral efficiency by data multiplexing using antenna arrays," in *Personal, Indoor and Mobile Radio Communications, 2002. The 13th IEEE International Symposium on*, 2002, pp. 610-613 vol.2.

[28] R. Mesleh, H. Haas, A. Chang Wook, and Y. Sangboh, "Spatial Modulation - A New Low Complexity Spectral Efficiency Enhancing Technique," in *Communications and Networking in China, 2006. ChinaCom '06. First International Conference on*, 2006, pp. 1-5.

[29] R. Y. Mesleh, H. Haas, S. Sinanovic, C. W. Ahn, and S. Yun, "Spatial Modulation," *IEEE Transactions on Vehicular Technology,* vol. 57, pp. 2228-2241, 2008.

[30] J. Jeganathan, A. Ghrayeb, and L. Szczecinski, "Spatial modulation: optimal detection and performance analysis," *IEEE Communications Letters,* vol. 12, pp. 545-547, 2008.

[31] N. R. Naidoo, H. J. Xu, and T. A. M. Quazi, "Spatial modulation: optimal detector asymptotic performance and multiple-stage detection," *IET Communications,* vol. 5, pp. 1368-1376, 2011.

[32] J. Yang, W. Yuanlu, W. Jiejun, S. Mingxing, and L. Yibo, "Spatial Modulation Scheme With Low-Complexity Detection Algorithms," *Communications Letters, IEEE,* vol. 19, pp. 1422-1425, 2015.

[33] A. Younis, N. Serafimovski, R. Mesleh, and H. Haas, "Generalised spatial modulation," in *Signals, Systems and Computers (ASILOMAR), 2010 Conference Record of the Forty Fourth Asilomar Conference on*, 2010, pp. 1498-1502.

[34] J. Jeganathan, A. Ghrayeb, L. Szczecinski, and A. Ceron, "Space shift keying modulation for MIMO channels," *Wireless Communications, IEEE Transactions on,* vol. 8, pp. 3692-3703, 2009.

[35] L. Han-Wen, R. Y. Chang, C. Wei-Ho, H. Zhang, and K. Sy-Yen, "Bi-Space Shift Keying Modulation for MIMO Systems," *Communications Letters, IEEE,* vol. 16, pp. 1161-1164, 2012.

[36] R. Mesleh and S. S. Ikki, "A High Spectral Efficiency Spatial Modulation Technique," in *Vehicular Technology Conference (VTC Fall), 2014 IEEE 80th*, 2014, pp. 1-5.

[37] S. Soon Up Hwang, Sangjin Lee and Jongsco Seo, "Soft-output ML detector for Spatial Modulation OFDM Systems," *IEICE Electronic Express,* vol. 6, p. 6, October 10 2009 October 2009.

[38] Y. Yang and B. Jiao, "Information-guided channel-hopping for high data rate wireless communication," *IEEE Communications Letters,* vol. 12, pp. 225-227, 2008.

[39] R. Rajashekar, K. V. S. Hari, and L. Hanzo, "Antenna Selection in Spatial Modulation Systems," *IEEE Communications Letters,* vol. 17, pp. 521-524, 2013.

[40] Y. Zhang, C. Ji, W. Q. Malik, D. C. O. Brien, and D. J. Edwards, "Receive antenna selection for MIMO systems over correlated fading channels," *IEEE Transactions on Wireless Communications,* vol. 8, pp. 4393-4399, 2009.

[41] M. Di Renzo, H. Haas, and P. M. Grant, "Spatial modulation for multiple-antenna wireless systems: a survey," *Communications Magazine, IEEE,* vol. 49, pp. 182-191, 2011.

[42] G. Mingxi, J. Ghong, and S. Yuehong, "Detection Algorithm for Spatial Modulation System under Unconstrained Channel," presented at the IEEE International Conference on Communication Technology (ICCT), Nov. 2010.

[43] A. Younis, R. Mesleh, H. Haas, and P. M. Grant, "Reduced Complexity Sphere Decoder for Spatial Modulation Detection Recievers," presented at the IEEE Global Telecommunications Conference (GLOBECOM), Dec. 2010.

[44] A. Younis, M. Di Renzo, R. Mesleh, and H. Haas, "Sphere Decoding for Spatial Modulation," in *Communications (ICC), 2011 IEEE International Conference on*, 2011, pp. 1-6.

[45] H. J. Xu, "Simplified ML Based Detection Schemes for M-QAM Spatial Modulation," *IET Communications,* vol. 6, pp. 1356-1363, Jul. 2012.

[46] J. Wang, S. Jia, and J. Song, "Signal Vector Based Detection Scheme for Spatial Modulation," *IEEE Communications Letters,* vol. 16, pp. 19-21, Jan. 2012.

[47] N. Pillay and H. J. Xu, "Comments on "Signal Vector Based Detection Scheme for Spatial Modulation"," *IEEE Communications Letters,* vol. 17, pp. 2-3, Jan. 2013.

[48] J. Zheng, "Signal Vector Based List Detection for Spatial Modulation," *IEEE Wireless Communications Letters,* vol. 1, pp. 265-267, Aug. 2012.

[49] R. Rajashekar and K. V. S. Hari. (Jun. 2012, Low COmplexity Maximum Likelihood Detection in Spatial Modulation Systems.

[50] C. Xu, S. X. N. Sugiura, and L. Hanzo, "Spatial Modulation and Space-Time Shift Keying: Optimal Performance at a Reduced Detection Complexity," *IEEE Transactions on Communications,* vol. 61, pp. 206-216, Jan. 2013.

[51] Q. Tang, Y. Xiao, P. Yang, Q. Yu, and S. Li, "A New Low-Complexity Near-ML Detection Algorithm for Spatial Modulation," *Wireless Communications Letters, IEEE,* vol. 2, pp. 90-93, 2013.

[52] J. Jeganathan, "Space Shift Keying Modulation for MIMO Channels," Master of Applied Science, The Department of Electrical and Computer Engineering, Concordia University,Canada, Montreal, Quebec, Canada, 2008.

[53] R. Mesleh, S. Engelken, S. Sinanovic, and H. Haas, "Analytical SER Calculation of Spatial Modulation," in *IEEE 10th International Symposium on Spread Spectrum techniques and Applications (ISSSTA '08)*, Aug. 2008, pp. 272-276.

[54] H. J. Xu, "Symbol Error Probability for Generalized Slection Combining Reception of M-QAM," *South African Institute of Electrical Engineers (SAIEEE) Africa Research Journal,* vol. 100, pp. 68-71, Sep. 2009.

[55] R. Govender, N. Pillay, and X. HongJun, "Soft-output space-time block coded spatial modulation," *Communications, IET,* vol. 8, pp. 2786-2796, 2014.

[56] P. T. P. Tang, "Table-lookup algorithms for elementary function and their error analysis," presented at the 10th IEEE International Symposium on COmputer Arithmetic, Jun. 1991.

[57] J. Jeganathan, A. Ghrayeb, and L. Szczecinski, "Generalized space shift keying modulation for MIMO channels," in *Personal, Indoor and Mobile Radio Communications, 2008. PIMRC 2008. IEEE 19th International Symposium on*, 2008, pp. 1-5.

[58] M. S. Alouini and A. J. Goldsmith, "A Unified Approach for calculating Error Rates of Linearly Modulated Signals over Generalized Fading Channels," *IEEE Transactions on Communications,* vol. 47, p. 11, September 1999.

[59] R. Mesleh, S. S. Ikki, and H. M. Aggoune, "Quadrature Spatial Modulation," *Vehicular Technology, IEEE Transactions on,* vol. 64, pp. 2738-2742, 2015.

[60] C. E. Shannon, "A Mathematical Theory of Communication," *Bell Labs Technical Journal,* vol. 27, July Jul. 1948.

[61] A. Agrawal and T. Pangti, "Block Layered Space-Time Code Design," presented at the 4th IEEE Workshop on Sensor Array and Multichannel Processing Waltham, M. A, 2006.

[62] E. Basar, U. Aygolu, E. Panayirci, and H. V. Poor, "Space-Time Block Coded Spatial Modulation," *Communications, IEEE Transactions on,* vol. 59, pp. 823-832, 2011.